ADVANCED MASTERS IN STRUCTURAL ANALYSIS
OF MONUMENTS AND HISTORICAL CONSTRUCTIONS

Master's Thesis

Georgios Vlachakis

Out-of-plane simulation of masonry structures using novel finite element techniques

UNIVERSITAT POLITÈCNICA DE CATALUNYA

Education and Culture

Erasmus Mundus

Spain | 2017

DECLARATION

Name: Vlachakis Georgios

Email: giorgovlachaki@gmail.com

Title of the Msc Dissertation: Out-of-plane simulation of masonry structures using novel finite element techniques

Supervisor(s): Professor Miguel Cervera & Savvas Saloustros

Year: 2016-2017

I hereby declare that all information in this document has been obtained and presented in accordance with academic rules and ethical conduct. I also declare that, as required by these rules and conduct, I have fully cited and referenced all material and results that are not original to this work.

I hereby declare that the MSc Consortium responsible for the Advanced Masters in Structural Analysis of Monuments and Historical Constructions is allowed to store and make available electronically the present MSc Dissertation.

University: Universitat Politècnica de Catalunya

Date: 14/07/2017

Signature:

_____

This page is left blank on purpose.

My wing is ready to fly
I would rather turn back
For had I stayed mortal time
I would have had little luck.
– Gerhard Scholem, "Angelic Greetings"

There is a painting by Paul Klee called Angelus Novus. An angel is depicted there who looks as though he were about to distance himself from something which he is staring at. His eyes are opened wide, his mouth stands open and his wings are outstretched. The Angel of History must look just so. His face is turned towards the past. Where we see the appearance of a chain of events, he sees one single catastrophe, which unceasingly piles rubble on top of rubble and hurls it before his feet. He would like to pause for a moment so fair, to awaken the dead and to piece together what has been smashed. But a storm is blowing from Paradise, it has caught itself up in his wings and is so strong that the Angel can no longer close them. The storm drives him irresistibly into the future, to which his back is turned, while the rubble-heap before him grows sky-high. That which we call progress, is this storm.

- Walter Benjamin, "Theses on the Philosophy of History"

This page is left blank on purpose.

ACKNOWLEDGEMENTS

First and above all, I would like to thanks deeply my three supervisors, who guided me through this process of creative learning. Professor Miguel Cervera, for his precious comments and endless discussions that widened my thinking horizons; Savvas Saloustros, for his meticulous support that provided a balance to this process; and last but not least, Gabriel Barbat, for being always next to my side and providing me immediately any of his “tools”. If “the object of teaching is to enable people to get along without a teacher”, as a paper states at their corridor, then unfortunately, I doubt that they should be satisfied. However, I can assure them that we are on the right track.

I am also grateful to all the great SAHC professors that provided to me this unique educational program, during the courses period in the University of Padova.

A special thanks is dedicated to all the organizers of the SAHC Master program for making this experience possible.

Furthermore, I would like to thank the MSc Consurtium for the generous financial support, which made it possible for me to participate in the program.

My thanks are further extended to my lovely parents, for their support about this journey, before it even started! In addition, my sister Eva is also greatly acknowledged, as the “last minute savior”.

Finally, I would like to sincerely thank all of my classmates in Padova and Barcelona for all the happy and sad moments we shared together.

It has been an experience I will never forget!

This page is left blank on purpose.

ABSTRACT

The out-of-plane response is a complex and at the same time key aspect of the seismic vulnerability of masonry structures. It depends on several factors, some of which are the material properties, the quality of the walls, the geometry of the structure, the connections between structural elements and the stiffness of the diaphragms. Despite its importance and due to the related difficulties, there is still lack of a robust and straightforward assessment technique.

During the last years, a wide variety of numerical methods has been employed to the out-of-plane assessment of unreinforced masonry structures (URM). Among the most famous of them are finite element macro-modelling approaches as they allow the modelling of large structures at a reasonable computational cost. However, macro-modelling approaches may result in the non-realistic representation of localized cracks and dependency of the numerical solution on the used finite element mesh.

As a remedy to this problem, the mixed strain/displacement finite elements have been recently proposed. Thanks to the independent interpolation of the strains and displacements, the proposed formulation is characterized by an enhanced accuracy in strain localization and crack propagation problems, being at the same time mesh bias independent. For these reasons, the mixed finite elements are employed in this thesis for the out-of-plane assessment of URM structures, being at the same time the first real-scale application.

A full scale experimental campaign of two masonry structures, namely a stone and a brick, subjected to shaking-table test is chosen here as benchmark problem (Candeias et al, 2017), and different nonlinear static analyses are performed. In order to assess the efficiency of the proposed model, the results are compared firstly with the experimental results, secondly with the results obtained by the standard elements and finally, with a previous similar simulation attempt existing in the literature. Furthermore, physical and numerical input parameters, such as the effect of the lintels, the damage model or the stabilization parameter used, are also examined.

As a general overview, the proposed model provides a good estimation in terms of collapse mechanism and PGA for both structures, while a sufficient estimation in terms of displacements is obtained only for the brick house. Several observed differences are attributed to shortcomings of the methodology adopted, related mainly to the homogenized nature of the model and the static monotonic loading applied. Moreover, the results of the mixed formulation do not appear to suffer by any mesh bias dependency, justifying their superiority, but arriving with an increased computational cost.

This page is left blank on purpose.

RESUMEN

La respuesta fuera del plano es un aspecto complejo y a la vez clave de la vulnerabilidad sísmica de las estructuras de mampostería. Depende de varios factores, algunos de los cuales son las propiedades del material, la calidad de las paredes, la geometría de la estructura, las conexiones entre los elementos estructurales y la rigidez de los diafragmas. A pesar de importancia del tema y debido a las dificultades asociadas a ella, todavía no existe una técnica de evaluación robusta y directa.

Durante los últimos años, se ha utilizado una amplia variedad de métodos numéricos para la evaluación fuera del plano de las estructuras de mampostería no reforzada. Entre los más populares están los métodos de modelado macro de elementos finitos, ya que permiten el modelado de grandes estructuras a un costo computacional razonable. Sin embargo, los enfoques de macro-modelado pueden resultar en una representación poco realista de las fisuras localizadas y en la dependencia de la solución numérica respecto de la malla de elementos finitos usada.

Como remedio a este problema, se han propuesto recientemente los elementos finitos mixtos deformación/desplazamiento. Gracias a la interpolación independiente de las deformaciones y desplazamientos, la formulación propuesta se caracteriza por una mayor precisión en los problemas de localización de las deformaciones y de propagación de fisuras, proporcionando al mismo tiempo resultados independientes de la malla. Por estas razones, los elementos finitos mixtos se emplean en esta tesis para la evaluación fuera de plano de estructuras de mampostería no reforzada, siendo al mismo tiempo la primera aplicación a escala real de esta técnica.

Se elige aquí como estudio de caso una campaña experimental (Candeias et al., 2017) a escala completa de dos estructuras de albañilería, a saber, una de piedra y una de ladrillo, sometidas a ensayo de mesa vibratoria, y se realizan diferentes análisis estáticos no lineales. Para evaluar la eficiencia del modelo propuesto, los resultados se comparan en primer lugar con los resultados experimentales, en segundo lugar con los resultados obtenidos por los elementos estándar y, finalmente, con una simulación numérica previa. Además, también se examinan parámetros de la simulación físicos y numéricos, tales como el modelo de daño utilizado, la influencia de los dinteles o el parámetro de estabilización.

Como resultado general, el modelo propuesto proporciona una buena estimación en términos de mecanismo de colapso y aceleración máxima del suelo para ambas estructuras, aunque sólo se obtiene una estimación satisfactoria en términos de desplazamientos para la casa de ladrillo. Varias de las diferencias observadas se atribuyen a las deficiencias de la metodología adoptada, relacionadas principalmente con la naturaleza homogeneizada del modelo y la carga monótona estática aplicada. Además, los resultados de la formulación mixta parecen no sufrir de ningún sesgo

debido a la malla, justificando su superioridad, pero comportando un coste computacional incrementado.

Τίτλος Μεταπτυχιακής εργασίας: **“**Προσομοίωση εκτός-επιπέδου απόκρισης κατασκευών από τοιχοποιία χρησιμοποιώντας καινοτόμα μέθοδο πεπερασμένων στοιχείων. “

ΠΕΡΙΛΗΨΗ

Η εκτός-επιπέδου απόκριση είναι μία σύνθετη και την ίδια στιγμή καίριας σημασίας πτυχή για την σεισμική τρωτότητα κατασκευών από τοιχοποιία. Εξαρτάται από αρκετούς παράγοντες, μερικούς από τους οποίους είναι οι ιδιότητες των υλικών, η ποιότητα της τοιχοποιίας, η γεωμετρία της κατασκευής, η σύνδεση μεταξύ των δομικών στοιχείων και η δυσκαμψία των διαφραγμάτων. Παρόλη την σπουδαιότητα και λόγω των σχετικών δυσκολιών, υπάρχει ακόμα έλλειψη μίας αξιόπιστης και άμεσης τεχνικής εκτίμησής της.

Τα τελευταία χρόνια, μία μεγάλη ποικιλομορφία αριθμητικών μεθόδων έχει χρησιμοποιηθεί για την εκτίμηση της εκτός-επιπέδου απόκρισης κατασκευών από τοιχοποιία. Μεταξύ των πιο διαδεδομένων είναι η προσέγγιση με πεπερασμένα στοιχεία μακρο-μοντελοποίησης, καθώς επιτρέπει την προσομοίωση μεγάλων κατασκευών με λογικό υπολογιστικό κόστος. Ωστόσο, η προσέγγιση μακρο-μοντελοποίησης μπορεί να οδηγήσει σε λανθασμένη αναπαράσταση των ρωγμών και εξάρτηση της αριθμητικής λύσης από το επιλεγμένο κάνναβο πεπερασμένων στοιχείων.

Για την αντιμετώπιση του παραπάνω προβλήματος, τα μεικτά πεπερασμένα στοιχεία παραμορφώσεων/μετατοπίσεων έχουν πρόσφατα προταθεί. Χάρις στην ανεξάρτητη ολοκλήρωση των παραμορφώσεων και των μετατοπίσεων, τα προτεινόμενα στοιχεία χαρακτηρίζονται από αυξημένη ακρίβεια σε προβλήματα συγκέντρωσης παραμορφώσεων και διάδοσης ρωγμών, όντας την ίδια στιγμή ανεξάρτητα από το προεπιλεγμένο κάνναβο. Για τους παραπάνω λόγους, τα μεικτά πεπερασμένα στοιχεία υιοθετούνται στην παρούσα εργασία για την εκτίμηση της εκτός-επιπέδου συμπεριφοράς άοπλης τοιχοποιίας, αποτελώντας συγχρόνως την πρώτη εφαρμογή τους σε κατασκευή πραγματικού μεγέθους.

Ως πειράματα αναφοράς της παρούσας εργασία έχουν επιλεγεί δύο πραγματικού μεγέθους κατασκευές, μία από οπτόπλινθους και μία πέτρινη, υποβαλλόμενες σε καταπόνηση σεισμικής τράπεζας (Candeias et al, 2017), και εκτελούνται διαδοχικές στατικές υπερωθητικές αναλύσεις για την εκτίμησή τους. Με σκοπό την αξιολόγηση της αποτελεσματικότητας του προτεινόμενου μοντέλου, γίνεται σύγκριση των αποτελεσμάτων πρώτα με τα πειραματικά, μετέπειτα με τα αποτελέσματα των καθιερωμένων πεπερασμένων στοιχείων, και τέλος με μία όμοια προσπάθεια ανάλυσης, προϋπάρχουσα στην βιβλιογραφία. Στη συνέχεια διερευνούνται ορισμένες φυσικές και αριθμητικές παράμετροι, όπως η επίδραση των ανωφλιών, το μοντέλο βλάβης και η παράμετρος σταθεροποίησης.

Εποπτικά, το προτεινόμενο μοντέλο πετυχαίνει μία καλή εκτίμηση των αποτελεσμάτων τόσο σε όρους μηχανισμού κατάρρευσης όσο και σε όρους μέγιστης εδαφικής επιτάχυνσης, ενώ ικανοποιητική εκτίμηση σε όρους μετατοπίσεων επιτυγχάνεται μόνο για την οπτοπλινθοδομή. Συγκεκριμένες

παρατηρούμενες διαφοροποιήσεις αποδίδονται στις αδυναμίες της υιοθετούμενης μεθοδολογίας, όπως την ομογενοποιημένη θεώρηση του μοντέλου και την μονοτονικά και στατικά εφαρμοζόμενη φόρτιση. Επιπλέον παρατηρείται ότι τα αποτελέσματα των μεικτών πεπερασμένων στοιχείων δεν εξαρτώνται από το προεπιλεγμένο κάνναβο, αποδεικνύοντας έτσι την ανωτερότητά τους, επιβαρυμένα ωστόσο με επιπλέον υπολογιστικός κόστος.

TABLE OF CONTENTS

TABLE OF TABLES

TABLE OF FIGURES

1. OUT-OF-PLANE FAILURE OF MASONRY STRUCTURES: A BRIEF INTRODUCTION OF AN OPEN TOPIC

1.1 Introduction to the problem

Unreinforced masonry structures consist one of the oldest construction types, are still worldwide inhabited and include the majority of the built heritage. Despite their significance, their material characteristics and structural behaviour remain still uncertain. Moreover, history has shown that unreinforced masonry structures are extremely vulnerable to seismic events, i.e. the recent earthquakes of Umbria-Marche 1997, Kashmir 2005, Pisco 2007, L'Aquila 2009, Haiti 20010, Christchurch 2011, Emilia Romagna 2012, Nepal 2015, Umbria 2016, Lesbos 2017.

Figure 1.1 Out-of-plane collapses of traditional Unreinforced Masonry (URM) houses during the earthquake in Lesbos 2017

Among the possible failures of the unreinforced masonry structures, the out-of-plane is undoubtedly the most crucial (Figure 1.1), according to several post-earthquake surveys (Rietherman, 1985; Moore et al, 1988; Hart et al, 1988; Bruneau, 1994; Lagomarsino, 1998; Lagomarsino & Podesta, 2004;

Decanini et al, 2004, etc.). In addition, out-of-plane is one of the most complex and yet inadequately addressed topics in seismic analysis (Menon & Magenes, 2008). In fact, the out-of-plane vulnerability of masonry structures is a widely known issue, with evidence perceived since Byzantine times (Binda et al, 2006) which was stated early in the 15th century by Leonardo da Vinci; since then, it has been suggested that improvements should be made on connections between different leafs and tie rods should be inserted to sustain out-of-plane motions (Milizia, 1554; Rondelet, 1802). Indeed, as Costa (2012) underlines, the low strength to mass ratio of masonry structures increases their vulnerability in the out-of-plane direction because inertia forces are not restrained due to the reduced stiffness and strength of the masonry walls in that direction. Moreover, local collapse mechanisms are likely to form, due to usual presence of local weaknesses or lack of global integrity. Figure 1.2 presents the Rondelet's out-of-plane mechanisms, one of the first sets of out-of-plane mechanisms reported in literature.

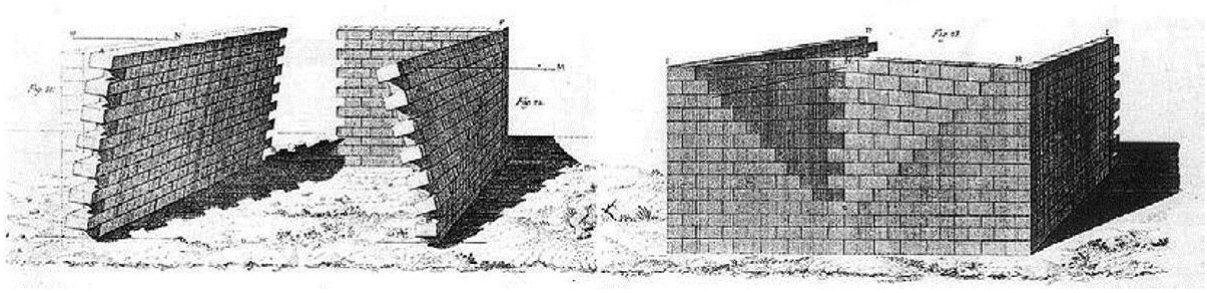

Figure 1.2 Rondelet's collapse mechanisms of masonry walls under out-of-plane horizontal action (Ferreira et al, 2015)

The main aspects of the seismic vulnerability of an unreinforced masonry building, as summarized and underlined by (Menon & Magenes, 2008), can be gauged by the presence of certain simple, yet critical features enumerated below:

- The quality of the load-bearing walls (masonry units, mortar, interlocking of units, regularity of courses) to facilitate monolithic behaviour right through the wall thickness
- Restricted slenderness of the walls to ensure out-of-plane stability
- Presence of efficient connections amongst walls (good interlocking at wall intersections), and between walls and horizontal structures (tie-rods, ring beams at all roof/floor levels) to ensure "box-action"
- Adequately rigid and resistant floor diaphragms providing restraint to the out-of-plane vibration of walls, increasing structural redundancy and facilitating internal force redistribution
- Presence of suitable elements such as ties, floor diaphragm, etc., or availability of in-plane resistance of strong walls or buttresses to counteract horizontal thrusts (from roofs, arches or

vaults) to form a “closed” self-equilibrating system. Out-of-plane failure of walls where horizontal thrusts are counteracted merely by their out-of-plane resistance is very frequent.

Furthermore, it is common that inadequate retrofitting or strengthening techniques are applied to masonry structures, which appear to create or boost local mechanisms rather than secure their integrity (Valluzzi, 2007). Actually, as Penazzi et al (2000) point out, “*the ineffectiveness of these techniques […] are mostly due to […] the lack of knowledge on the material and structural behaviour of historic buildings”*.

Summarizing, the out-of-plane response is a complex and at the same time crucial aspect of the seismic vulnerability of masonry structures. It depends on several factors, some of which are the material properties, the quality of the walls, the geometry of the structure, the connections between structural elements and the stiffness of the diaphragms. Consequently, adequate methods and tools are needed, able to reproduce correctly this response in order to assess correctly and decide properly possible interventions.

1.2 Brief review of the assessment methodologies

Several methods, techniques and computational tools have been developed as a constant effort towards the assessment of the out-of-plane response of unreinforced masonry structures. A complete and detailed categorization and presentation of all these techniques is far beyond the scope of this thesis. However, a brief but representative overview is attempted here, based mainly on the remarkable work of Ferreira et al (2015).

The different assessment techniques developed so far could be categorized in two main groups: analytical methods and numerical approaches. Therefore, the brief overview presented herein is based on this distinction, and are schematically presented in Figure 1.3.

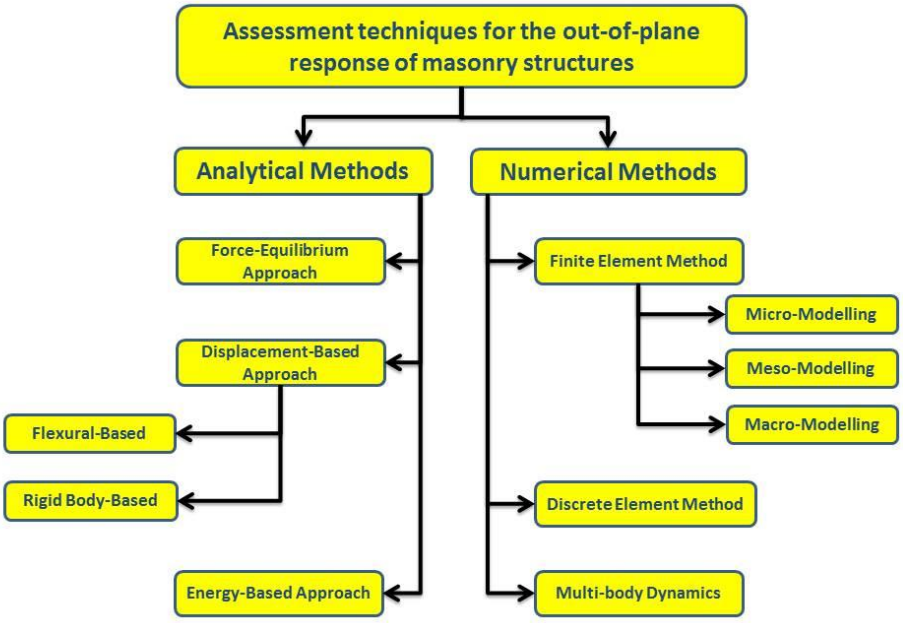

Figure 1.3 Assessment techniques for the out-of-plane response of masonry structures

1.2.1 Analytical methodologies

As already presented in Figure 1.3, the several alternative analytical approaches developed so far could be further classified into three groups:

- the force-equilibrium approach, based on the assumption that the out-of-plane failure phenomenon is related to forces and their equilibrium,
- the displacement-based approach, established on the assumption that the out-of-plane instability of masonry structures is more related to maximum displacements reached by the structure, rather than forces,
- the energy based approach, in which a correlation between the strength of the wall and the velocity of the input motion is assumed.

Force-equilibrium approach

The force-equilibrium approach is based on the assumption that the out-of-plane failure phenomenon is related to forces and their equilibrium. Therefore, the expected force capacity of the structure is compared with the expected force demand, which is directly correlated with the PGA.

Graphic-statics mark the beginning of the equilibrium approach to analyse masonry structures. Starting back to the 16th century's parallelogram rule (Stevin, 1586) and based on the static equilibrium analysis of rigid body mechanisms, the equilibrium method would be later combined with the limit theorems of plasticity by (Heyman, 1966) as a first application to masonry structures. Having as main assumption that failure of masonry can only occur due to instability rather than material failure, Heyman proposed that equilibrium equations could provide a lower-bound while the kinematic theorem an upper-bound solution to the problem. Despite its further development (Giaquinta & Giusti, 1985; Del Piero, 1989; Block et al. 2006; DeJong, 2009) and potential, the method is characterized by un-conservatism by its intrinsic nature, since local crushing, crack propagation and sliding effects are neglected.

However, several developments have been done on the use of the so-called non-standard limit analysis (Giuffrè, 1990; Giuffrè et al, 1993; Casapulla, 1999; Picchi, 2002; Restrepo-Vélez, 2004; D'Ayala & Speranza, 2003, Casapulla & D'Ayala, 2006, Novelli & D'Ayala, D. 2012). According to this proposal, the possible failure mechanisms that might appear at the examined structure should initially be identified based on a thorough collection/abacus, proposed at the aforementioned works (Figure 1.4). Thenceforth, a collapse load factor, λ_c, is calculated for each case so that a limit equilibrium state is verified, and the mechanism with the lower value is the most probable to occur. The load factor, λ_c, describes the ratio between the lateral seismic acceleration, a, and the gravitational acceleration, g; the masonry walls are assumed as rigid bodies connected with hinges according to the mechanism examined; while the method can take into account the effects of friction, cohesion, loading configuration, connections or restraints and special devices, such as ties. The main advantage characterizing this method is its practical simplicity, since a reduced number of input parameters are only needed.

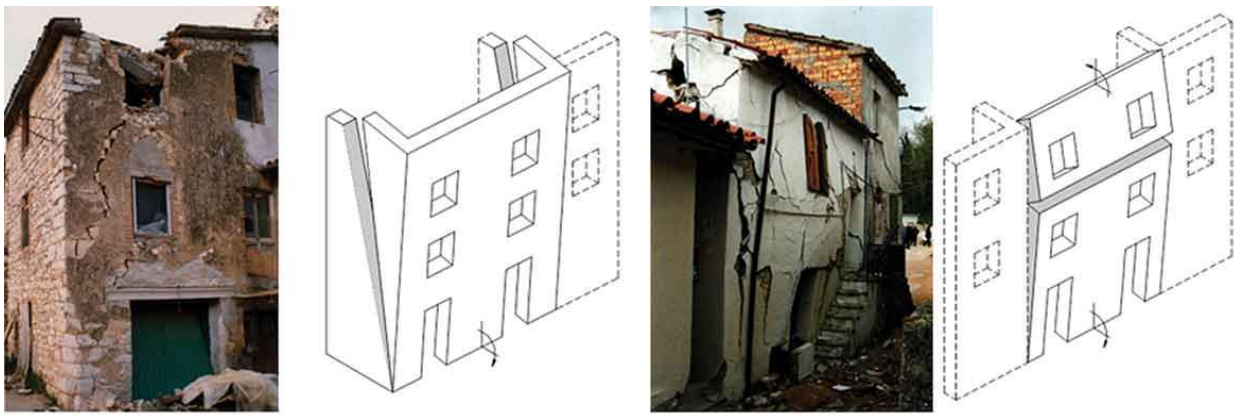

Figure 1.4 Collapse mechanisms as observed and modelled (D'Ayala & Speranza, 2003)

Using the principles of the force-based approach, several works have been also dedicated into defining the flexural strength of masonry, derived by a yield-line analysis of plates (Hendry et al, 1997; Felice & Giannini, 2001, Milani et al, 2006). Such an approach can take into account two dimensional bending phenomenona, the lateral restrains and the effect of friction.

Finally, despite the simplicity of all the aforementioned methodologies, the experimental research has shown that the masonry walls can sustain higher accelerations than their "quasi-static" capacity, and therefore their collapse tends to be ruled by their maximum displacement or velocity rather than by their maximum strength, possessing non-negligible post-cracking behavior (Venture, 1981; Bruneau, 1994; Doherty et al, 2002). Consequently, the displacement-based approach has attracted the attention of researchers and engineers.

Displacement-based approach

The displacement-based approach is established on the assumption that the out-of-plane instability of masonry structures is more related to maximum displacements reached by the structure, rather than forces (Abrams et al, 1996; Doherty, 2000; Griffith et al, 2003). Therefore, the collapse or not of the structure should be assessed by comparing the expected displacement capacity of the structure with the expected displacement demand.

The proposal to replace the traditional force-based methods was already done in (Priestley, 1985), by attempting a correlation between the capacity of masonry walls and the spectral velocity of the input motion (energy). Later on, Tomaževič underlined once more that the seismic vibration is "filtered" by the structure and as a result, out-of-plane vibrations could be amplified at higher stories, due to local resonance effects (Tomaževič, 1997). Following this research line, (Doherty el al, 2002) proposed a simplified displacement-based approach, with a trilinear force-displacement relationship, which would form the basis for further development, later on by (Griffith et al, 2003; Derakhshan et al, 2013, Lagomarsino 2015). Moreover, recently in (Ferreira, 2015), the same model is even more explored and a four-branch model was proposed, able to take into account also the elastic behaviour (Figure 1.5). The main concept of the method is that the geometric instability of an unreinforced masonry wall will only occur when the mid-height displacement of the assumed rigid block exceeds its ultimate displacement stability limits. Moreover, the maximum force that a load bearing wall can attain is lower than the "rigid-block" case, since the vertically loaded wall can initially deform and therefore the displacement at static instability is lower (Menon & Magenes 2008). According to the method, the assumed mechanism is idealized by a SDOF system, with the aforementioned three/four-branch relationship, while the only necessary parameters to proceed are the geometry, the boundary conditions and the vertical forces. Thereafter, the effective mass and effective stiffness can be calculated and in turn the displacement demand, by using the spectrum. Finally, the parameters Δ_1, Δ_2 and Δ_f (or θ_{cr}, θ_y, θ_l, θ_u respectively), representing the displacement of the initial stiffness reduction,

strength reduction and maximum stable displacement, should be provided for application by previous experimental calibrations. The two main disadvantages of the method are the need of experimental calibration of those parameters and in addition the a priori knowledge/assumption of the collapse mechanism, as discussed also in the force-based approach.

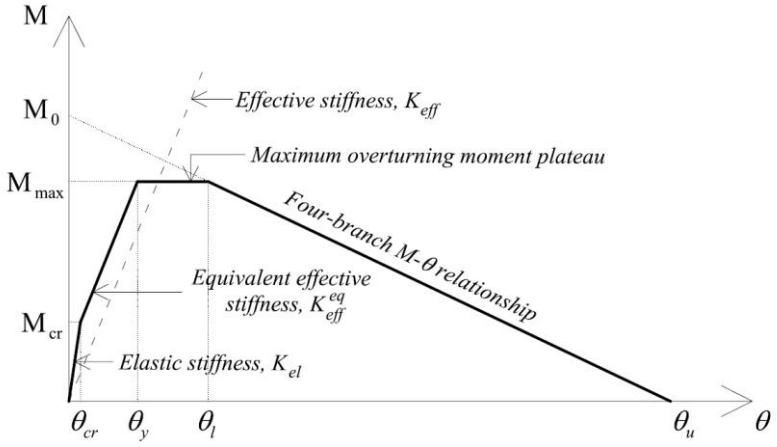

Figure 1.5 Four-branch idealization of the static M - θ relationship (Ferreira, 2015)

A parallel research line focused on the rocking motion of rigid blocks, which appeared to be a quite complex topic. Initially studied by (Housner, 1963) and continued by several researchers (Priestley et al, 1978; Yim et al, 1980; Psycharis, 1990; Spanos et al, 2001; Makris & Konstantinidis 2003), it was pointed out that the main characteristics which affect such a response are the slenderness, the geometry of the base of the block and the details of the ground motion. Moreover, analytical solutions presented extreme difficulties even for two stacked blocks, while it was proposed that spectrum approaches should refer to rocking spectra instead of flexural response spectra, since the phenomenon was shown to be more similar to the inverted pendulum problem rather than the regular pendulum oscillator. Applications to masonry walls were later on developed by (Sorrentino et al, 2008; Shawa et al, 2012; D'Ayala & Shi, 2011; Gabellieri et al, 2013; Derakhshan et al, 2011). More specifically, the former two works examined the rocking response of a masonry façade using a SDOF rocking system, taking into account the restrains provided by the transversal walls and horizontal structural elements, while energy dissipation was considered through the restitution coefficient. On the other hand, two-DOF rocking systems were examined in the rest of the studies (Figure 1.6), simulating portions of a cracked vertical spanning wall, and taking into account different conditions such as the flexible diaphragm, the crack height, the overburden loads, the mortar compressive strength and the mortar repointing.

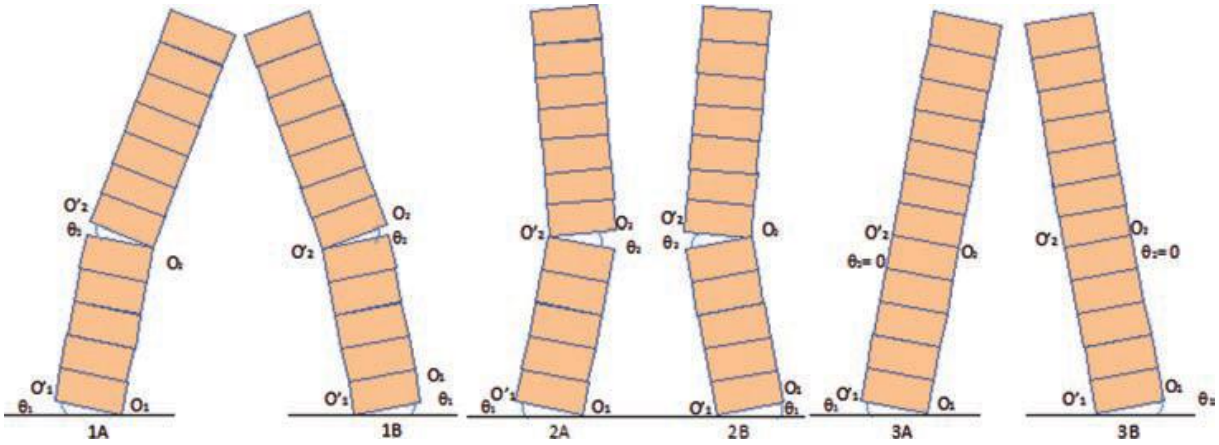

Figure 1.6 . Theoretical model simulating out of plane deformation of the centre strip of the facade of the experimental model, and the possible six patterns of relative rotation of the two rocking blocks (D'Ayala & Shi, 2011)

Energy approach

A possible energy-based approach has been recently proposed in (Sorrentino et al, 2017), despite it is not yet thoroughly examined. The origins of such an approach can be traced once more to (Housner, 1963) and (Sorrentino et al, 2006). The approach is based in the comparison between the energy demand and the energy requested to overturn the structure.

More specifically, the energy demand is estimated as the kinetic energy of the system in the rest position under a given initial velocity v, which in turn could be given either by the PGV of the seismic input either by the pseudo-spectral velocity. In the latter case the secant period, T_s, can be assumed similarly as all the aforementioned works. The energy capacity is simply given by the area below the assumed three/four-branch capacity curve. Moreover, in the same study (Sorrentino et al, 2017), the proposed energy approach is compared with reference non-linear time history analyses, for one-sided, two-sided and vertical spanning walls, and the results show a better correlation than the displacement-based approach. However, as the authors state, more systematic analyses is needed to be performed.

1.2.2 Numerical approaches

Due to the recent astonishing advance of computational capacities, there has been a significant development of computational methods and tools, available both for researchers and practitioners. This variety of methods and tools might resort to different theories, assumptions and field of applications, and as stated in (Lourenço, 2002), they result in: different levels of complexity (from simple graphical methods and hand calculations to complex mathematical formulations and large systems of non-linear equations), different availability for the practitioner (from readily available in any

consulting engineer office to scarcely available in a few research oriented institutions and large consulting offices), different time requirements (from few seconds of computer time to a few days of processing) and, of course, different costs. Moreover, since different tools might provide different results and the complexity to accuracy are not necessary analogous, the choice of a certain tool is not straightforward. In fact, it should be sought under the physical problem examined and within the aforementioned framework, bearing always in mind the alternative possibilities.

Consequently, in order to have a clear view of the possible numerical methods and tools used for the assessment of out-of-plane response of masonry structures, a brief overview of the three main approaches is presented here, following the outline of (Ferreira et al, 2015).

Finite Element method

The high complexity that characterizes masonry as a material (i.e. its composite nature and anisotropic behaviour) makes FE simulation a difficult task. Nevertheless, several strategies can be adopted, depending on the accuracy, simplicity and model scale desired. More specifically, according to (Lourenço, 2009), it is possible to use one of the following strategies, presented also in Figure 1.7: (a) Detailed micro-modelling, in which unit and mortar in the joints are represented by continuum elements, whereas the unit–mortar interface is represented by discontinuum elements; (b) Simplified micro-modelling or meso-modelling, in which expanded units are represented by continuum elements, whereas the behaviour of the mortar joints and unit–mortar interface is lumped in discontinuum elements; (c) Macro-modelling, in which units, mortar and unit–mortar interface are smeared out in a homogeneous continuum.

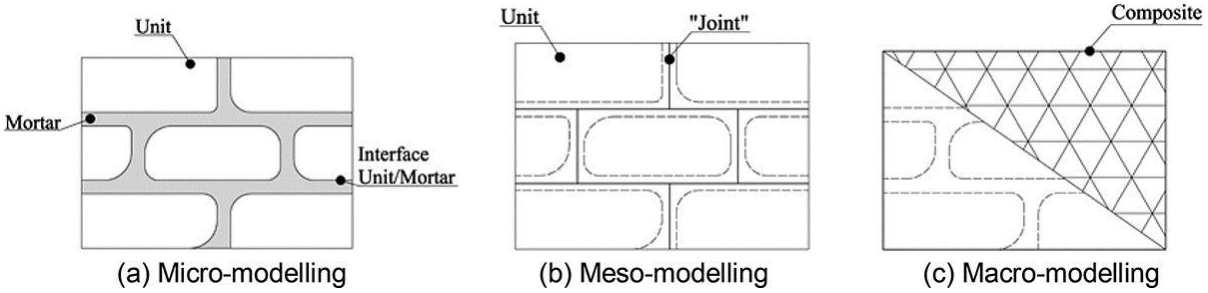

Figure 1.7 Modelling strategies of masonry structures (Lourenço, 2002)

Although the first attempts to model masonry with finite elements dates back to 1978 (Page, 1978), until the recent past very few works were devoted to the out-of-plane response. The most important are hereafter presented, being categorized according to the modelling strategies just mentioned.

Micro-modelling approach

As failure of masonry structures is usually expected to appear at the weak joints rather than the units, special care and importance should be given to the interfaces elements, when using a micro-modelling technique (Theodossopoulos & Sinha, 2013). One of the first works devoted to interfaces was (Lourenço & Rots, 1997) and was based on softening plasticity in tension, shear and compression.

In the work of (Cecchi et al, 2007), a micro-modelling technique was employed, combined with a kinematic limit analysis approach; in order derive and present the macroscopic failure surfaces of masonry loaded out-of-plane. In this work, infinitely resistant 3D blocks connected by interfaces with a Mohr-Coulomb failure criterion are considered and an associate flow rule for joints is adopted.

Furthermore, in (Zuccarello et al, 2009) a comparison of a heterogeneous (Figure 1.8) and a homogeneous model was done for out-of-plane loaded panels. As the authors conclude, a heterogeneous approach is more reliable in terms of collapse load evaluation, giving also detailed information of out-of-plane bricks sliding.

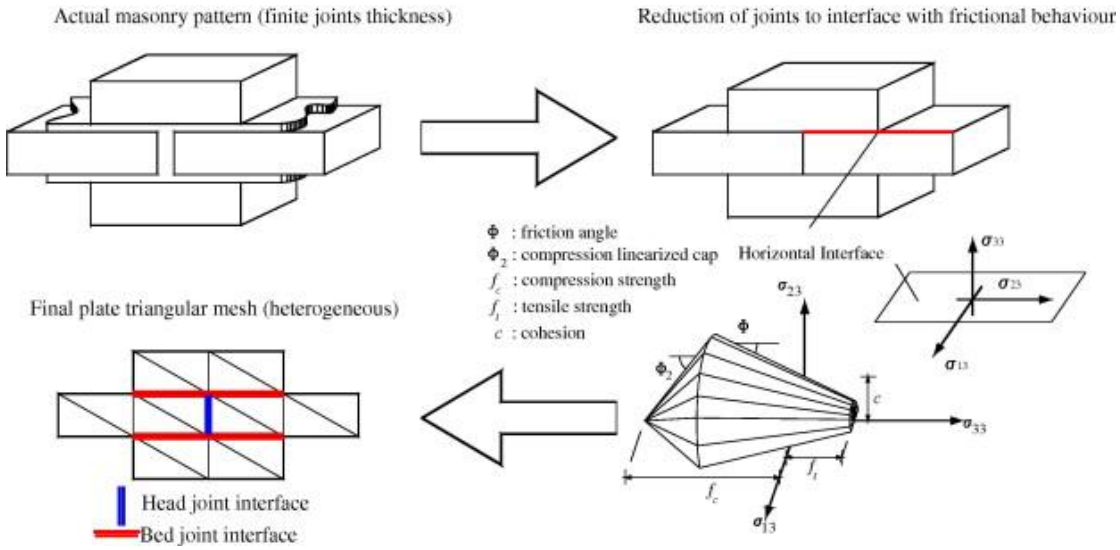

Figure 1.8 Numerical heterogeneous model proposed in (Zuccarello et al, 2009)

Simplified micro-modelling (meso-modelling) approach

Although meso-modelling presents an interesting intermediate alternative to micro- and macro-modelling, it has been mainly applied for in-plane cases. As has been underlined by (Macorini & Izzuddin, 2011), such models present several difficulties when subjected to complex loading conditions, such as the out-of-plane response; however, in the same work, the problem is tackled by defining new interface elements. More specifically, non-linear 2D surfaces with 3D brick elements are

employed to simulate the initial and damage-induced anisotropy, while multi-surface softening plasticity models are used to take into account the different failure modes (Figure 1.9).

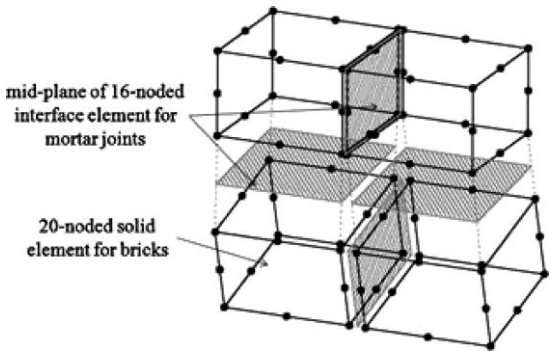

Figure 1.9 Three-dimensional (3D) mesoscale modeling for brick-masonry solid elements and two-dimensional (2D) non-linear interfaces (Macorini & Izzuddin, 2011)

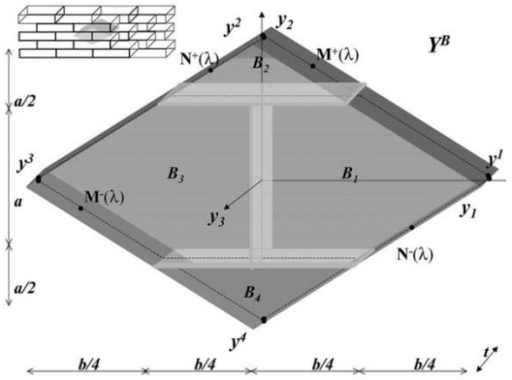

Figure 1.10 Characteristic 3D elementary pattern in the masonry whit discontinuity surface (Cecchi & Sab, 2002)

Macro-modelling approach

According to the macro-modelling approach, all the different phases of masonry are combined in an attempt to reproduce its properties and anisotropic behaviour adequately in a continuum model.

Following a series of previous works, Cecchi & Sab (2002) proposed a 3D model in order to define the bending stiffness of the structure, while the periodic nature of masonry was obtained by repetition of a 3D elementary representative module (Figure 1.10). On the contrary, in the work of Milani et al (2006), a simplified homogenization technique is used; employing the models proposed in (Lourenço, 2000) and following a lower and upper bound analysis approach.

In 2011, Milani & Venturini (2011) presented a 3D homogenized FE limit analysis software, in which the homogenized strength of three-leaf walls are obtained with a simplified kinematic procedure and are later implemented at a structural level. Moreover, in the work of Casolo & Milani (2013) different approaches are proposed for the modelling of three-leaf masonry, who's importance is also highlighted.

Second order effects, of slender walls subjected to out-of-plane, are examined in (Milani et al, 2013), where a FE model able to take into account both geometrical and material non-linearity is used.

Discrete Element method

Several discrete element formulations have been developed the past years, used both for the qualitative identification of possible deformation and failure modes, and in the interpretation of experimental data or damage observation (Lemos, 2007).

The first cited work that employed this method for the seismic analysis of structures was (Kawai, 1978). In this work, small rigid bodies were used, connected with springs. As a first attempt, the model appeared to be very effective in non-linear dynamic analysis. Furthermore, in (Lemos, 1998), a 3D rigid block model was employed in order to study the out-of-plane failure modes of masonry arches, while the effect of joint stiffness was also examined.

In the two works of (Sincraian et al, 1998; Drei et al, 2001) 2D discrete element models have been used in order to study the out-of-plane failure of aqueducts (Figure 1.11), and as it is stated in the last one, the use of block elements similar to the real stone bocks seems a realistic modelling of the structure. Moreover, in the same work it was underlined that according to this approach, the resistance of the model depends on the regular texture of the blocks and the uniformity of the structure, while small weak elements act as failure triggering devices.

In (Casolo, 1999), a simplified model, based on the concepts of (Kawai, 1978), was presented for investigating the out-of-plane behaviour of masonry walls. Plane rigid elements are used, in which only the out-of-plane displacements are considered, while they are connected by hinges that can be regarded as spherical joints, calibrated to approximate the brittle failure of masonry. This flexural-torsional model appears to provide with good accuracy the most likely local mechanism and the level of loading causing severe damage. As a further development of this work, the same author (Casolo, 2000) presented a new model able to perform cyclic dynamic analysis, by including the material hysteretic behaviour in the connection joints. As a conclusion, the author notes the suitability of the proposed model for the out-of-plane assessment of masonry structures, indicating the reduced computational resources needed and its robust accuracy.

The work of (Roberti & Spina, 2001) used the discrete element method in order to investigate the out-of-plane behaviour of irregular masonry. Specifically, 2D polygonal blocks are used, in order to reproduce the real irregular characteristics of the dry stone masonry. As it is finally stated by the authors, the DEM analysis seems to be an efficient tool for the stability analysis of masonry structures, focusing more on the block stability and equilibrium, rather than on accurate stress determination inside the blocks, which could occasionally be a critical aspect if blocks start to crack

One year later, (Oliveira et al, 2002) employed a 3D model with a small number of large blocks, in order to interpret the observed damage caused in a lighthouse by earthquakes. This is an example of the type of model wherein the numerical blocks are not intended to represent the real masonry units,

but correspond simply to a partition of the structure into large components, sufficient to define the range of possible collapse mechanisms (Lemos, 2007).

Following the same research line, (Alexandris et al, 2004) studied the collapse mechanisms of traditional masonry houses with 2D and 3D models. Since the out-of-plane mechanisms appear to be the dominant ones, the 2D models are considered incapable for such analysis. Moreover, the 3D models are able to capture the collapse mechanism quite well (Figure 1.12), however, the base excitations needed to do so are much higher. This is attributed to the fact that the stones are modelled perfectly cut, while in reality, corners break during the rocking response and therefore the overall strength is reduced. Consequently, the authors propose the use of cut or rounded corners.

A further application of discrete element models on the study of out-of-plane behaviour of masonry has been presented in (De Felice, 2005). Following the same research line, the study investigates the case of multiple leaf masonry and the influence of transversal bond. As expected, the results show that the transversal section level is crucial to provide a monolithic behaviour avoiding disaggregation.

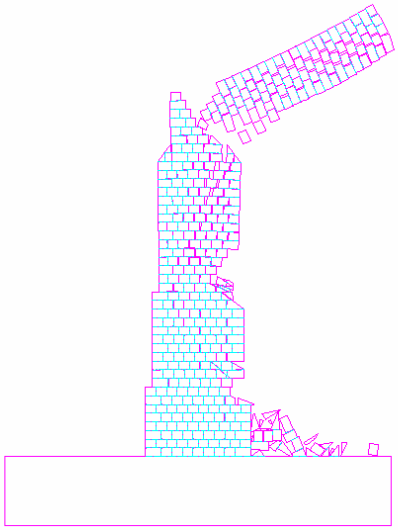

Figure 1.11 Out-of-plane failure of an aqueduct (Drei et al, 2001)

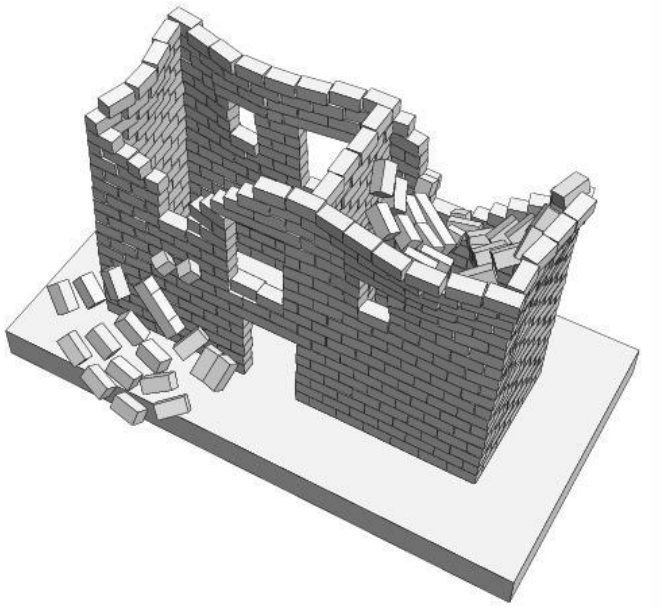

Figure 1.12 Collapse mechanism in a two-story house (Alexandris et al, 2004)

Multi-body Dynamics

Multibody dynamics is an analysis tool widely used in other engineering fields, and has been recently also proposed by (Costa, 2012) for the simulation of the out-of-plane failure of masonry buildings. In this work, masonry portions, considered representative of the out-of-plane local mechanisms activated

by seismic loads, are modelled as kinematic chains (normally assumed as infinitely rigid bodies) whose non-linear behaviour is concentrated at the contact regions (Figure 1.13). More specifically, the non-linearity is represented by a sliding friction law (of Coulomb type with cohesion), as well as by unilateral contacts where impacts between bodies lead to energy dissipation. In addition, the contact regions are assumed to have infinite compressive and null tensile strengths.

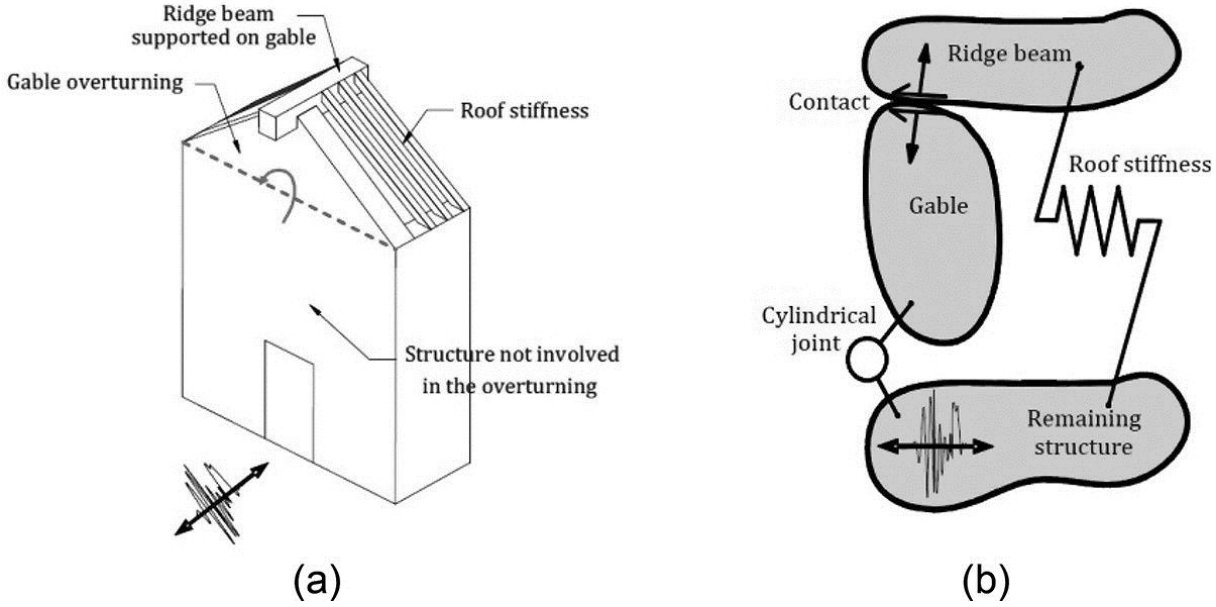

Figure 1.13 Multi-body dynamics-based approach: (a) schematic representation of a local mechanism; (b) equivalent multi-body system (Costa, 2012)

The main advantages of the method are its time efficiency and input parameters required, since only the geometry, the mass, the friction coefficient and the energy restitution coefficient are needed. On the other hand, two main shortcomings of the method, as have been underlined by the author, are namely the influence and uncertainties introduced by the energy ratio coefficient and the need to predefine the local mechanisms in order to create the multibody model.

1.3 Aim of the thesis

The out-of-plane response consists the most crucial and at the same time very complex behavior of unreinforced masonry structures. Despite its importance and due to the related difficulties, there is still lack of a robust and straightforward assessment technique. More specifically, although the tools available may significantly contribute to the estimate of seismic safety of existing masonry structures, they appear themselves not yet sufficient for a refined prediction of the failure mechanism and a reliable estimate of the seismic displacement demand (De Felice et al, 2017).

Bearing in mind the above, the objective of this thesis is to explore the possibilities of a novel finite element technique for the assessment of the out-of-plane response of masonry structures. More specifically, a simplified macro-modelling approach is used, employing a mixed strain/displacement finite element formulation. The specific finite element formulation has already been tested in small scale numerical tests, and has proved to be a remedy for the common shortcomings of standard irreducible elements in strain localization problems: the spurious mesh dependency and lack of convergence of the computed solution. A first application of this enhanced accuracy model in real scale engineering is attempted in this study.

A full scale seismic experimental campaign of two masonry structures is chosen as case study (Candeias et al, 2017), while static non-linear analyses are performed. The problem is examined under the framework of crack propagation and strain localization, having as main task to reproduce the collapse mechanism of the structures.

As already mentioned, out-of-plane failure of masonry structures is usually controlled by their stability rather than their strength, and therefore an assessment of the complete response and failure is not able only through a push-over analysis, since dynamic behavior is not considered and inertial dynamic effects and cyclic damage accumulation are neglected. Nevertheless, the highly non-linear problem of the collapse mechanism formation presents by it self still an open topic. Furthermore, as it is underlined in (Mendes et al, 2017), the correct collapse mechanism identification is crucial and affects significantly the final results of any assessment attempt. This is also clear by the literature review of assessment techniques presented above, since several approaches premise the knowledge of the collapse mechanism (see force-based approach, displacement-based approach, energy-based approach, multibody dynamics), which is usually assumed by intuition. Consequently, a numerical and straightforward approach seems of great importance. Moreover, this attempt could also be seen as a first step, whose next could be the dynamic analysis using the mixed formulation, exploring higher possibilities of the finite element method.

2. MIXED FINITE ELEMENTS

2.1 Motivation for a novel technique

Despite the great advance of numerical methods and techniques in the last decades, strain localization and crack propagation of quasi-brittle materials, such as masonry, is still an open issue. Within the framework of the finite element method, the solution obtained with the standard finite elements might appear to be mesh-dependent, thus resulting in an incorrect fracture direction. This shortcoming is not inherent in the continuum mathematical idealization of the physical problem, but arises at the discretization phase of the procedure, since the discrete model is capable of representing only an approximated numerical projection of the problem over the computational domain (Cervera et al, 2010b), while flawless solutions can be obtained if the mesh is perfectly aligned with the expected crack. However, in general, the correct crack direction is the unknown rather than given information of the problem, and therefore an objective procedure towards the solution is needed.

This drawback has caught the attention of many researchers in the last decades; and numerous attempts have been made in order to tackle it, following mainly two different approaches: a continuous and a discontinuous approach. Within the continuous approach, the failure process is modelled by the degradation of the material at the constitutive level; while within the discontinuous approach, an explicit crack representation is accounted for the computed geometry and handled as geometrical discontinuity. A detailed review of these proposals is considered far beyond the scope of this thesis, but the reader is referred to (de Borst, 2002; Mosler & Meschke, 2004; Rabczuk, 2013) for a general overview.

Within the continuous approach, the mixed finite elements have been recently employed and developed for solid mechanics, as an alternative remedy to the aforementioned problem of mesh-bias dependency (Cervera et al, 2010a; Cervera et al, 2010b; Cervera et al, 2011; Cervera et al, 2015; Benedetti, 2017). Mainly used in fluid mechanics, the main characteristic of the mixed formulation is the simultaneous approximation of multiple fields of interest. Consequently, and particularly for the strain localization problem, the mixed elements are indented to interpolate the strains, in addition to the displacements. In this way, an enhanced accuracy for the strains (and in turn the stresses) is achieved, which is crucial for quasi-singular points that are leading the fracture progress. In other terms, in the mixed formulation a higher order of local convergence is guaranteed for the strains; and therefore the strains and stresses are more accurately computed. Therefore, theoretically speaking, an objective procedure towards the solution can be claimed, since the approximated solution is refined upon discretization refinement without any mesh bias dependency.

Furthermore, the performance of the mixed strain/displacement formulation has been tested under several experimental problems both in 2D and 3D, such as Mode I, Mode II, Mode III and mixed Mode

fracture (Cervera et al, 2010b; Cervera et al, 2011; Cervera et al, 2015; Cervera et al, 2017; Benedetti, 2017). As a result, the mixed finite elements show, in practice, to be capable of overcoming many of the challenges posed by strain localization in solids, providing reliable and accurate solutions, without the need of auxiliary crack tracking techniques.

According to the studies devoted to this topic and mentioned above, the following strong points of the mixed formulation can be summarized:

- it can be used with any 2D or 3D finite element of any order
- it can be used with any constitutive law (i.e. plasticity or damage), since it follows the classical local constitutive mechanics framework
- it can model structural size effect and is virtually mesh independent
- it ensures local convergence of strains and stresses
- it presents enhanced strain accuracy and is observed to be superior in predicting peak loads, strain localization patterns and failure mechanisms
- it can model Mode I (extension), Mode II (shear) and Mode III (tearing) and mixed mode fracture
- it can be extended to include inertial forces in dynamics

2.2 Formulation of the mixed finite elements

In this section, the matrix formulation of the mixed strain/displacement finite elements is presented, following the outline of (Cervera et al, 2017). The matrix and vector notation follows the Voigt's convention for symmetric tensors.

2.2.1 Variational form

In a 3D problem, the displacements, the strains, the stresses and the body forces can be defined as vectors: $\boldsymbol{u} = (u, v, w)^{\boldsymbol{T}}$, $\boldsymbol{\varepsilon} = \left(\varepsilon_x, \varepsilon_y, \varepsilon_z, \gamma_{xy}, \gamma_{yz}, \gamma_{xz}\right)^T$, $\boldsymbol{\sigma} = \left(\sigma_x, \sigma_y, \sigma_z, \tau_{xy}, \tau_{yz}, \tau_{xz}\right)^T$, $\boldsymbol{f} = \left(f_x, f_y, f_z\right)^T$. Moreover, the displacements and strains are locally related through the compatibility equations (Zienkiewicz et al, 2005):

$$\boldsymbol{\varepsilon} = \boldsymbol{\mathcal{S}}\boldsymbol{u} \tag{1}$$

where $\boldsymbol{\mathcal{S}}$ is the differential symmetric gradient operator.

The stresses and body forces are related through the Cauchy's equilibrium equation:

$$\boldsymbol{\mathcal{S}}^T\boldsymbol{\sigma} + \boldsymbol{f} = \boldsymbol{0} \tag{2}$$

while the stresses and the strains through the constitutive equation:

$$\boldsymbol{\sigma} = \boldsymbol{D}_s\boldsymbol{\varepsilon} \tag{3}$$

where $\boldsymbol{D}_s$ is the secant constitutive matrix.

It is underlined here, that in the mixed strain/displacement formulation presented herein, the strains are also considered as unknowns in addition to the displacements, and therefore are not substituted further on.

Therefore, the strong form can be obtained by pre-multiplying equation (1) by the secant constitutive matrix $\boldsymbol{D}_s$ and introducing equation (3) into (2):

$$-\boldsymbol{D}_s\boldsymbol{\varepsilon} + \boldsymbol{D}_s\boldsymbol{\mathcal{S}}\boldsymbol{u} = \boldsymbol{0} \tag{4}$$

$$\boldsymbol{\mathcal{S}}^T(\boldsymbol{D}_s\boldsymbol{\varepsilon}) + \boldsymbol{f} = \boldsymbol{0} \tag{5}$$

Equation (4) and (5), together with boundary conditions of the problem compose the strong form of the mixed formulation. The boundary conditions are acting on the boundary Γ of the body, either as prescribed displacements Γ_u either as prescribed tractions Γ_t.

Furthermore, the variational form can also be obtained: firstly, by pre-multiplying equation (4) with an arbitrary virtual strain vector $\delta\boldsymbol{\varepsilon}$ and integrating over the spatial domain Ω, and secondly, pre-multiplying equation (5) with an arbitrary virtual displacement $\delta\mathbf{u}$ and integrating over the spatial domain Ω. Then, the Divergence Theorem is used in the later equation, while the boundary conditions on Γ_u are assumed $\mathbf{u=0}$. Thus, the variational form of the problem is finally obtained:

$$-\int_{\boldsymbol{\Omega}} \delta\boldsymbol{\varepsilon}^T\boldsymbol{D}_s\boldsymbol{\varepsilon}d\Omega + \int_{\Omega} \delta\boldsymbol{\varepsilon}^T\boldsymbol{D}_s\boldsymbol{\mathcal{S}}\boldsymbol{u}d\Omega = 0 \quad \forall\delta\boldsymbol{\varepsilon} \tag{6}$$

$$\int_{\Omega} (\boldsymbol{\mathcal{S}}\delta\boldsymbol{u})^T(\boldsymbol{D}_s\boldsymbol{\varepsilon})d\Omega = \int_{\Omega} \delta\boldsymbol{u}^T\boldsymbol{f}d\Omega + \int_{\Gamma_t} \delta\boldsymbol{u}^T\bar{\boldsymbol{t}}d\Gamma \quad \forall\delta\boldsymbol{u} \tag{7}$$

Summarizing, the problem of the mixed formulation is to find the unknowns $\boldsymbol{u}$ and $\boldsymbol{\varepsilon}$ of the aforementioned equations, which verify the boundary conditions on Γ_u and Γ_t.

2.2.2 Finite element approximation and stabilization

Moving to the discretized domain ($\Omega=\cup\Omega_e$) of the finite element approximation, the displacements $\mathbf{u}$ and the strains $\boldsymbol{\varepsilon}$ are approximated by:

$$\boldsymbol{u} \cong \hat{\boldsymbol{u}} = \boldsymbol{N}_u\boldsymbol{U} \tag{8}$$

$$\boldsymbol{\varepsilon} \cong \hat{\boldsymbol{\varepsilon}} = \boldsymbol{N}_\varepsilon\boldsymbol{E} \tag{9}$$

where $\mathbf{U}$ and $\mathbf{E}$ are the displacements and strains, respectively, at the nodes of the finite element mesh, while $\mathbf{N}_u$ and $\mathbf{N}_\varepsilon$ are the interpolation functions adopted for finite elements.

Furthermore, if equal interpolations are adopted for the strains and the displacements in equations (8) and (9), then the solvability and the stability of the problem is not verified since they don't satisfy the Inf-Sup condition (Brezzi, 1974)). Therefore, the stabilization Orthogonal Subscales Method is used in order to overcome this problem, and ensure the necessary stability.

More specifically, this is done by substituting the approximated strains of equation (9), with the following form:

$$\boldsymbol{\varepsilon} \cong \hat{\boldsymbol{\varepsilon}} = \boldsymbol{N}_{\varepsilon}\boldsymbol{E} + \tau_{\varepsilon}(\boldsymbol{B}_{u}\boldsymbol{U} - \boldsymbol{N}_{\boldsymbol{\varepsilon}}\boldsymbol{E}) = (1-\tau_{\varepsilon})\boldsymbol{N}_{\varepsilon}\boldsymbol{E} + \tau_{\varepsilon}\boldsymbol{B}_{u}\boldsymbol{U} \tag{10}$$

where $\boldsymbol{B}_u$ is defined as $\boldsymbol{B}_u = \boldsymbol{\mathcal{S}}\boldsymbol{N}_u$, and τ_ε is a stabilization parameter that might range from 0 to 1. Particularly, for τ_ε=0 the stabilization effect is lost, while for τ_ε=1 the standard irreducible formulation is recovered.

After substituting equation (8) and (10) to the variational form of the problem, the system of equations written in matrix form is:

$$\begin{bmatrix} -\boldsymbol{M}_{\boldsymbol{\tau}} & \boldsymbol{G}_{\boldsymbol{\tau}} \\ \boldsymbol{G}_{\boldsymbol{\tau}}^{T} & \boldsymbol{K}_{\boldsymbol{\tau}} \end{bmatrix} \begin{bmatrix} \boldsymbol{E} \\ \boldsymbol{U} \end{bmatrix} = \begin{bmatrix} \boldsymbol{0} \\ \boldsymbol{F} \end{bmatrix} \tag{11}$$

such that:

$$\boldsymbol{M}_{\boldsymbol{\tau}} = (1-\tau_{\varepsilon}) \int_{\boldsymbol{\Omega}} \boldsymbol{N}_{\boldsymbol{\varepsilon}}^{\boldsymbol{T}} \boldsymbol{D}_{\boldsymbol{s}} \boldsymbol{N}_{\boldsymbol{\varepsilon}} d\boldsymbol{\Omega} \tag{12}$$

$$\boldsymbol{G}_{\boldsymbol{\tau}} = (1-\tau_{\varepsilon}) \int_{\boldsymbol{\Omega}} \boldsymbol{N}_{\boldsymbol{\varepsilon}}^{\boldsymbol{T}} \boldsymbol{D}_{\boldsymbol{s}} \boldsymbol{B}_{\boldsymbol{u}} d\boldsymbol{\Omega} \tag{13}$$

$$\boldsymbol{K}_{\boldsymbol{\tau}} = \tau_{\boldsymbol{\varepsilon}} \int_{\boldsymbol{\Omega}} \boldsymbol{B}_{\boldsymbol{u}}^{\boldsymbol{T}} \boldsymbol{D}_{\boldsymbol{s}} \boldsymbol{B}_{\boldsymbol{u}} d\boldsymbol{\Omega} \tag{14}$$

$$\boldsymbol{F} = \int_{\boldsymbol{\Omega}} \boldsymbol{N}_{\boldsymbol{u}}^{\boldsymbol{T}} \boldsymbol{f} d\boldsymbol{\Omega} + \int_{\boldsymbol{\Gamma}_{\boldsymbol{t}}} \boldsymbol{N}_{\boldsymbol{u}}^{\boldsymbol{T}} \bar{\boldsymbol{t}} d\boldsymbol{\Gamma} \tag{15}$$

where $[\boldsymbol{E}\ \boldsymbol{U}]^{\mathrm{T}}$ are the strains and displacements at the nodes of the mesh, being the unknowns of the problem to be computed.

3. EXPERIMENTAL AND NUMERICAL RESEARCH ON THE TOPIC

In 2014, an integrated workshop on “Methods and challenges on the out-of-plane assessment of existing masonry buildings” (Lourenço et al., 2017) was held in Guimarães in Portugal. The works that were carried out the next years have been published as a separate, special issue on the International Journal of Architectural Heritage, Volume 11, Issue 1, pages 1-160, 2017. This issue includes several articles, including a review article on the out-of-plane assessment techniques (Sorrentino et al., 2017), a conceptual discussion article on research needs and modelling issues (Abrams et al., 2017), an experimental campaign of two real scale mock-ups (Candeias et al. 2017), an article of blind test prediction of the experiments by several experts (Mendes et al., 2017), a series of post-diction analysis (Derakhshan et al., 2017; AlShawa et al., 2017; Gams et al., 2017; Chácara et al., 2017; Lemos & Campos-Costa, 2017; Cannizzaro & Lourenço, 2017), and a final concluding article (de Felice et al., 2017).

These experimental tests are chosen as a reference setup/case-study for this thesis, and for this reason an extended description of its setup and results is presented herein.

3.1 Experimental Campaign

For the purpose of the aforementioned workshop, the experimental tests include two structures, namely a brick and a stone masonry, which are subjected to shaking-table seismic motion. The tests have been carried out in the National Laboratory of Civil Engineering, in Lisbon, Portugal, and the results are published in (Candeias et al. 2017).

3.1.1 Test Setup

Geometry and Construction process

Two structures are tested, namely a brick and a stone masonry. The mock-ups have three walls and a U-shape plan, which include the façade facing East with a central opening, and two transversal walls (return walls) with one (South) being blind and the other one (North) having a window. The detailed geometry of each mock-up is presented in Figure 3.1. As can been seen, there are two important differences between the two structures: on the one hand, the brick mock-up has a thin wall thickness of 0.235 m and therefore is more slender than the stone mock-up which has a 0.5 m wall thickness and, on the other hand, the stone mock-up has a door on the façade, while the brick mock-up has just a window.

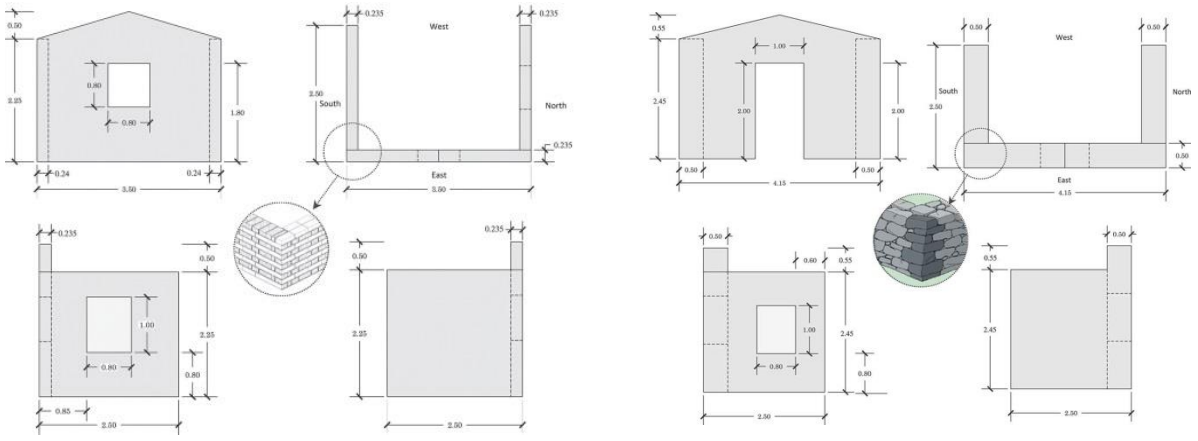

Figure 3.1 Geometry of (a) the Brick mock-up and (b) the Stone mock-up (Candeias et al, 2017)

Concerning the construction process and details, fired clay bricks together with industrial pre-batched hydraulic lime mortar are used to build the brick mock-up, while rough stones together with a lime-based mortar are used for the stone mock-up. Moreover, an English bond arrangement is employed for the brick mock-up building process; while the stone mock-up is built with a typical multiple leaves arrangement, where the two outer ones are with larger stones and the inner one with rubble masonry. Two timber lintels are placed above each openings of the brick mock-up, while two stone lintels are placed side by side for each opening of the stone mock-up. In addition, cement has been added to the mortar used in the first layer of the masonry in order to secure the bond between the masonry wall and the reinforced concrete slab of the shaking table, where the mock-ups are built on. Finally, it is important to underline the absence of any diaphragm of the mock-ups, and as a sequence the lack of any box behaviour. A general view of the two mock-ups is presented in Figure 3.2.

Figure 3.2 General view of the mock-ups (Candeias et al, 2017)

The material characterization for both tests is done by six wallets, for each case, of dimensions 1m x 1m and the corresponding thickness. Three of the wallets are tested in vertical compression and the rest three in diagonal compression aiming at obtaining the diagonal tensile (or shear) and compressive strength of masonry, respectively. The mean values of the tests are presented in Table 1.

Table 1: Results of material characterization

	Young's Modulus (GPa)	Specific mass (kg/m^3)	Tensile strength (MPa)	Compressive strength (MPa)
Brick	5.17	1890	0.102	2.48
Stone	2.08	2360	0.224	5.44

During the dynamic test, 6 LVDTs and 20 accelerometers were used as the instrumentation of the mock-ups.

Seismic action simulation

Both mock-ups are subjected to unidirectional seismic loading up to collapse, in the direction perpendicular to the façade. As reference seismic input motion, the N64E strong ground motion component of the February 21, 2011 Christchurch (New Zealand) earthquake is used. The signal is firstly properly filtered in the low frequencies ranges, so that no trouble would be created to the shake-table actuators and its final form is presented Figure 3.3.

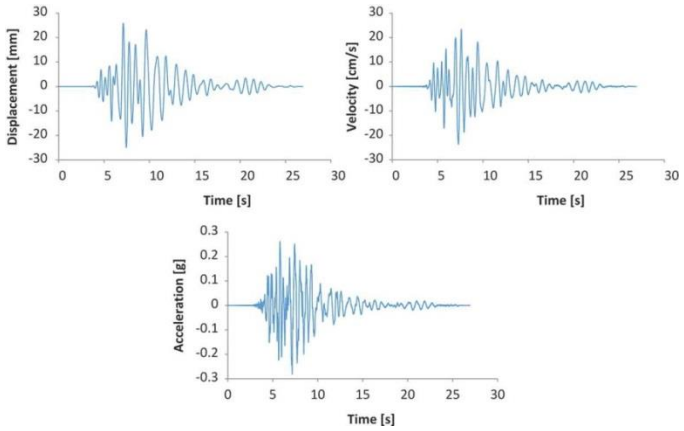

Figure 3.3 Reference seismic input motions (displacement, velocity and acceleration) (Candeias et al, 2017)

The mock-ups are tested up to collapse to the sequence of the reference signal. The sequence of the tests is presented in Table 2, for both of the structures.

Table 2 Test sequence

Brick Masonry		Stone Masonry	
Sequence	PGA [g]	Sequence	PGA [g]
TEST01	0.179	TEST00	0.382
TEST02	0.292	TEST01	0.403
TEST03	0.358	TEST02	0.419
TEST04	0.405	TEST03	0.657
TEST05	0.517	TEST04	1.024
TEST06	0.782	TEST05	1.051
TEST07	0.843		
TEST08	1.273		

3.1.2 Results of the experiment

Brick House

The brick house mock-up behaved linear up to the TEST05, where the first cracks started to appear near the windows. During TEST06, the existed cracks extended and new appeared. In TEST07 the cracks developed even more, mainly horizontally towards the corners following the brick layout and, forming practically a mechanism. The formed mechanism was consisted by 4 separated parts: 1) the gable of the façade, 2) the northeast corner of the mock-up limited by the windows and the horizontal crack at the window's lower height, 3) the northwest pier and 4) the spandrel of the north wall. The evolution of the damage and the formation of the collapse mechanism are illustrated in Figure 3.4.

Finally, the house was extensively damaged at TEST08 (1.27g), when the gable of the façade, the spandrel of the north wall and the northwest pier collapsed. More specifically, the collapse evolution during TEST08 can be described by the following steps: 1) the northern part of the gable fell towards the east, 2) simultaneously, the northeast pier rocked without falling, while the northwest pier was also rocking, 3) consequently, the lintel of the north window fell vertically due to lack of support, 4) afterwards the northwest pier rotated and fell towards west 5) finally the southern part of the gable façade fell also towards the east direction.

Figure 3.4 Brick mock-up: Damage evolution and collapse mechanism (Candeias et al, 2017)

Concerning the strong motion response of the brick mock-up, the top of the gable wall exhibited displacement of 5.4 mm one test before the collapse and at the last test 136.5 mm due to the out-of-plane collapse of that part. The maximum displacements recorded during each test are shown in Figure 3.5 (b).

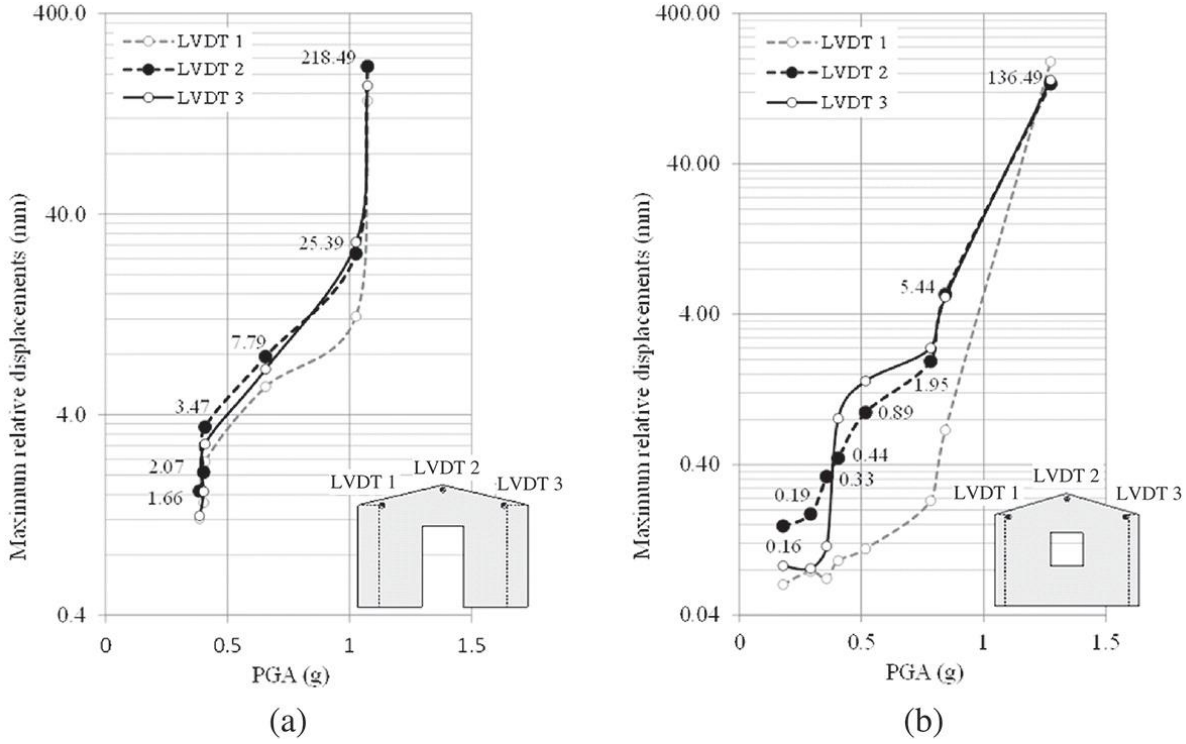

Figure 3.5 Maximum relative displacements recorded: (a) Stone structure and (b) Brick structure (Mendes et al, 2017)

Trying to summarize the response of the Brick mock-up, the following important points are underlined:

- The dynamic response of the mock-up was characterized by significant torsional effects, due to asymmetric configuration of the openings,
- The damage started developing at TEST05 and was already extended at TEST07,
- Two main mechanisms were formed: 1) the main mechanism that involved the out-of-plane failure of the gable and the north part of the façade, together with the in-plane failure of the weak return wall (both spandrel and piers), 2) the secondary mechanism of the partial collapse of the northern part of the gable, which was in fact activated due to the formation of the first, although it collapsed earlier in the end.
- Large displacements of 136.5 mm were reached, but mainly after the mechanisms were formed.

Stone House

The Stone house mock-up showed an almost linear behaviour up to TEST03. However, it should be mentioned that initial damage state was observed before the seismic testing plan started. This initial damage included a horizontal crack on the south wall, above the first layer of stones that continues into the east wall up to the door, with some additional minor cracks at the other side of the door. Also it was observed a small horizontal crack at the northwest corner. A clear cause of the aforementioned cracks has not been provided by the authors. In any case, the stone house appeared to extend its damage state during TEST03, when some cracks propagated from the corners of the door and the window and a horizontal one near the base of the northeast corner. During TEST04 significant diagonal cracks extended at the east façade, propagating from the top south corner down to the mid height of the door. Moreover, the cracks at the north wall extended and new appeared at the top northwest corner and in the window lower west corner. Finally, the last TEST05 was marked by the extensive crack pattern that developed around the stones in the east façade, mainly at the north corner, the damage and rocking response of the northwest pier with the detachment of two stones, and finally some damage development in the south wall. Once more, the evolution of the damage and the formation of the collapse mechanism are illustrated in Figure 3.6.

The damage/collapse sequence of the last test can be described as: 1) the two stones on the top northwest corner fell off the structure, due to the impulses that the large lintel stone of the window imposed to them, 2) the respective pier rocked in-plane around diagonal cracks that formed from the lower corner of the window, 3) the northeast corner rocked in the east-west direction, initially as a single element, around a crack that started from the lower corner of the window and extended at the lower part of the corner, and later on split into two parts by diagonal cracks one of them stabilized by the weight of the large lintel stone of the window and the other slightly rotated around the vertical axis, 4) the east façade rocked out-of-plane around the diagonal cracks of its south part and the (approximately) horizontal ones at the mid height of its north part, 5) the central part of the gable top rocked also out-of-plane, but almost independently due to the vertical cracks formed on both sides of the lintel stone. 6) Finally, the south wall, been detached due to the horizontal crack developed initially and some cracks at its interlocking with the facade, behaved like a solid block.

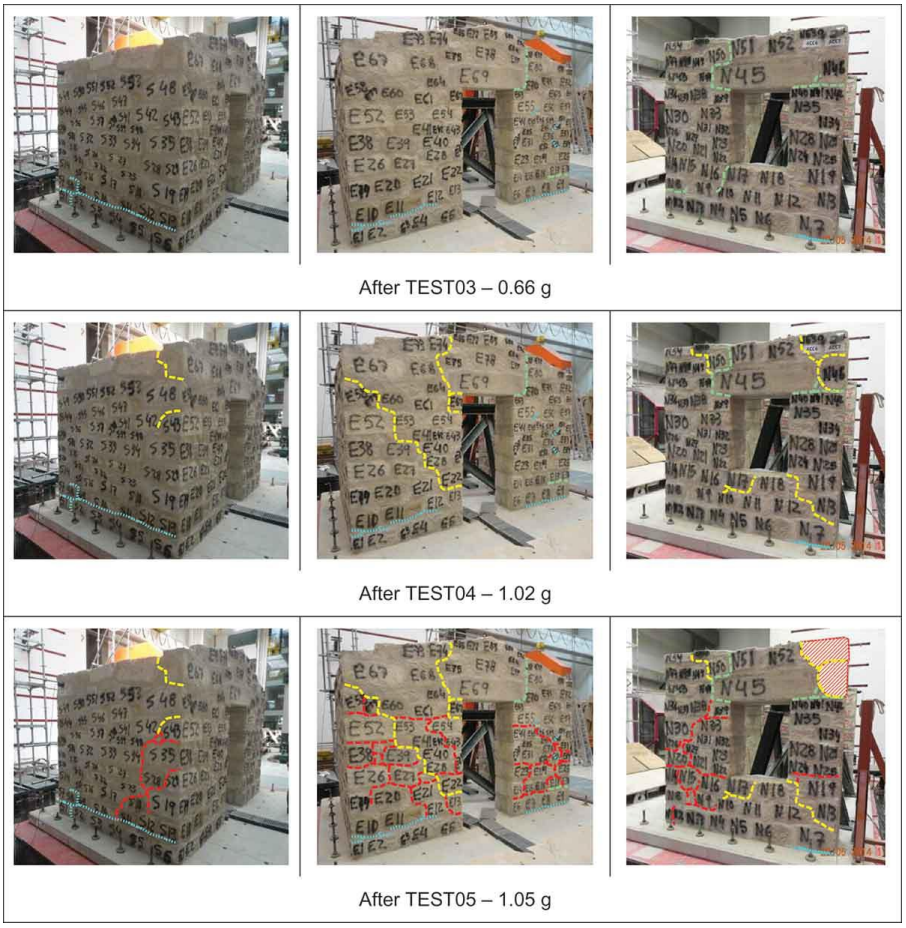

Figure 3.6 Stone mock-up: Damage evolution and collapse mechanism (Candeias et al, 2017)

Moreover, the stone house developed displacement at the gable top of 25.4 mm in TEST04, while in the last TEST05 a value of 218.5 mm was measured.

Summing up the significant points of the response of the stone house:

- As the brick house, the dynamic response of the stone mock-up was decided by significant torsional effects, due to asymmetric configuration of the openings,
- the highly unit-to-structure size ratio led to the domination of the crack pattern by the actual arrangement of the stones and joints,
- Initial damage was observed on the mock-up, but the damage mainly extended during TEST03 to TEST05.
- The collapse mechanism formed involved a portion of the south part of the façade, the gable, the northeast corner, the spandrel of the window and the northwest pier.

- Only some large stones at the northwest corner fell down, while the low slenderness of the walls avoided the out-of-plane overturning of big portions.
- The big lintels of the openings significantly affected the local crack and collapse mechanism formation.
- A large displacement of 218.5 mm was reached, but mainly after the mechanism was formed, and the structure was experiencing rocking behaviour.

3.2 Assessment Campaign

Besides the aforementioned experimental campaign, the workshop “Methods and challenges on the out-of-plane assessment of existing masonry buildings” and the published articles include also an assessment campaign, composed by two different phases: a blind pre-diction and a post-diction assessment phase. During the pre-diction phase, 25 world experts on the field were asked to provide an assessment of the experiments, without knowing their results. On the other hand, six post-dictions were also done in a later time, when the results of the experiments were already provided to the groups. A quick description of their main points is here presented, so that a comparison with the assessment developed in this thesis will be possible later. However, the reader can refer to (Mendes et al., 2017; Derakhshan et al., 2017; AlShawa et al., 2017; Gams et al., 2017; Chácara et al., 2017; Lemos & Campos-Costa, 2017; Cannizzaro & Lourenço, 2017) for a more detailed description.

3.2.1 Blind Pre-dictions

Before any results of the experimental campaign were published, 25 world experts were asked to provide a blind pre-diction assessment for the two mock-ups tested (Mendes et al., 2017). The only information provided were the geometrical configuration, the mass, the results of the wallets tests (Young’s modulus of elasticity, tensile and compressive strength), the normalized accelerogram envelopes of the seismic action that was used in the shaking table and the corresponding response spectra.

Each expert was free to decide what modelling approach or type of analysis to use. Therefore, several modelling approaches were used, namely: - rigid blocks, according to the expected collapse mechanism, - finite element models, either using a macro-modelling either a simplified micro-modelling approach, - discrete element models, using rigid elements and interface elements with a Mohr-Coulomb law, - or even combined FEM and DEM, that could also simulate the deformability of the units.

Concerning the type of analysis, three different types were used: 1) limit analysis, based on the kinematic approach, 2) static non-linear analysis (pushover), and 3) non-linear dynamic analysis, at which artificial accelerograms, generated by the experts, were used.

From a methodological point of view, the collapse mechanisms were defined based either on FEM or DEM models, either by personal judgement. Furthermore, the collapse of the structures were mainly evaluated through a force-based or displacement-based approach.

Figure 3.7 presents examples of models prepared by the experts using different modelling approaches and different tools of structural analysis.

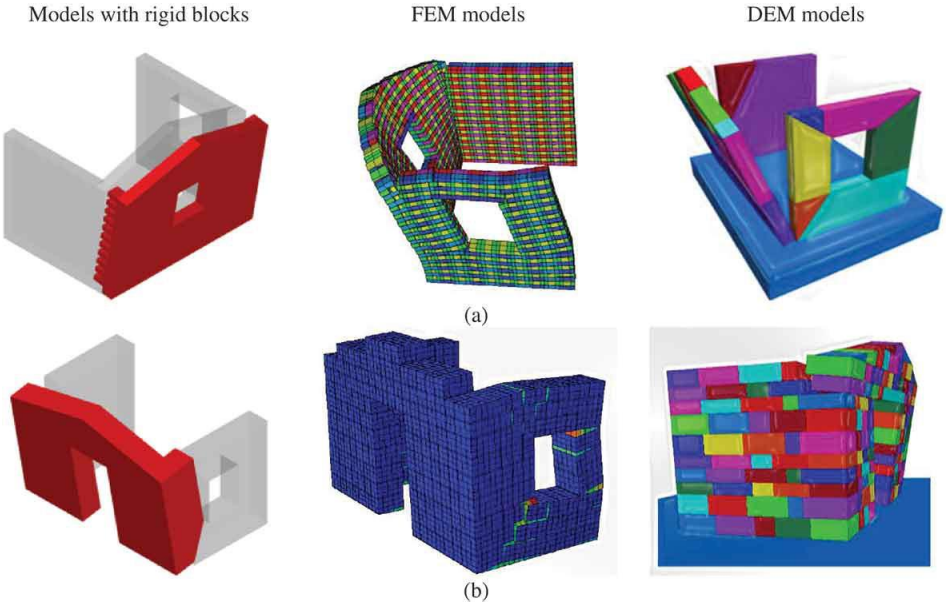

Figure 3.7 Examples of models developed by the experts (a) brick structure and (b) stone structure (Mendes et al, 2017)

For the stone house, 17 predictions were made, while 19 predictions were made for the brick house. Based on the capability of the predictions to identify the experimental collapse mechanism, according to (Candeias et al. 2017), it was observed that 6 (out of 17) good pre-dictions were achieved for the stone mock-up, while 9 (out of 19) were achieved for the brick house. Moreover, concerning the prediction of the capacity of the structures, the obtained values were significantly spread. More specifically, the estimated average value of PGA for the stone house (Figure 3.8 (a)) was 0.91g with a COV=63%, while the experimental PGA was 1.07g. Meanwhile, the estimated average value of PGA for the brick house (Figure 3.9 (a)) was 0.64g with a COV=39%, while the experimental PGA was 1.27g. It is clear that, a better capacity estimation for the stone house was achieved (15% lower average estimation), but with a wide range of values. On the other hand, a much more divergent estimation was achieved for the brick house (49% lower). Meanwhile, if only the fair predictions in terms of collapse mechanisms are considered, a better capacity estimation was achieved for the stone house (PGA=0.93g with COV=31%) (Figure 3.8 (b)), while the capacity estimation of the brick house is worst (PGA=0.48g with COV=50%) (Figure 3.9 (b)).

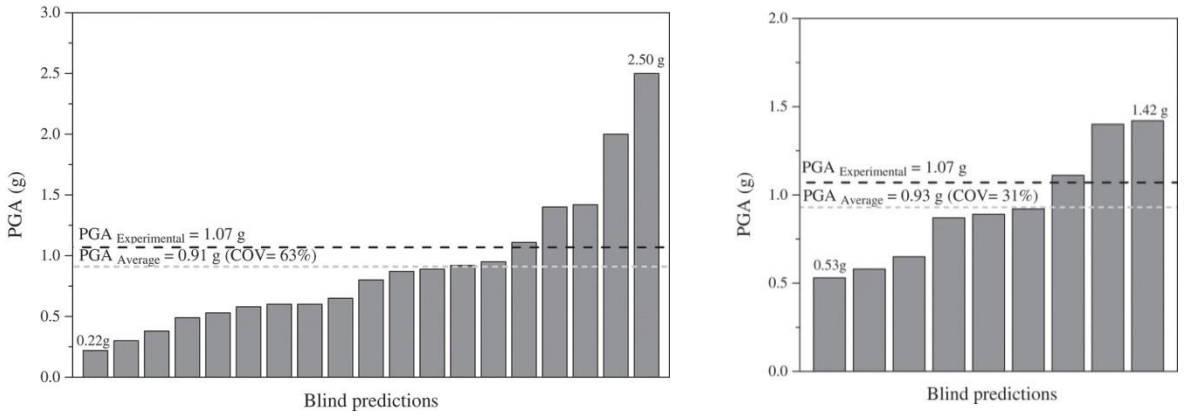

Figure 3.8 PGAs of the predictions for the stone structure: (a) for all blind predictions and (b) for the good blind predictions (Mendes et al, 2017)

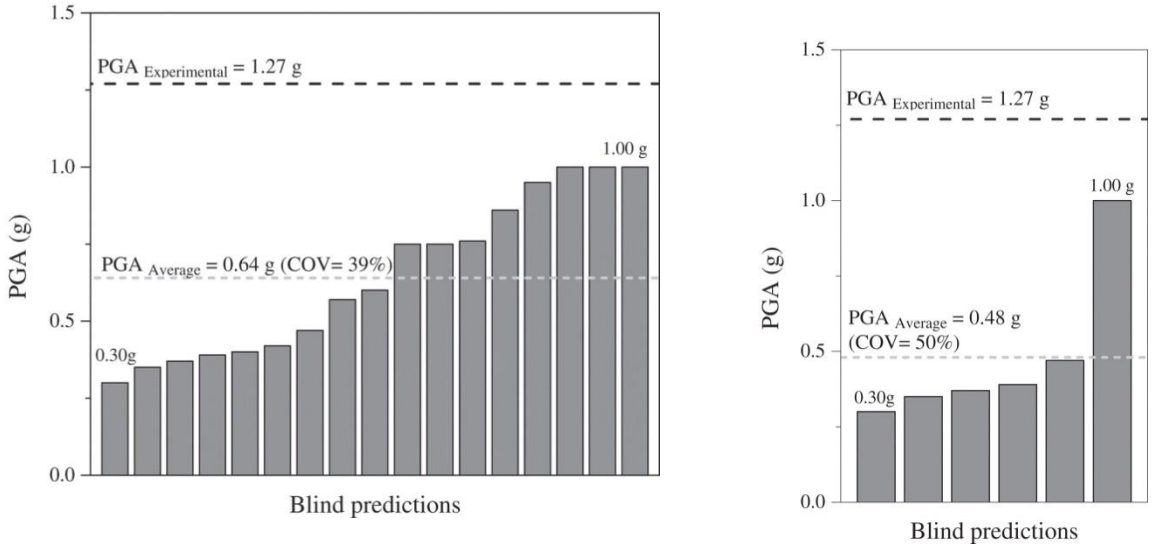

Figure 3.9 PGAs of the predictions for the brick structure: (a) for all blind predictions and (b) for the good blind predictions (Mendes et al, 2017)

In conclusion, the large spread of capacity estimations for the stone house was mainly attributed to predicting the correct collapse mechanism, while the correct prediction for the brick house couldn't provide any better capacity estimation. This was traced to the difficulties related to the high slenderness of walls and flexibility of the corners, and the simultaneously activation of a secondary mechanism. Therefore, the article suggested that FEM approaches (in contrast with DEM approaches)

seem to be less reliable in predicting the bending strength of facades and the strength of the walls connections.

Moreover, although better capacity estimation could not always be achieved by assuming the correct mechanism, it is generally accepted that correct mechanism identification was a fundamental step in the whole assessment procedure. At the same time, several collapse mechanisms assumed in the pre-dictions were estimated based on expert's judgement, which indicated that further research in needed within this topic.

3.2.2 Post-dictions

After the experimental results were given to the expert groups, six of the groups continued their assessment campaign, providing and publishing thus a more detailed comparison of their methods with the experimental outcomes (Derakhshan et al., 2017; AlShawa et al., 2017; Gams et al., 2017; Chácara et al., 2017; Lemos & Campos-Costa, 2017; Cannizzaro & Lourenço, 2017). A posteriori at that point, the groups were able to calibrate their models or even test them under known conditions and phases. More specifically, in one case (Derakhshan et al., 2017) the experimental collapse mechanism was assumed as known for the assessment, while in other cases the capability of the model to estimate both the collapse mechanism and the seismic capacity or response in time was investigated. In addition, since there were not strict time limits, some of the cases took the advantage to realize sensitivity analysis of the results to some variables, such as meshing, strength properties, analysis parameters and input characteristics.

As a general trend, the collapse mechanisms proposed by the post-dictions were all in good agreement with the experimental, although in some cases the mechanisms were difficult to be exactly identified by the model and the a posteriori knowledge of the real ones was necessary. In fact, all cases indicated the north wall as a weak part that led to torsional behaviour. However, the bending response/strength of the façade was not correctly represented in most cases. Moving to the displacement demand, the results weren't considered satisfactory. Specifically, the average value for the brick house was 159 mm (+17% than the experimental) and for the stone house 104 mm (-52% than the experimental). These values were significantly scattered, with the COV being 149% and 72%, respectively. It should however be underlined that the displacements (both in the experiments and the numerical assessments) hugely increased just before the collapse. Therefore, the displacement demand appeared to be very sensitive to even a slight wrong estimation of the displacement capacity.

A brief presentation of the different cases is introduced here, which focus, on one hand, on the methods and models used and on the other hand, on the results in qualitatively terms, rather than the exact values obtained.

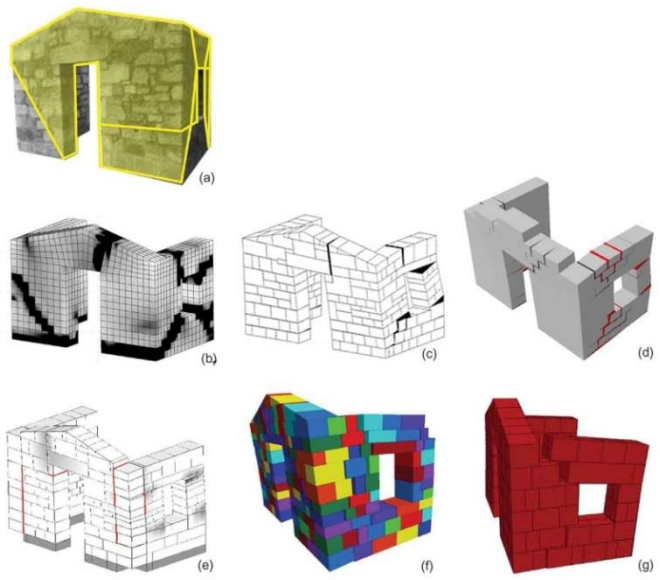

Figure 3.10 Failure mechanism of the Stone House experimental outcome (a) and simulations with macro-FEM (b), micro-FEM (c,d), discrete macro-elements (e), distinct elements (f), and combined finite-discrete elements (g) (de Felice et al, 2017)

Limit analysis with equivalent block systems

This study (Derakhshan et al., 2017) examined the problem with the analytical displacement-based approach. Firstly, the mechanisms assumed during the pre-diction were qualitatively evaluated, but afterwards the corresponding experimental mechanisms were examined, by neglecting the side walls for simplification reasons. The problem was addressed by analysing the assumed collapse mechanism as a SDOF rigid block, with a rigid foundation and a rocking motion. In addition, the seismic demand was evaluated by the corresponding response spectra.

The method showed to be a viable simplified procedure in estimating the peak displacement demands near collapse. However, several uncertainties characterized the method, such as: 1) firstly, the evaluation of the seismic demand by the response spectra depends on the period, which in turn relies on a simplified estimation of the elastic stiffness, 2) secondly, as the authors addressed, since the period of the rocking system depends on the amplitude of the oscillations, the obtained estimation could be reliable only when displacements larger than half of the capacity occur, 3) finally, the displacement demand was found to be very sensitive to viscous damping, which is still an open research issue. As a sequence, the method may significantly overestimate the seismic demand if rocking is not activated, or some parameters are not well addressed.

Finite Element Method

Two of the post-diction studies used the finite element method, but each one with a different strategy (Gams et al., 2017; Chácara et al., 2017).

Macro and Micro FEM based approaches

In the study (Chácara et al., 2017), the authors examined the problem by using different scale modelling (both macro and micro) and running several analysis (both pushover and time history), in order to capture both the corresponding collapse mechanism and the displacement demand. The numerical analyses were performed using the FEM commercial software Diana.

More specifically, both macro-modelling and micro-modelling approaches were employed, each one presenting well known advantages and shortcomings. For the macro-modelling, a homogenized, isotropic material was used with limited tensile and shear strength, while for the micro-modelling, elastic units were used connected with nonlinear interfaces with limited compressive and shear strength. Moreover, the total strain crack model, included in the software, was employed to represent the material's nonlinear behaviour. Finally, both pushover and non-linear dynamic analysis were implemented, using a mass proportional loading and the test ground motion records of the test, respectively.

Regarding the collapse mechanism estimation (Figure 3.10 (b&c), Figure 3.11 (b&c)), the results of both micro- and macro-modelling were able to correctly reproduce the weak response of the north side wall of both mock-ups, which resulted in torsional behaviour. Good agreement of the collapse mechanism was also attained for the façade of the stone house, although, neither of the micro- or macro- models could reproduce correctly the damage of the main façade for the brick house, as both models underestimated the damage due to vertical bending (horizontal cracking) and therefore represented wrongly damage development due to horizontal bending (vertical cracking). The same problem of underestimating the vertical bending appeared also in the stone model, but not in such a level that could influence the correct mechanism.

The base-shear, correlated to the self-weight W, provided by the push-over analysis were: 1) for the brick house i) pulling: 0.82 W for the macro-modelling and 1.75 W for the micro-modelling, ii) pushing: 1.15 W for the macro-modelling and 2 W for the micro-modelling, 2) for the stone house i) pulling: 1.2 W for the macro-modelling and 0.73 W for the micro-modelling, ii) pushing: 1.6 W for the macro-modelling and 1.18 W for the micro-modelling.

Concerning the displacement demand, the time-history analysis provided displacement estimations for both mock-ups, but the estimations were a level of order lower than the experimental ones, revealing the difficulties of simulating large displacements with continuum models that are almost completely cracked (Figure 3.12).

Two step FEM approach

In the second study that uses finite elements (Gams et al., 2017), a different strategy was adopted: a two-step approach was used, in which the collapse mechanism was identified in the first step, while the displacements were evaluated at the second, by using a different FEM configuration. In both cases the analysis was performed with the commercial software Abaqus.

More specifically, at the first step a micro-modelling approach was employed, in which elastic units were assumed connected together with non-linear 3D material that simulates the mortar. Moreover, a pushover analysis was performed, applying horizontal loads proportional to the mass. As already mentioned, this step of the procedure had as objective to simulate the cracking development and finally the formation of the collapse mechanism of the mock-ups. The obtained results (Figure 3.10 (d), Figure 3.11 (d)) were very similar with the ones obtained in (Chácara et al., 2017), being capable to represent correctly the damage concentration at the north side wall, but not adequately in the façade. Nevertheless, the damage concentration could only provide useful indications regarding the collapse mechanism.

The next step of the analysis had as objective to simulate the response of the structure just after the mechanism is formed, and until the loss of stability at collapse. Taking this into account, a simplified model of macro- 3D linear elastic elements was used, that corresponded to the collapse mechanism macro-elements. In order to check the capability of this modelling strategy, the experimental mechanism was assumed as known. Finally, the connection of these elements was modelled with frictional interfaces with zero cohesion, and non-linear dynamic analyses were performed using the accelerations of the shaking table. The response of the analysis was in quite good agreement for the brick house, where even the exact time of collapse could be predicted, by observing the displacements diverging. However, the response of the stone house could be adequately estimated only until a specific time of the test, in which during the experimental test the structure crumbled into more parts than the initial mechanism. This could be highlighted as a shortcoming of the analysis method used.

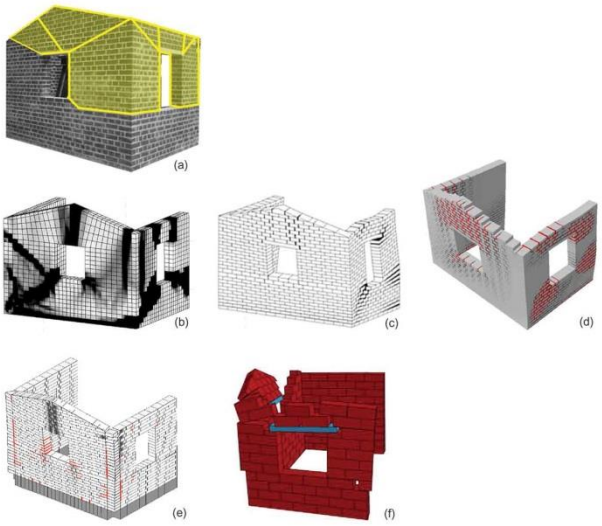

Figure 3.11 Failure mechanism of the Brick House experimental outcome (a) and simulations with macro-FEM (b), micro-FEM (c,d), discrete macro-elements (e), and combined finite-discrete elements (f) (de Felice et al, 2017)

Discrete element method

Two of the studies (Lemos & Campos-Costa, 2017; Cannizzaro & Lourenço, 2017) used the discrete element method, in which the structure is modelled as an assembly of blocks separated by contact interfaces. The two studies employed a different version of the method, differentiating mainly at the interfaces used.

Simplified macro-element approach

In (Cannizzaro & Lourenço, 2017) quadrilateral elements were used, connected by interfaces provided with discrete non-linear springs. These springs have been calibrated in order to approximate all the possible masonry failures (including the out-of-plane), and the main advantage of using them is their low computational cost. Concerning the two mock-ups analysed, two different models were created for each one: one with large elements and the other one with element size comparable to the real units (analogous to micro-modelling). In all cases, pushover analyses were performed with a mass proportional loading.

The collapse mechanism obtained by the analysis was again similar with the ones obtained with the finite element simulations (Figure 3.10 (e), Figure 3.11 (e)): good agreement with the experimental was achieved at the north wall and the torsional effects created, but the damage of the gable wall was overestimated. Concerning the maximum base shear capacity: on one hand 1) for the brick house i)

0.85 W was obtained for the model with large elements, while ii) 1.00 W was obtained for the model with small elements, on the other hand 2) for the stone house i) 1.3 W was obtained for the model with large elements, while ii) 1.4 W was obtained for the model with small elements.

Discrete element approach

In (Lemos & Campos-Costa, 2017), rigid quadrilateral elements were used, separated with Mohr-Coulomb interfaces that have limited tensile and shear strength and constant friction angle. Both pushover and non-linear dynamic analysis were performed. Moreover, several input parameters had to be checked and calibrated when needed during the whole procedure, since the model appeared to be very sensitive to their values.

The results of the analysis showed good agreement with the experimental values. More specifically, both the natural frequencies and the modal shapes were correctly captured, while the failure mode was also approximately reproduced (Figure 3.10 (f)). In addition, the displacement response was remarkably well simulated during all the different tests and intensities (Figure 3.12 (b)). Although, the method showed to have some drawbacks, such as: on one hand, in order to achieve such a good agreement of the results, an extensive and very specialized sensitivity analysis was necessary since the method require a lot of input variables which are in turn very sensitive, and on the other hand, the damage obtained appeared to be incorrectly distributed, and couldn't localize and accumulate.

Combined FEM-DEM

A combined finite-discrete element method was used in (AlShawa et al., 2017). The mock-ups were modelled using 3D units, separated by interfaces. The units were composed of deformable, linear, elastic finite elements, while the interface had limited tensile and shear strength; while after failure, separation and re-contact could occur, during which a compressive-frictional interaction could take place. Regarding the analyses, non-linear dynamic analysis was performed, according to the shaking table motion. In addition, the influence of several parameters was also investigated by sensitivity analysis, such as: the material properties and mechanical parameters, the mesh, the corner interlocking, the ground motion amplitude and the damage accumulation.

The model achieved a good representation of the collapse mechanism (Figure 3.10 (g), Figure 3.11 (f)), and a good estimation of the displacement demand at the collapse (Figure 3.12). Moreover, it was revealed that the seismic demand of such a methodology is highly sensitive to the tensile strength, which is in turn hardly estimated by the experimental campaign. As a result, since the identification of the collapse mechanism didn't seem to be affected by this uncertainty, the author proposed that a two-step strategy might be more robust in such problems.

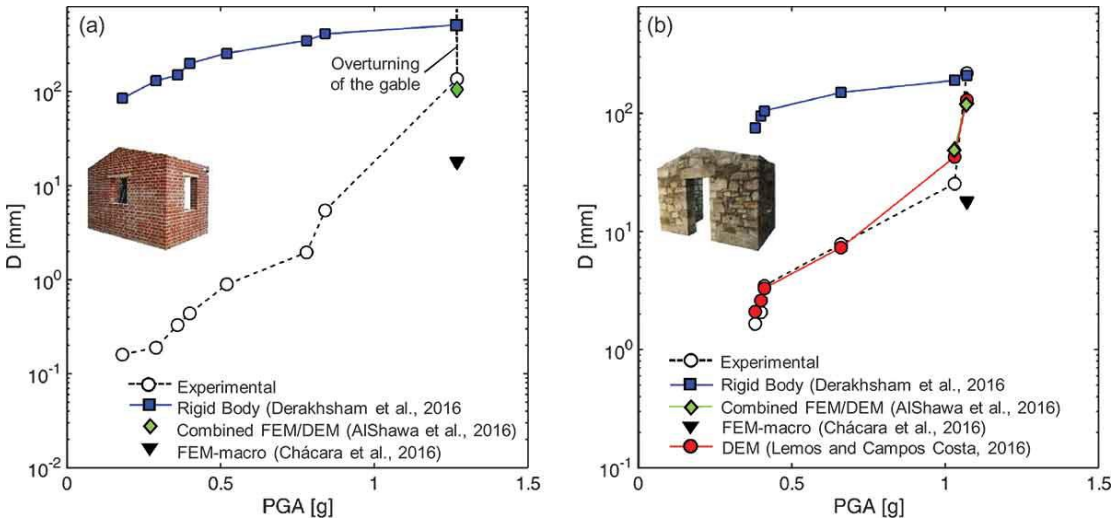

Figure 3.12 Comparison between experimental displacements and displacement demand estimated by postdictions for the Brick House (a) and for the Stone House (b) (de Felice et al, 2017)

3.3 Summary of previous research on the topic

The difficulties of assessing the out-of-plane behaviour of masonry structures has led into an extensive research campaign, which included a state-of-the-art review, a real scale experimental campaign, and both blind pre-dictions and a posteriori post-dictions of experts on the experiment.

The experimental campaign included a real-scale shaking-table test of two mock-ups, one made of brick masonry and the other one of stone. The main characteristics that played a decisive role on the response of the mock-ups were the effective wall-corners connections, the weak north wall that led to torsional behavior, and finally the presence of the opening at the façade. As a result, a combined both in-plane and out-plane mechanism appeared in both cases. Finally, it was highlighted the importance of geometrical and construction details, and therefore the accurate survey always needed is such constructions.

Before any results of the experiment were published, several groups of experts performed blind prediction of the response. This task appeared to be extremely challenging, especially for the brick mock-up due to its higher flexibility. The results proposed varied significantly and were widely scattered, mainly due to assumption on the main factors that governed the response and were mentioned above. Moreover, although different modelling approaches or analysis were tested, none of them appeared to be completely robust. Therefore, it was pointed out that more research is needed to develop reliable techniques.

Right after the results of the experimental campaign were provided to the groups, a second assessment campaign was carried out, at that time a posteriori and with the ability to re-calibrate their models. In some cases, the experimental collapse mechanism was assumed as known for the assessment, while in other cases the capability of the model to estimate both the collapse mechanism and the seismic capacity or response in time was investigated.

Both analytical and numerical models were used. The former ones, based on rigid body mechanisms, are faster and need very few variables, and as a result are usually recommended for codes. Although, it is important to underline that they may lead to wrong estimations. On the other hand, sophisticated numerical models are quiet complex and time consuming to analyse, but if used with precision they could provide more robust solutions.

A limit analysis based approach is the fastest way to estimate the out-of-plane capacity, but with the important limitation that the mechanism should be known. At the same time, it is characterized by several shortcomings or uncertainties, such as: i) it doesn't account any size effects, ii) the mechanism and its boundary conditions need to be known, iii) the crushing strength is usually neglected and the position of hinges is unclear, and finally iv) uncertainties related to the use of response spectrum (period, damping).

Several numerical approaches were employed, being the finite element method, the discrete element method or combined finite-discrete method, and were investigated by their efficiency to predict the collapse mechanism and the displacement capacity.

The finite element method was used, with various different modelling strategies, consisted of micro- or macro- modelling approaches. The method was able to simulate adequately the damage at north, weak wall, but not at the façade. Moreover, its continuum nature appeared to be inappropriate to simulate large rigid body displacements, which are always present during the rocking response of such phenomena.

The discrete element method revealed that a better representation can be achieved by modelling the possible occurrence of cracks with surfaces of discontinuity. Once more, several different models and strategies were performed, some of which were the distinct element method, macro-elements, combined finite/discrete elements, or even equivalent FEM micro-models. The results were able to predict the collapse mechanism, and in addition a good reproduction of the dynamic response was achieved. However, the high computational effort needed combined with the high sensitivity to the input variables, are the main drawbacks of the discrete element method.

As a conclusion, it is clear that the tools available to assess the complex phenomenon of out-of-plane response and failure of masonry structures are either extremely sophisticated and costly, either not yet completely sufficient. Therefore, more research is needed in the topic towards more reliable methods

and tools that could provide refined predictions of the failure mechanisms and the dynamic displacement response.

4. METHODOLOGY

The aforementioned experimental campaign, presented in (Candeias et al, 2017), is selected as case-study of this thesis. In Chapter 3, it is shown that despite the numerous attempts to assess the problem, it is a difficult and challenging task. In this Chapter, the methodology adopted to approach the problem is stated, together with its shortcomings and the expected outcomes.

4.1 Methodology and Objective of the analyses

4.1.1 Modelling approach

A finite element macro-modelling approach is adopted, using the mixed strain/displacement formulation presented in Chapter 2.

- The finite element method is considered an adequate method for modelling the linear and non-linear response of the structure, however, not capable of reproducing correctly the rocking phenomena, which characterize the out-of-plane response before collapsing (see Chapter 1.2).
- A macro-modelling approach is selected, instead of a micro- or meso- approach. This choice is done mainly under the scope of a reasonable computational cost, since a direct simulation of the masonry components of a complete structure becomes unaffordable both in terms of model preparation and computation time. Moreover, a more detailed simulation would require many more input parameters, which are not provided by the experimental campaign selected. On the other hand, such a modelling approach excludes the ability to represent phenomena related to the units' lay-out, i.e the anisotropic behaviour of masonry, lintels' effect, interlocking of units, high unit/structure size ratio of the stone house etc.
- The mixed strain/displacement finite element formulation is used, due to the accuracy it presents in strain localization problems, extensively described in Chapter 2. On the one hand, it is capable to overcome problems related to mesh bias dependency and can assess more correctly the load peak, the crack path and the failure mechanism. On the other hand, in computational terms, it is more costly, since there are nine unknowns per node instead of three.

4.1.2 Analyses strategy

The non-linear static analysis (pushover) is used here as a simple but sufficient tool that can provide an assessment of the collapse mechanisms that might form, if applied in all directions. Since the mock-up structures were subjected to a unidirectional seismic action, the pushover analysis is applied twice per case, both for pushing and pulling, according to a mass proportional loading. The plotted capacity curves that are presented for each analysis, correspond to the total base shear of the structure, and the displacement to the top of the gable of the façade.

However, the pushover analysis is also characterized by several shortcomings, attributed to its intrinsic static-monotonic nature. More specifically, the dynamic behaviour is not considered and inertial dynamic effects and cyclic damage accumulation are neglected, while as it has been experimentally shown that the masonry walls can sustain higher accelerations than their “quasi-static” capacity (see Chapter 1.2, Venture, 1981; Bruneau, 1994; Doherty et al, 2002).

Moreover, a complete ability of the analysis to predict the exact collapse displacement, cannot be claimed; since such a task cannot be achieved by a numerical tool that might lose its convergence due to loss of stability/equilibrium in the horizontal direction, while it is the vertical one which is in the end the determinant factor for the collapse or not of the structure.

4.1.3 Objectives of the analyses

Considering all the above, the main objectives of the thesis can be summarized in:

- To assess the proposed model by comparing with the experimental results. More specifically, due to the aforementioned limitations inherent in the model adopted, such a comparison is mainly focused on the identification of the collapse mechanism, being though of great importance as underlined by (Mendes et al, 2017), and of significant need for other methods as is observed in Chapter 1.2. Furthermore, a correlation is also attempted for the load peak and the displacements, despite the difficulties.
- To assess the performance of the mixed finite elements by comparing with the results obtained with the standard elements. Being the first big scale application of this formulation, the analyses performed consists a challenge for the claimed advantages of the mixed finite elements, and in particular for the mesh bias dependency remedy. Therefore, the comparison is done both in terms of crack pattern and the load peak. Moreover, since the mixed formulation includes a higher computational cost, a relative discussion is also opened.
- To assess the proposed model by comparing with similar previous assessment attempts. Between the previous assessment attempts presented in Chapter 3.2 and within the framework of the adopted modelling approach, a similar assessment analysis has been done (Chácara et al., 2017). The two proposed models are set side by side, in order to investigate possible shortcomings or advantages of both models.
- To perform sensitivity analyses and examine the influence of secondary parameters, such as the lintel’s effect, the damage model used, or the stabilization parameter. More specifically, the lintels are distinctly modelled and their influence on the results is examined. Furthermore, the differences of two alternative damage models, namely an isotropic and an orthotropic, are studied. In addition, since an explicit value of the stabilization parameter is not yet available, its influence on the results is also examined.

4.2 Simulation Model

The finite element numerical analyses are performed using the finite element program COMET (Cervera et al., 2002), while the pre- and post-processing is done using GiD (GiD, 2002). Both softwares been developed at CIMNE (International Center for Numerical Methods in Engineering).

4.2.1 Material properties, geometry and finite element mesh

The experimental campaign (Candeias et al, 2017) provides the material parameters of the two structures (Table 3), which were obtained by testing six wallets of each masonry type, in vertical compression and diagonal compression (see Chapter 3.1).

We should also underline that the fracture energy is not given by the experiment, but the value is obtained according to (Lourenço, 2009), as was done also in (Chácara et al., 2017; Cannizzaro, & Lourenço, 2017). This choice would latter on give us the opportunity to compare our results with the aforementioned works, since all the mechanical parameters used are identical.

Table 3 Mechanical Parameters for brick and stone structures

				Tensile parameters		Compressive parameter
	Young's Modulus (GPa)	Specific mass (kg/m^3)	Poisson's ratio	Tensile strength (MPa)	Fracture energy (N/m)	Compressive strength (MPa)
Brick	5.17	1890	0.20	0.102	12	2.48
Stone	2.08	2360		0.224	48	5.44

3D hexaedra solid elements are used for the simulation, representing the complete geometry of the two mock ups (Figure 4.1 and Figure 4.2). Furthermore, linear/linear interpolations are employed for the mixed finite elements, while the configuration scheme of the integration points is investigated during the creation of the reference model (see Chapter 5.1.1 & 5.2.1). Finally, a fully structured mesh is used, with a mesh size of approximately 0.1 x 0.1 m^2 over the plane of the walls, while in order to estimate the necessary elements needed across the thickness, a sensitivity analysis is initially done to ensure that the structural performance is stable upon further refinement (see Chapter 5.1.1 & 5.2.1).

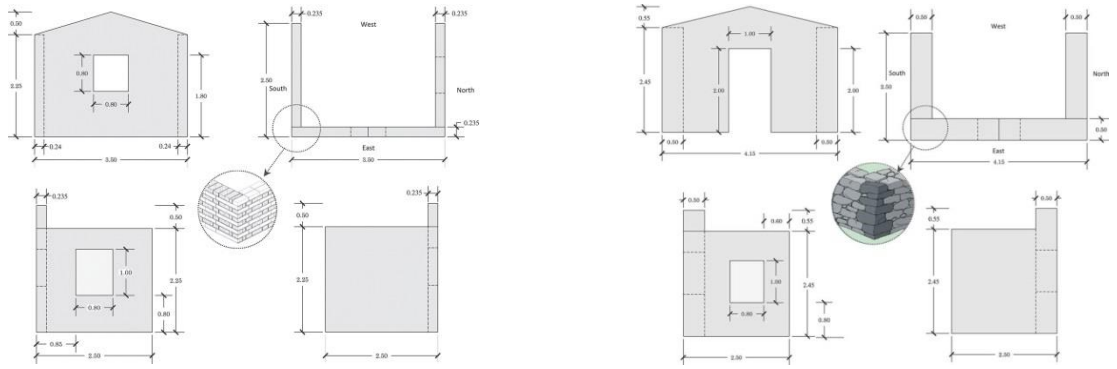

(a) (b)

Figure 4.1 Geometry of (a) the Brick mock-up and (b) the Stone mock-up (Candeias et al, 2017)

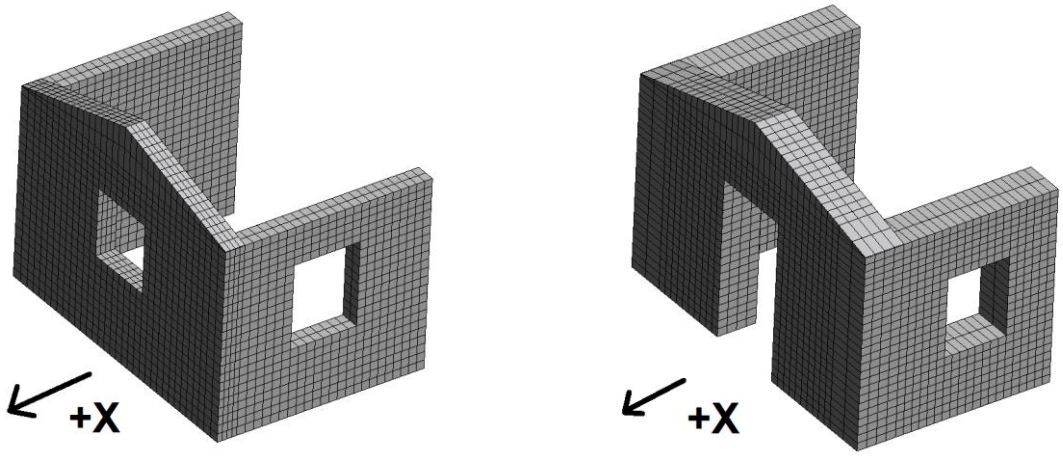

(a) (b)

Figure 4.2 FE mesh model and axis definition of (a) the Brick structure and (b) the Stone structure

4.2.2 Damage model and damage criterion

A continuum damage mechanics model is adopted (Cervera et al, 2003) for the non-linear behaviour of the material. In this model, the actual stresses of a damaged material are related to the equivalent stresses of the intact material (effective stresses) with the internal damage index d (equation (16)). This scalar-type variable represents the damage of the material and it ranges from 0 (intact) to 1 (completely damaged).

$$\boldsymbol{\sigma} = (1 - d)\bar{\boldsymbol{\sigma}} \tag{16}$$

Moreover, this is a damage model with isotropic behavior, which doesn't take into account any cracks re-closure phenomena and is adopted since a monotonic loading is applied. Although, in order to assess this choice, the performance of the isotropic damage model in the final results is compared

with an orthotropic damage model. A comprehensive or detailed comparison of the different possible damage models is considered out of the limits of this thesis and therefore is skipped. Although, in order to have a more practical and clear understanding of the differences of the isotropic and orthotropic damage models, a simple example of a single hexaedra element has been tested and is presented in the Annex.

The Rankine damage criterion (Figure 4.3) is used herein, since such structures show a very low and brittle tensile failure, while their compressive strength is relatively high. This damage criterion is comparing the principal tensile stress σ_1 with the corresponding threshold, defined initially as the tensile strength of the material f_t, and after that as the stress of the exponential path corresponding to the maximum strain appeared until that time.

Concerning the non-linear behaviour of the material, an exponential softening branch is considered for tension (Figure 4.4), while the compressive behaviour is considered elastic, since a Rankine-type damage criterion is used. Moreover, the traditional crack-bandwidth approach (Bažant & Oh, 1983) is adopted and the fracture energy concept is used in order to tackle mesh-size dependency by regularizing with respect to the resolution of the FE mesh.

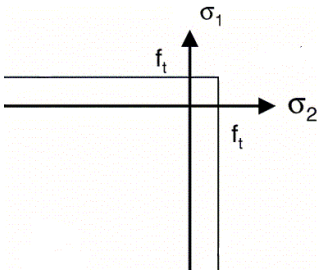

Figure 4.3 Rankine damage criterion

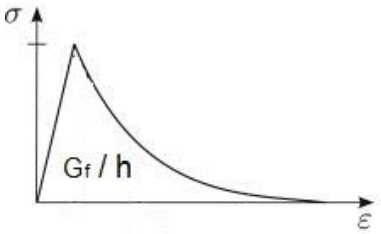

Figure 4.4 Exponential softening under tension

4.2.3 Numerical parameters

The material non-linearity of such push-over analysis implemented here requires an incremental procedure, which is done here in a pseudo-time step-by-step way. At each step, iterations are repeated until the equilibrium is achieved. The equilibrium condition is considered by checking the convergence of the norm of residual forces and the norm of the total external forces. The admissible tolerance of convergence is set to 1%, which a common value for such structures. Moreover, the initial stiffness matrix is used in every step of the iterative procedure.

Furthermore, the non-linear behaviour of such brittle structures shows numerical difficulties in order to follow the equilibrium path, such as the presence of “snap-through” and “snap-back” response. For this reason, the numerical tool of arc-length has been used, so that a solution could be found for the post peak regimes. More specifically, every analysis is initially run with the spherical algorithm of arc-

length and therefore any possible snap-back can be identified. However, the spherical algorithm tends usually to follow the unloading path, when during a “snap-back” the tangent of the solution turns negative for the second time. Although, at that time the physical interpretation of the “snap-back” can be identified by looking at the results, and a second analysis is then run, using the displacement control algorithm of the arc-length, by controlling a DOF of a point of the structure that monotonically develops. In particular, since in most cases the “snap-back” response of parts of the structure was happening due to the early and brittle failure of the weak return wall, as a control point of the displacement arc-length was set the north-east, or north-west top of the structure that followed the failure of the return wall.

5. ANALYSES AND COMPARISONS

The results of the analyses are presented in this chapter. More specifically, each mock-up is studied at the same time for both pulling and pushing, in order to have a holistic point of view of the total response. In the beginning of each case, a reference model is chosen by comparing, discussing and selecting different input parameters. After that, the reference model is compared with the experimental results and several aspects that are studied, such as: comparison with standard finite element formulation, comparison with previous FEM simulations, physical or numerical parameters (lintel's effect, use of isotropic or orthotropic damage model, influence of stabilization parameter τ_{ε},), and finally the computational cost of the analysis.

5.1 Brick Masonry

5.1.1 Reference Model

Mesh refinement

The finite element method provides by its intrinsic nature an approximation of the "real" solution. However, several parameters should provide convergence towards the "real" solution upon refinement. One such parameter is the mesh size. More specifically, since the out-of-plane behaviour of walls is affected mainly by the elements across the thickness, a sensitivity analysis is firstly performed in order to find out a number of elements that can provide an adequate solution. This means that several models with different elements across the thickness are employed and their solution is compared so that the results don't change significantly by a further refinement.

First, the adequate number of elements across the thickness of the façade is investigated (Figure 5.1 (a)). 1, 2, 4 and 6 elements are tested and it is observed that the difference between the model with 4 and 6 elements is small. Therefore 4 elements across the thickness of the facade are employed.

Secondly, the number of elements across the thickness of the side walls is investigated, having at the same time 4 elements at the façade. This time only 1, 2 and 4 elements are tested since there is not significant change between 2 and 4 elements. Therefore, 2 elements across the thickness of the side walls are employed.

Concluding, 4 elements are used across the thickness of the façade and 2 across the thickness of the side walls. This difference of elements needed can be explained by the fact that the façade in subjected to out-of-plane response and therefore the precision of the solution across the thickness is more important than the mainly in-plane response of the side walls.

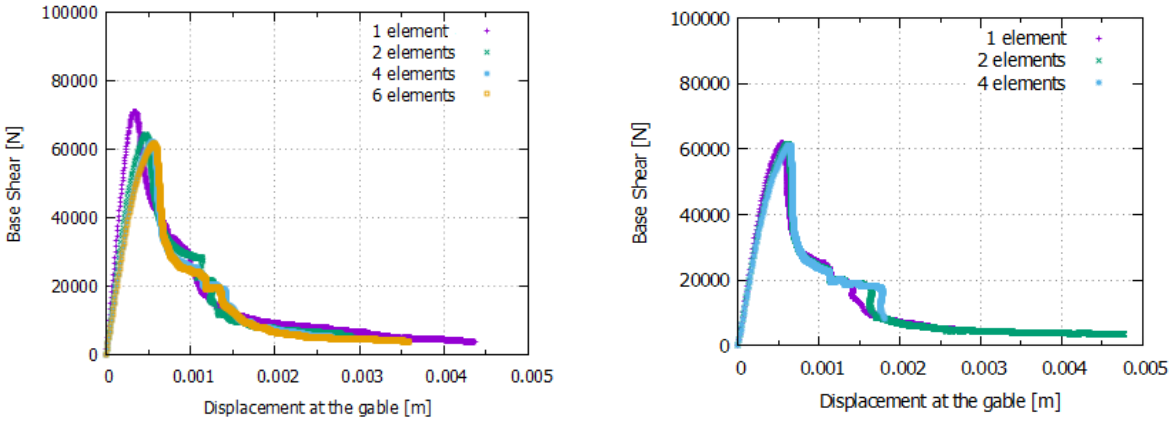

(a) (b)

Figure 5.1 Brick House Pulling(+X): Mesh refinement for (a) Façade elements and (b) Side walls elements

Integration points configuration scheme

In some previous works that used the mixed strain/displacement finite element formulation (Cervera et al, 2010b), the nodes of the elements were used as integration points, instead of the "classical" Gaussian points. For this reason, a simple comparison is done in order to assess these two possibilities.

The comparison of these two different integration points' schemes is shown by plotting their two different capacity curves in (Figure 5.2).

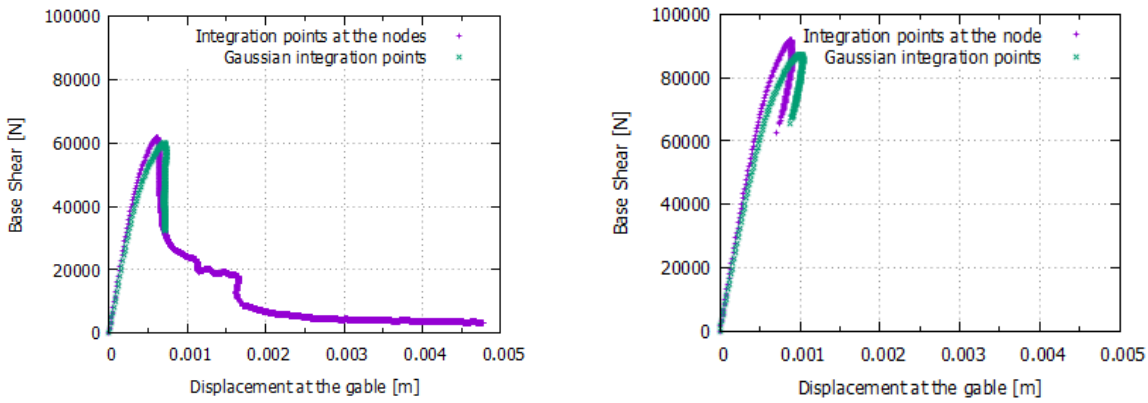

(a) (b)

Figure 5.2 Brick House: Different Integration points configuration for (a) Pulling(+X) and for (b) Pushing (-X)

As can been observed by the graphs, the scenario of the integration points at the nodes provides slightly stiffer results at the elastic regime. Nevertheless, the non-linear response appears to be identical both in the capacity curves, but also in the response of the structure, and therefore a more detailed comparison is skipped here.

We can say that this result is as expected, and it approves why the Gaussian points are preferred than the nodes as integration points (Zienkiewicz et. al, 2005). However, we should mention that if a mesh refinement is done, then the curve of the integration points at the nodes converges towards the curve with the Gaussian integration points.

Finally, it is important to underline that the analysis with the integration points at the nodes can provide a more consistence numerical solution (not physically, but numerically), since the strains and stresses are calculated at the same points with displacements, and therefore no interpolations are needed. This is the reason why here a further solution is achieved with the integration points at the nodes (Figure 5.2 (a)), while the Gaussian scheme results in the complete damage of some nodes (due to interpolations needed), which can then move freely in the space domain, causing then equilibrium instabilities.

Summarizing, although the Gaussian configuration provides a better approximation, the nodes configuration can catch a further solution and therefore highlight the complete mechanism. Considering that the main task of the problem, as addressed in 4.1.3, is to identify the collapse mechanism, therefore the nodes configuration is preferred and selected as reference case.

Elastic base

During the experimental campaign, the mortar used at the base (first layer of bricks/stones) of the mock-ups was enhanced with cement, in order to ensure their bond and prevent the sliding between them (Candeias et al. 2017).

The aforementioned construction detail had a direct, physical consequence: a crack formation and propagation was avoided at the base of the structures, since the material had locally enhanced strength properties. This physical response detail is initially neglected during the modelling procedure, as of minor importance. However, when the first analyses of the models are performed, the models appear to fail at their base when pushed (-X direction) (Figure 5.3 (a)). Therefore, since this response was not permitted to happen in reality, it is decided to simulate the base of the models with only elastic behaviour, not allowing them to crack. For this reason the first two layers of elements are assigned the same material properties but with an elastic behaviour.

The results of the model with the elastic base are presented in (Figure 5.3 (b), Figure 5.4) and at the same time are compared with the results without an elastic base. As can be observed, the damage that develops at the base of the facade doesn't evolve horizontally across the entire base of the structures any more, and therefore the formation of other mechanisms is allowed. For this reason, the reference model is modelled with an elastic base when performing a pushing (-X) analysis.

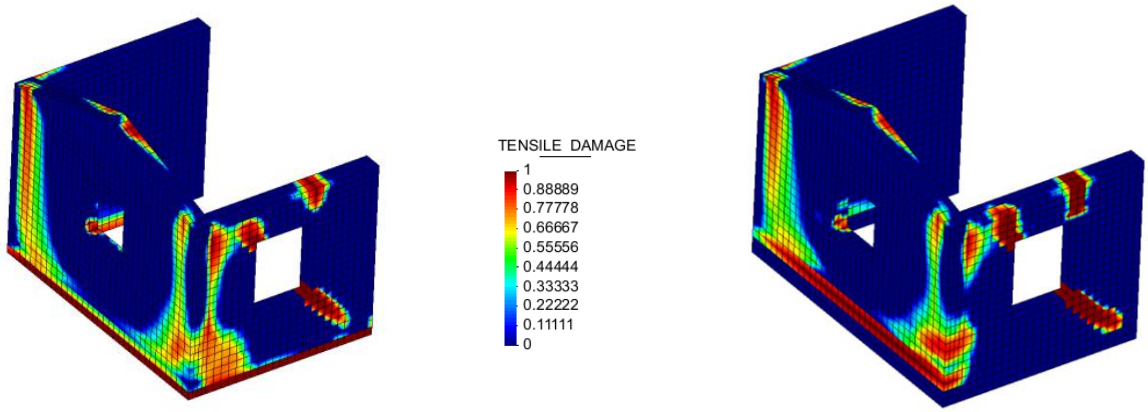

(a) (b)

Figure 5.3 Brick House: Pushing (-X) (a) without an elastic base and (b) with an elastic base

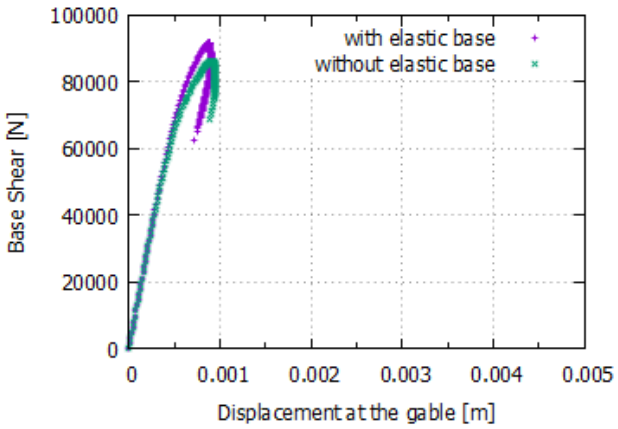

Figure 5.4 Brick House: Pushing (-X), with & without elastic base

Reference model results

The results of the of the reference model in terms of capacity curves are presented in Figure 5.5.

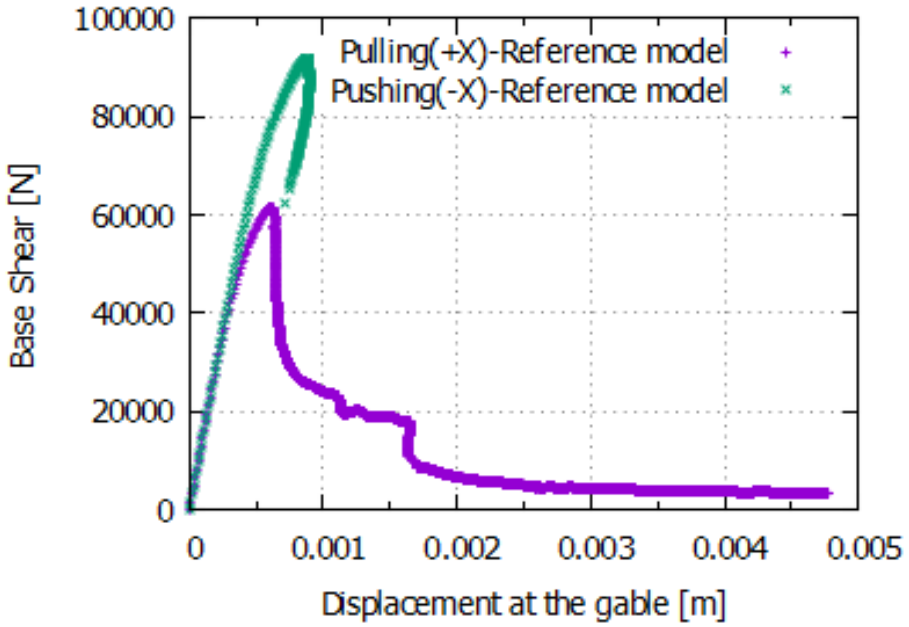

Figure 5.5 Brick House, Reference model: Pulling(+X) and Pushing(-X)

The first clear outcome of the results is that the structure appears to have a much higher peak load at the pushing (-X) direction than the pulling (+X). In order to give an explanation about this fact, the stress states of both models are compared, just some steps before the pulling (+X) model goes non-linear and their response is diverging. As can be seen in the Figure 5.6, when the model is loaded in the (+X) direction, more points with tensile stress concentration appear, mainly due to two reasons: 1) on one hand, if the plan of the structure is considered, then the model that is loaded in (-X) appears to have as “tensile resisting flange” the whole façade, while the model that is loaded in (+X), involves as “tensile resisting flange” only the west corners of the side walls, and therefore more stress concentration is present, and on the other hand, 2) when the constraints of the facade are considered, the tensile stresses reach higher values when the façade is loaded “outwards” than “inwards” (Figure 5.6). This is happening due the tensile stress flow path that is formed in the two cases, since in the case of inwards loading the tensile stress flow needs to form three turning points in plan, while in the case of outwards loading, one turning point is formed and therefore the stress flow can easier reach the outer surface. In other words, the corners of the façade are more vulnerable when loaded outwards than inwards. At the same time, it is interesting to note that this different response of the corners in the two directions is also a physical phenomenon and happened also in the experiment, as it was mentioned in (Candeias et al, 2017).

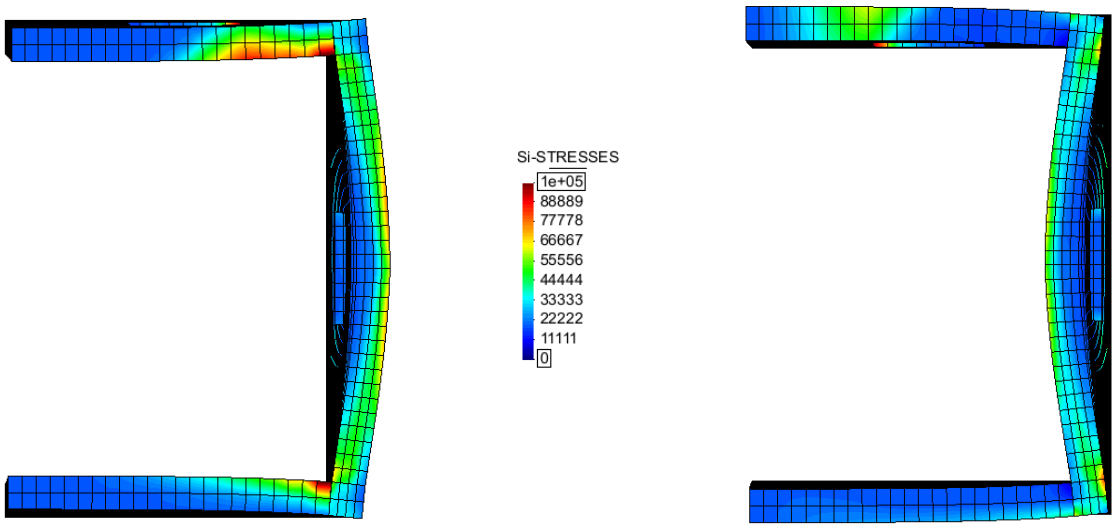

(a) (b)

Figure 5.6 Brick House (top view): Elastic tensile stresses (a) for pulling (+X) and (b) for pushing (-X)

Summarizing, the structure appears to be more vulnerable in the pulling (+X) direction. Therefore it is expected to be the crucial direction of failure. For this reason, the response of this direction is firstly presented.

Pulling (+X)

The response of the model subjected to loading in pulling (+X) direction is characterized mainly by two phases: i) the elastic response and initiation of damage until the peak load, and ii) the brittle loss of load capacity and the formation of the collapse mechanism.

Initially, the structure responds almost elastically until the base shear is around 40,000 N. At that point, damage initiates and stiffness starts to decrease until the peak load is reached around 60,000 N. The damage that develops at that early response is presented in (Figure 5.7 & Figure 5.8) and described here:

- The facade is damaged at the west side of its base, which is caused by the vertical bending, amplified by the relatively slender wall.
- The gable of the facade is scarcely damaged, due to the horizontal bending of the upper part of the gable wall. It is interesting to note here that this damage doesn't localize and at the same time it remains at low levels, as can be observed by looking at the strains.
- In addition, the horizontal bending of the gable results also in damaging significantly the connections with the return walls, especially at the top part.

- Both of the return walls are slightly damaged at the west side of their base, due to the in-plane bending.
- The north wall is extensively damaged, due to its in-plane behaviour and the presence of the window.
- More specifically, there is a significant diagonal shear crack starting at the low east corner of the window propagating towards the north-east corner of the structure, tending to join with the crack at the base of the gable wall,
- the spandrel of the window has started cracking at its connection with the piers, due to its bending behaviour, and
- the west pier appears to be damaged at its west “base”, also due to its bending response.

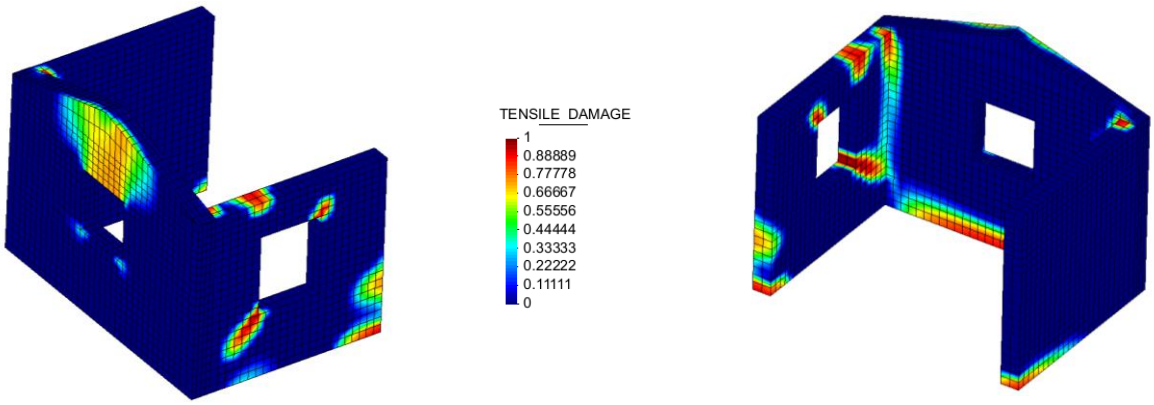

(a) (b)

Figure 5.7 Brick House Pulling (+X): damage at peak load (a) NE view and (b) SW view

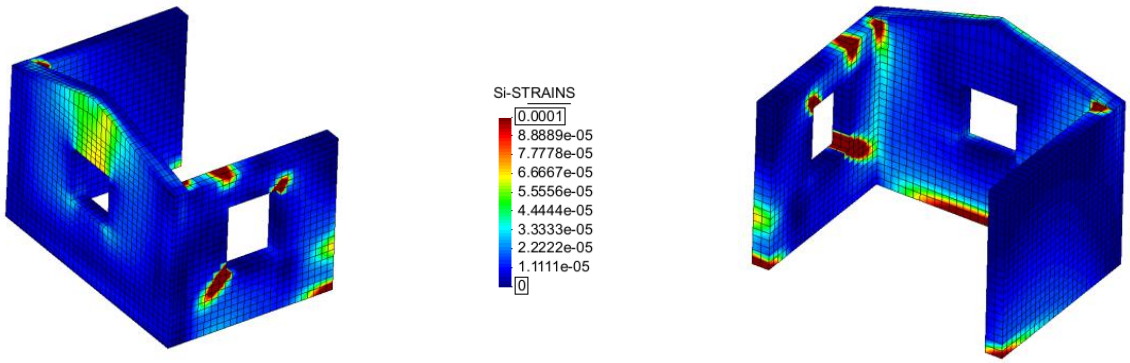

(a) (b)

Figure 5.8 Brick House Pulling (+X): principal strains at peak load (a) NE view and (b) SW view

After the peak load is reached, the response of the structure shows a very brittle behavior which leads to significant loss of load capacity. This is happening due to the great extension of the damage at the north side wall, which leads to the loss of local elements and their resistance contribution. More specifically, the first element that is completely damaged is the spandrel at its two sides, due to bending. At the same time, the west pier loses also its carrying capacity due to bending failure of its base. At that point, the structure presents some retaining strength, while the façade is no longer bending horizontally, since its constrain of the north side wall is lost. However, the whole north-east corner of the structure is weakly supported, since it has lost its resistance of the spandrel, the east pier of the north return wall due to the diagonal crack and finally its base due the vertical bending crack at the base of the gable wall.

As a result, a second significant loss of load capacity appears at the capacity curve, which corresponds to the development of a diagonal crack that connects the north lower and south upper corners of the façade, crossing the window (Figure 5.10). The complete development of this crack marks the formation of a collapse mechanism of the façade, and therefore, the top of the gable presents large displacements with very low resistance, until the crack expands across the thickness of the façade and the equilibrium is lost.

In the end, the collapse mechanism of the structure is composed by three macro-elements, namely the west pier of the north wall, the spandrel of the north wall and the north-east corner which includes the east pier of the north wall and the upper north part of the façade (Figure 5.9, Figure 5.10, Figure 5.11).

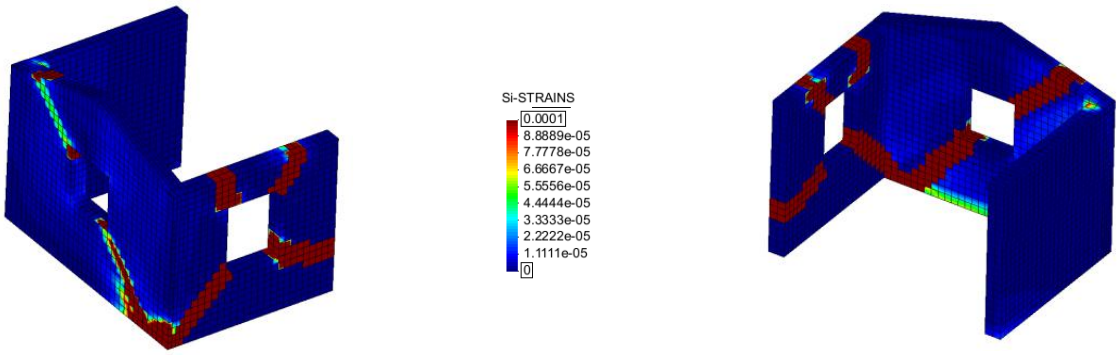

(a) (b)

Figure 5.9 Brick House Pulling (+X): principal strains at failure (a) NE view and (b) SW view

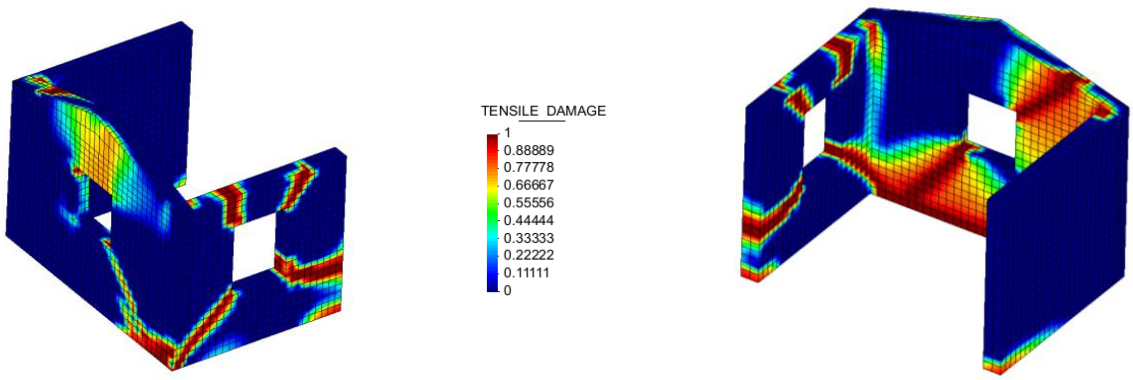

(a) (b)

Figure 5.10 Brick House Pulling (+X): damage at failure (a) NE view and (b) SW view

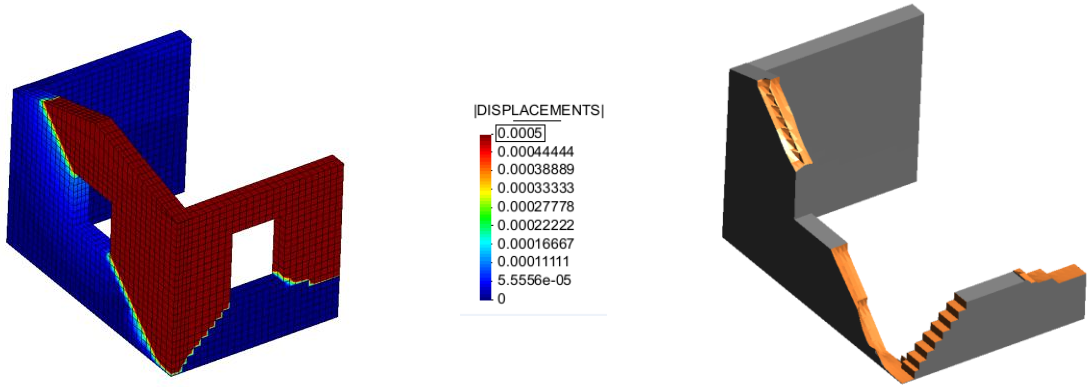

(a) (b)

Figure 5.11Brick House Pulling(+X) NE view: displacements at failure (a) contour and (b) iso-surface

Pushing (-X)

As already mentioned, the response of the structure is less vulnerable when pushed (-X direction). The structure responds almost elastically until a load peak of around 60,000 N and reaches a load peak of around 90,000 N.

At this area of the response, damage develops simultaneously in several parts of the structure (Figure 5.12):

- At the base of the facade, due to vertical bending.

- As the crack of the base develops, the resistance of the out-of-plane of the façade is transferred to the side walls and therefore horizontal bending of the façade causes vertical damage at the gable of the façade and at the corners of the walls. Moreover, diagonal cracks appear at the lower corners of the window.
- At the same time, significant in-plane damage is observed at the north side wall, due to the weakness introduced by the window.
- More specifically, the spandrel develops damage at its both sides due to bending, and
- a diagonal crack develops at the west lower corner of the window, towards the west low corner of the wall.

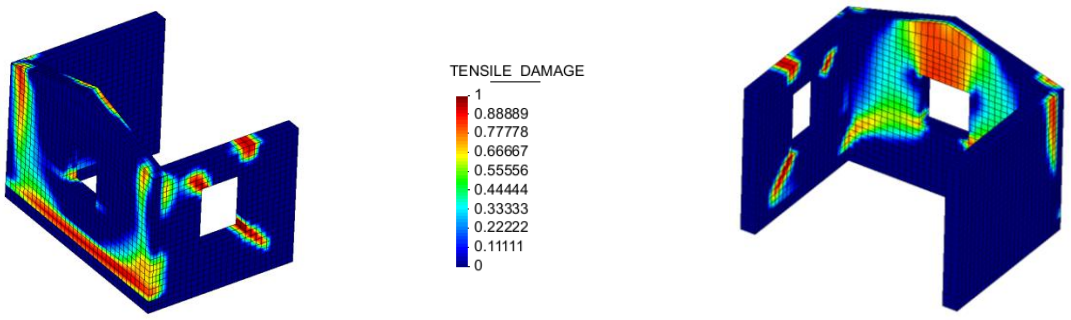

(a) (b)

Figure 5.12 Brick House Pushing (-X): damage at peak load (a) NE view and (b) SW view

Finally, right after the load peak, the spandrel and the west pier of the north wall fail completely, form a local collapse mechanism and the equilibrium is lost (Figure 5.13, Figure 5.14). As a result, a global collapse mechanism is not captured, due to the lack of convergence.

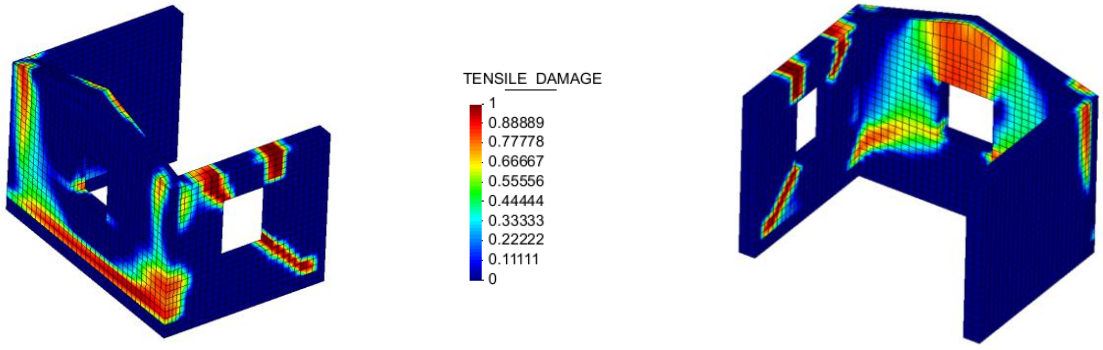

(a) (b)

Figure 5.13 Brick House Pushing (-X): damage at failure (a) NE view and (b) SW view

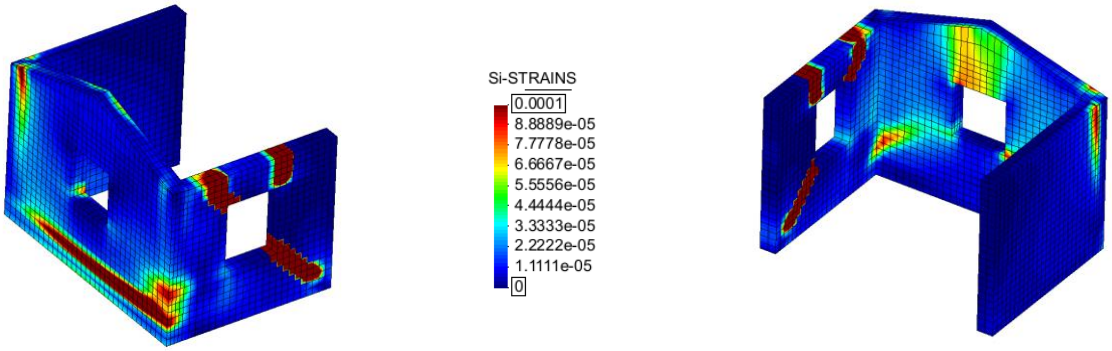

(a) (b)

Figure 5.14 Brick House Pushing (-X): principal strains at failure (a) NE view and (b) SW view

5.1.2 Comparison with Experimental results

Collapse mechanism

The main object of the analysis strategy that has been adopted in this thesis (Chapter4.1.3) is to identify the failure mechanism of the structure. Therefore, the results obtained during the analysis should be compared meticulously with the experimental results in terms of failure mechanism.

The main failure mechanism of the brick mock-up structure involved a part of the gable wall and a big portion of the north return wall (Figure 5.15), while a secondary local failure mechanism appeared earlier that involved a part of the tympanum. More specifically, the main failure mechanism was already developed during the TEST07 as can be seen in Figure 5.15, and involved 4 macro-elements: the north-west pier of the north wall, the spandrel of the north wall, the north-east corner including the two piers of the transversal walls and finally the gable of the façade. Consequently, during the TEST08, the aforementioned mechanism was already formed and initially presented a rocking response. This rocking response, which was governed by torsional effect, was more intense at the north side, and therefore caused the formation of the secondary mechanism at the north part of the gable.

Figure 5.15 Damage evolution and collapse mechanism formation in the Brick structure

(Candeias et al, 2017)

Moreover, the mock-up appeared to be more vulnerable in the outward direction of the façade, both before and after the complete formation of the mechanism (Candeias et al, 2017), while the numerical model was able to assess correctly this vulnerability.

The results of failure mechanism that are obtained with the FEM pull-over and push-over analysis are the following: Both directions represent correctly the in-plane collapse mechanism of the north wall, while there are some differences for the out-of-plane simulation of the façade (Figure 5.16, Figure 5.17, Figure 5.18).

Firstly, the FEM model appears to develop some vertical damage at the gable of the façade due to horizontal bending (Figure 5.10), while none of this damage appears at the experiment. This inconsistency might appears due to underestimation of the horizontal bending strength of the masonry, or due to the presence of the wooden lintel in the real structure which prevents the development of crack localization at its centre while provokes crack initiation at its corners. As a result, the final collapse mechanism that is formed by the simulation model appears to have one less macro-element, which is formed in the experiment due to the diagonal cracks developing from the facade window towards the top corners.

Secondly, there is a difference of the crack propagation at the north-east corner: the experimental structure develops a horizontal crack connecting the low corners of the two windows of the façade and the north wall, while the numerical model develops two diagonal cracks which start at the corners of

the windows and join at the lowest point of the corner. This difference might have been introduced due to the high orthotropic behaviour of the experimental brick structure, or partially due to the cyclic loading of the experiment, since when looking at the push-over (-X direction) damage pattern (Figure 5.13, Figure 5.14) it can be observed a damage localization at that corner.

Finally, it is clear that the secondary failure mechanism which appeared during the experiment cannot be simulated in the numerical model. This is attributed to the numerical tool employed for these analyses, which cannot simulate adequately the rocking response and therefore can't capture any new mechanism formation within an initial one. It is an intrinsic shortcoming of the strategy used herein, and as it is observed, its influence is not negligible.

Considering all the above, it is clear that the most important difference with the experiment is the directionality of the appeared cracks, following the mortar joints (Figure 5.15), which can't be represented by the adopted macro-modelling strategy. Nevertheless, the location of the damage is well captured and that shows that the model can simulate the structural response at a great extent.

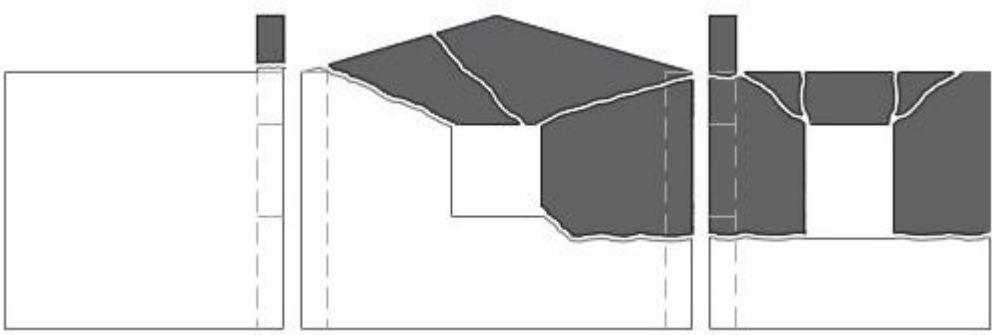

Figure 5.16 Brick house: Experimental collapse mechanism (Mendes et al, 2017)

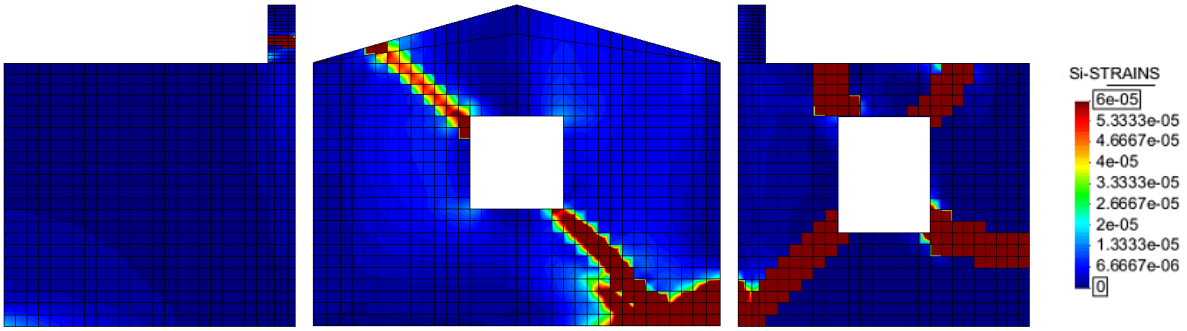

Figure 5.17 Brick house Pulling(+X): Principal strains at failure

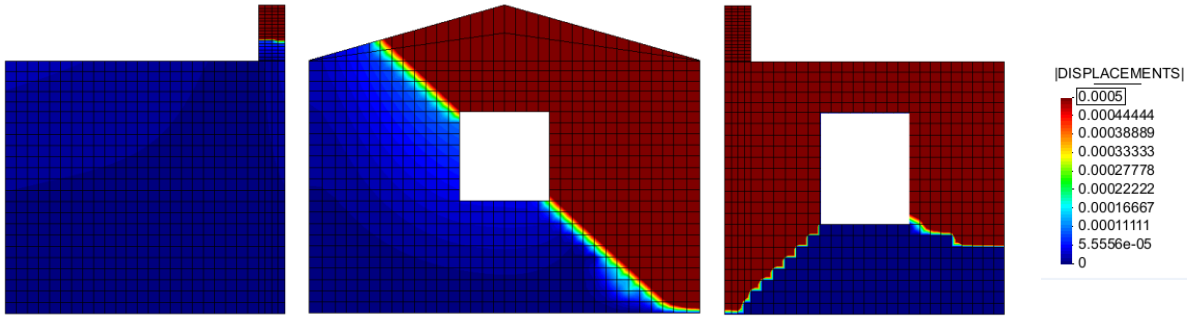

Figure 5.18 Brick house Pulling(+X): Displacements at failure

Peak load – PGA

A comparison of the experimental and the numerical models in terms of PGA is attempted in the subsection. However, this comparison is not straightforward for several reasons: 1) As has been identified by (Costa et al, 2013a), the characteristics of the ground motions may significantly influence the out-of-plane behavior of the specimen if for example near-field inputs are used, while the pushover

analysis would always provide the same results. 2) The shaking table test included cyclic loading with dynamic effects taking place, while the pushover analysis used here performs monotonic static loading in one direction at a time and no inertial or damping effects are taken into account. 3) The experimental procedure included a sequence of 8 steadily increasing excitations until the collapse is reached. Therefore, the damage of the structure was accumulated at every test, while the numerical analysis involves only one excitation until the loss of stability. 4) Finally, the analysis strategy used here is not able to reproduce the response of the structure after the collapse mechanism formation. For this reason, a comparison can be done only for the PGA's that correspond to damage initiation up to the completed mechanism formation.

According to (Candeias et al, 2017), the collapse mechanism of the brick house started to form at TEST05 and was completed at TEST07. The corresponding base shear of the PGAs' of these two TESTs have been plotted together with the pushover curves (Figure 5.19). More specifically, the orange line corresponding to TEST05 should highlight the damage initiation of the structure, while the red should indicate the load peak after which the mechanism is formed. Taking into account all the aforementioned uncertainties and difficulties of this attempt, it can be observed a good correlation between the experimental and the numerical results, specifically for the vulnerable pulling (+X) direction.

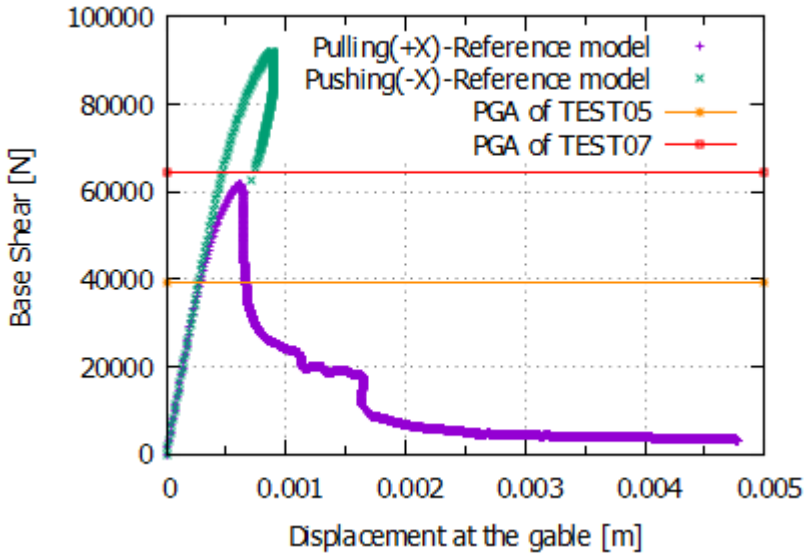

Figure 5.19 Brick model: pushover curves and corresponding PGA's of TEST05 and TEST07

Displacements

An attempt to correlate the numerical results with the experimental ones in terms of displacements faces the same difficulties as the correlation of PGA's, mentioned in the previous subsection. At the same time, the not exact collapse mechanism assessed here plays a significant and sensitive role in the displacement estimation.

Despite all the above, a comparison is attempted here in Figure 5.20, corresponding to completion of the mechanism formation. The corresponding PGA is selected as the load peak and the displacements at the last point of the capacity curve where the complete mechanism is formed. Moreover, it should be mentioned that since there is a very small difference in the declination of the crack at the top-south of the façade and the point of LVDT1 was included in the mechanism of the experiment, while in the numerical not; the plot point for the displacements corresponding to LVDT1 was chosen 4 elements to the north, so that it would be included in the mechanism.

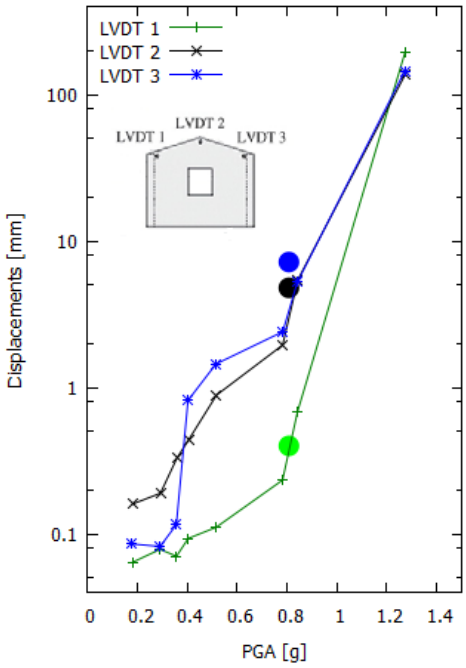

Figure 5.20 Brick house: Displacements of LVDTs during the experiment (lines) & corresponding numerical estimation (dots)

A relatively good agreement is observed at the results, although the difficulties described above. More specifically, the displacement of LVDT1 is correctly estimated, while there is a small divergence of LVDT3. This difference is appearing due to the experimental formation of the diagonal crack at the top-north part of the facade, which resulted in the "detachment" of the gable of the façade and therefore its individual macro-element response, including LVDT2 and LVDT3. This is depicted by the

difference of the two LVDTs until just one test before, when this mechanism was not completely formed and LVDT3 presented higher displacements, due to the torsional response.

5.1.3 Comparison with Standard elements

The solution obtained using the mixed finite elements is here compared with the solution that is obtained using the standard finite elements, in order to assess the efficiency of the mixed formulation and also identify and point out the shortcomings of the standard formulation that are overcome with the mixed one.

Firstly, a comparison is done in terms of capacity curves in Figure 5.21. The comparison of the two curves shows clearly a difference, especially at the initial stiffness, the load peak and the softening region. More specifically, the standard elements appear to be initially stiffer, develop a higher load peak and present a retaining strength at the softening region.

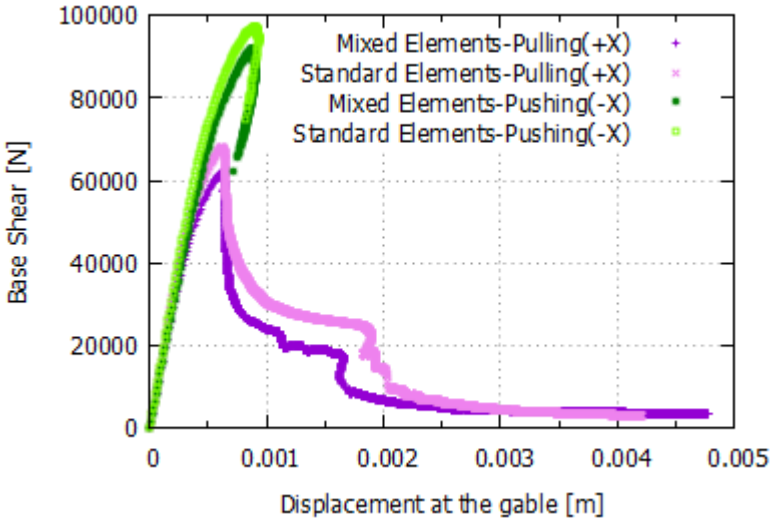

Figure 5.21 Brick house: Capacity curves in both directions for mixed & standard formulation

Finally, a comparison is made in terms of crack propagation (Figure 5.22), only for pulling (+X) direction, for the softening region where significant difference is observed in the capacity curves. Two differences can be identified: 1) the crack at the top west corner of the window in the return wall with the standard elements is propagating only vertically, while with the mixed elements the crack has a diagonal orientation, and 2) the crack that is propagating from the east low corner of the same window and is arriving at the north-east corner of the structure is finally “locking” at the facade with the mesh orientation at the third layer of elements and can’t join/connect with the crack of the base of the facade, which happens when using the mixed formulation. This is the reason of the aforementioned retaining strength that appears in the softening region of capacity curve. Both of the above mentioned

differences are what is generally called as mesh-bias dependency, and the overcome of this problem is one of the main advantages of the mixed finite element formulation.

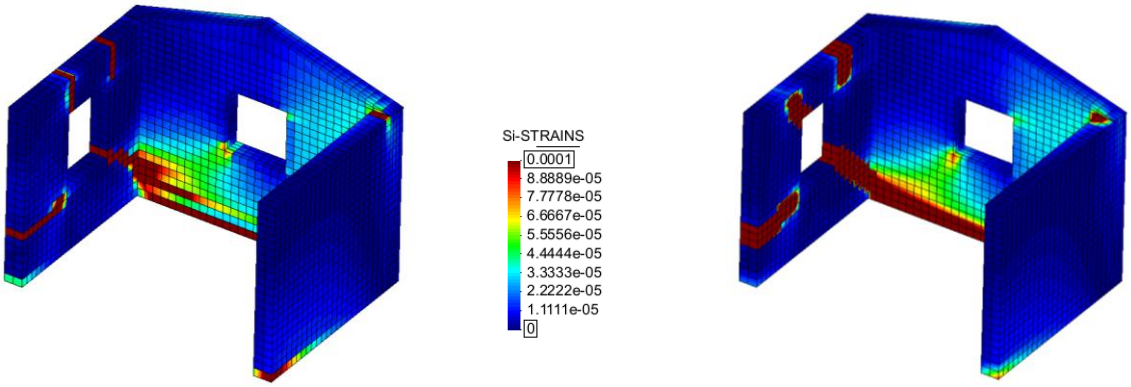

(a) (b)

Figure 5.22 Brick House Pulling(+X) NE view: Principal strains at softening region (a) with Standard elements and (b) with Mixed elements

5.1.4 Comparison with previous simulation attempts

Within the framework of the workshop presented in Chapter 3, between the several different approaches that the experts used for pre- and post-diction, a similar macro-element FEM strategy has been adopted for the assessment of the out-of-plane behaviour of the experiment, using the Diana commercial FEM software (Chácara et al., 2017). This previous work has produced some results that could be compared with the results obtained in this thesis. However, before moving forward to any comparison, firstly all the significant differences adopted in both works should be noted.

Starting with finite elements, it is underlined that in this thesis simple linear/linear interpolation elements have been used, but with the mixed formulation; while in the Diana simulation, elements with quadratic interpolations have been used, but with the standard irreducible formulation. Moreover, a rotating total strain smeared cracking model has been used during the Diana simulation, while an isotropic damage mechanics model has been used here.

Once more, the comparison between the two different simulations is made both in terms of capacity curves and cracks or mechanisms developed (Figure 5.23, Figure 5.24, Figure 5.25).

As a general overview, it is observed that a similar load peak is achieved, while the simulation using Diana dissipates much more energy by developing more damage at the façade and the corners and therefore a different mechanism is finally formed.

More specifically, although the load peak appears to be almost equal for both simulations, the initial stiffness of the mixed formulation is observed to be higher. This can be interpreted by two main points:

1) different order of elements is used in the two analyses, namely quadratic and linear for the Diana simulation and the reference formulation, respectively; 2) the integration point's configuration is also different, and as is shown in Subsection 5.1.1, the Gaussian configuration used in Diana simulation provides less stiffer results. In addition, the response of the two different models show to diverge a lot after the load peak. This can be clearly observed at the capacity curves, but can better be interpreted by looking at the damage and mechanism formed (Figure 5.24, Figure 5.25). Although that initially the two models develop similar damage at the gable of the façade and the north side wall, then their localization and development are diverging, with the mixed elements model concentrating at the north side wall, while the Diana model concentrating at the gable and the corners of the façade. As a result, the Diana model appears to dissipate much more energy since the capacity is lost much more gradually, compared with the brittle loss of the north wall at the model developed herein. Finally, a striking difference of displacements is obvious in the pushing (-X) direction, which is attributed to the early and brittle loss of the north-west pier and spandrel, which cause the partial loss of equilibrium in the case of the model developed herein, while in contradiction a much more distributed damage over the structure is noted in the Diana simulation.

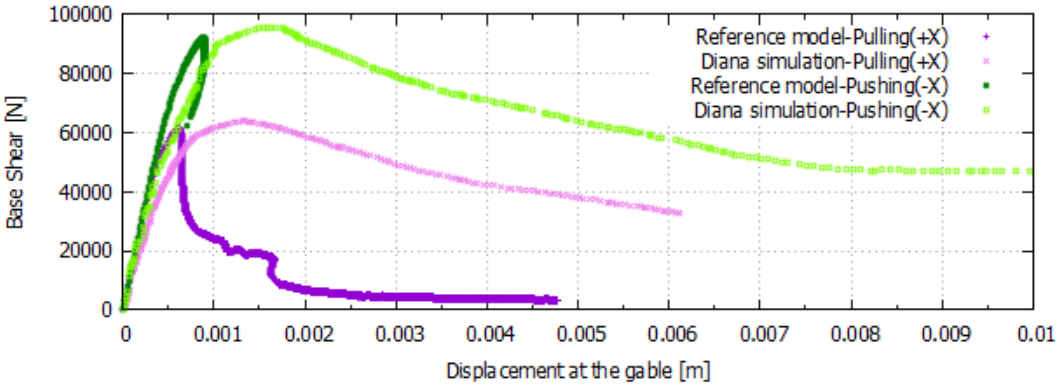

Figure 5.23 Brick House: Comparison of capacity curves of the reference and DIANA simulation

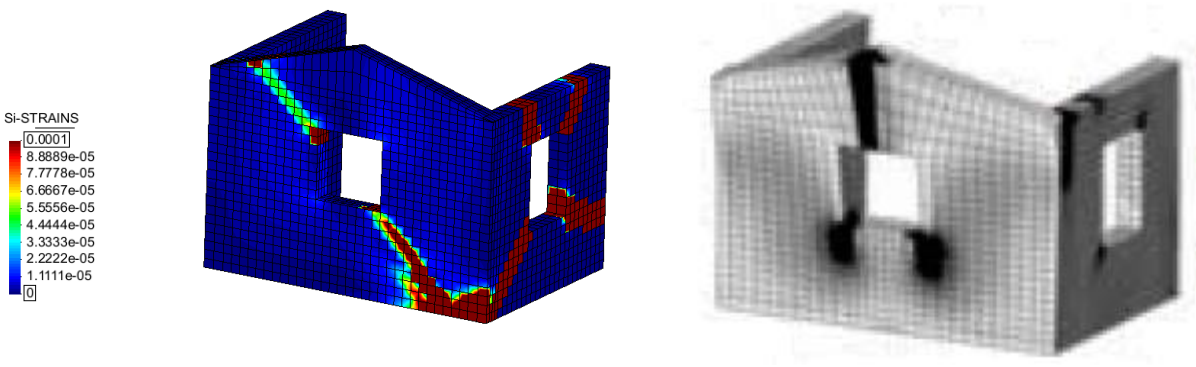

(a) (b)

Figure 5.24 Brick House Pulling(+X): Principal strains (a) reference model and (b) simulation with DIANA

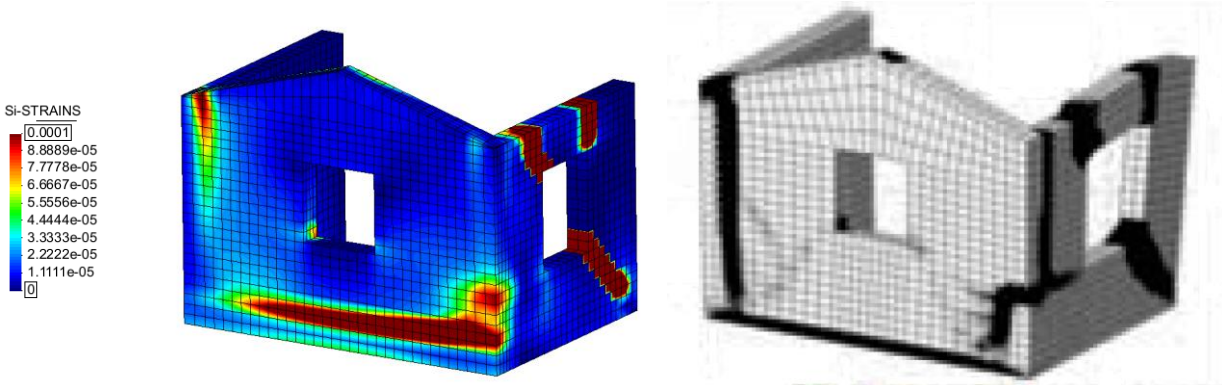

Figure 5.25 Brick House Pushing(-X): Principal strains (a) reference model and (b) simulation with DIANA

5.2 Stone Masonry

5.2.1 Reference Model

Mesh refinement

Once more, a mesh sensitivity analysis is performed, in order to assess the adequate number of elements needed through the thickness of the walls (Figure 5.26). Similarly with the brick house in Subsection 5.1.1, four elements across the thickness are adopted for the façade and two elements for the side walls.

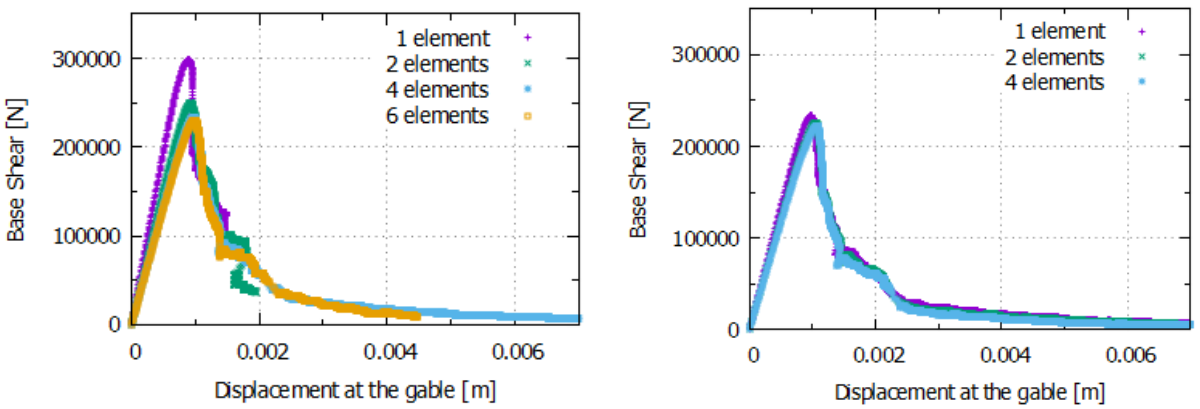

(a) (b)

Figure 5.26 Stone House Pulling(+X): Mesh refinement for (a) Façade elements and (b) Side walls elements

Integration points configuration scheme / Alternative solution

A similar strategy with the brick-house reference model is adopted here, concerning the integration points: the integration points have been selected at the nodes of the finite elements, since a more numerically consistence solution can be achieved, although the convergence to the “actual” solution is slower (Figure 5.27).

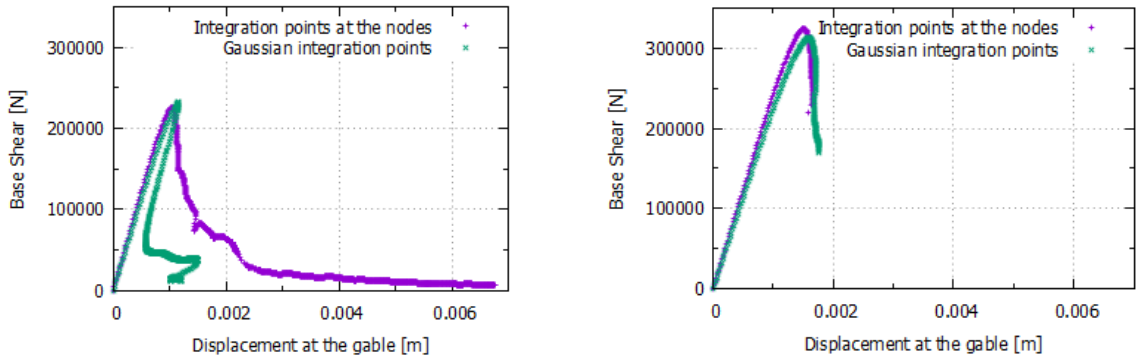

(a) (b)

Figure 5.27 Stone House: Different Integration points configuration for (a) Pulling(+X) and for (b) Pushing (-X)

However, during the investigation of all possible input parameters and their solution, an alternative solution is obtained in the case of pulling (+X), with Gaussian integration points (Figure 5.27). This alternative solution is underlined here, not because of a short divergence at the peak load or the initial stiffness, but because of the completely different collapse mechanism formed. As can be observed at the Figure 5.28 (a), although the structure initially develops identical cracks until the load peak, at that point the crack at the west base of the south side wall starts propagating all across the base towards the façade, causing also a severe snap-back at the capacity curve.

After the identification of this solution, a sensitivity analysis of all the possible parameters investigated in this thesis is performed, having as temporary reference model this solution. Parameters such as the integration points configuration scheme, the stabilization parameter τ_ε , use of standard finite elements, the elastic base consideration and even the number of the integration points are investigated; while none of them could replicate the same solution, leading always to the initial reference model that fails due to damage at the north side wall. However, this alternative solution can't be neglected for three main reasons: Firstly, because it clearly points out the highly non-linear nature of the problem examined here and therefore its sensitivity to all the input parameters. Secondly, since it provides a brittle failure which dissipates less energy and therefore could be "preferred" by the structure, if it appears as a bifurcation point. And finally, in view of the fact that the real stone house appeared to develop a similar crack, at the base of the south side wall, initially, before any other crack was extended (Candeias et al, 2017) , shown in Figure 5.28 (b). The reason of appearance of this crack at the experiment was not clearly explained and therefore a strict matching is not argued here, however, any similarities are of interest. Of course, the crack developed at the experimental mock-up appeared right above the first layer of stones, since cement was added at the first layer.

(a) (b)

Figure 5.28 Stone house: (a) Numerical failure at the base of the south wall and (b) experimental early failure at the base of the south wall

Despite the aforementioned considerations, the initial reference solution, obtained with the integration points at the nodes, is selected here for the rest of the chapter, since it appears more persistently

during the sensitivity investigation and at the same time is the only one that could provide a similar failure mechanism as the final experimental mechanism.

Elastic Base

Similarly with the brick mock-up, cement was also added at the base of the stone mock-up, and therefore the crack formation was avoided at the base (Candeias et al, 2017). Consequently, the base of the model is considered elastic for the case of pushing (-X) of the reference model, since otherwise a solution with failure at the base is obtained (Figure 5.29, Figure 5.30).

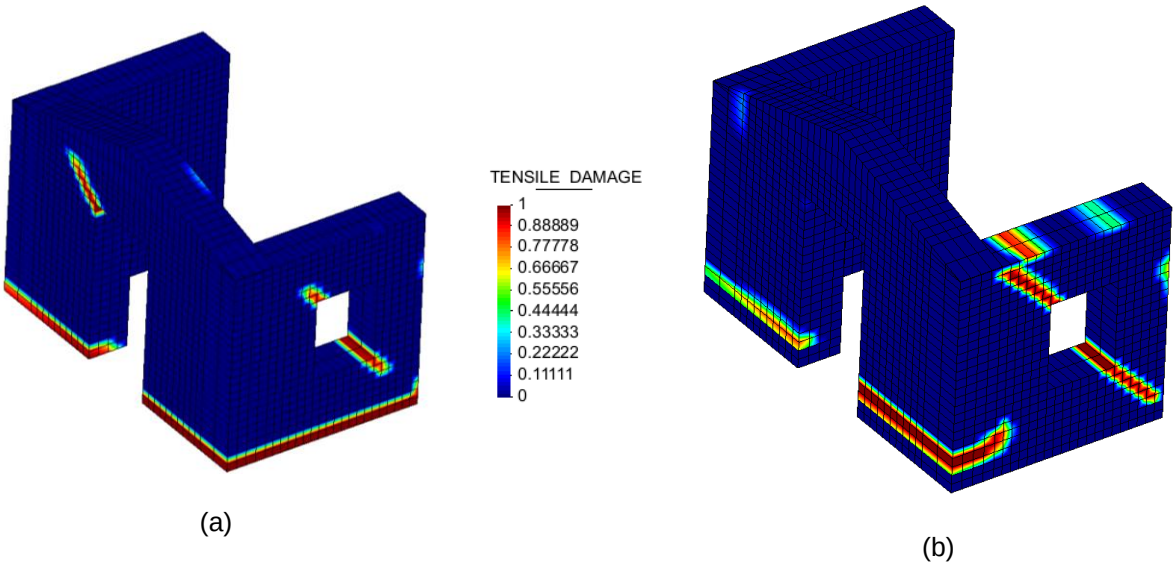

(a) (b)

Figure 5.29 Stone House: Pushing (-X): (a) without an elastic base and (b) with an elastic base

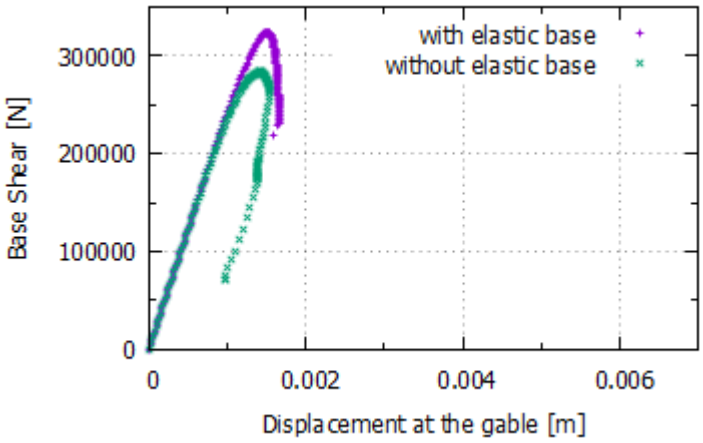

Figure 5.30 Brick House: Pushing (-X): with & without elastic base

Reference model results

Taking into account all the above considerations, the results of the reference model are presented in this subsection.

By looking at the capacity curves of both directions (Figure 5.31), similar outcomes with the brick house can be attained: the structure appears to be more vulnerable in the pulling (+X) direction. For this reason, the crucial for the collapse direction is expected to be the pulling (+X) and therefore its response is firstly studied.

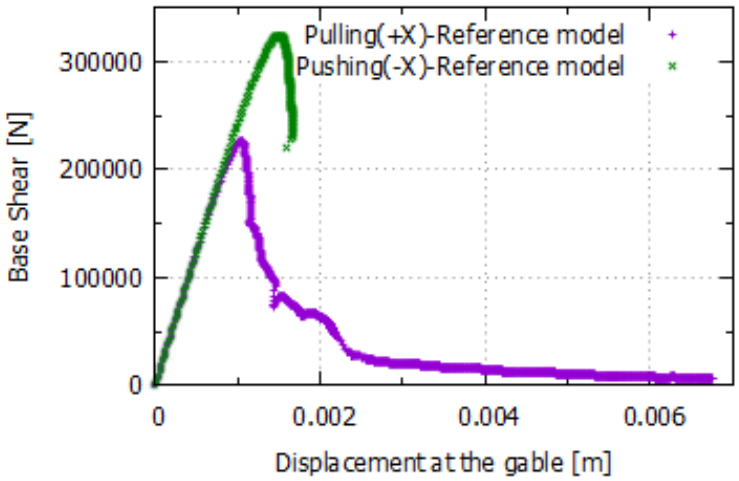

Figure 5.31 Brick House, Reference model: Pulling(+X) and Pushing(-X)

Pulling (+X)

The response of the model subjected to loading in pulling (+X) direction is characterized mainly by two phases: i) the elastic response and initiation of damage until the peak load, and ii) the brittle loss of load capacity and the formation of the collapse mechanism.

Initially, the structure responds almost elastically until the base shear is around 150,000 N. At that point, damage initiates and stiffness starts to decrease until the peak load is reached around 230,000 N. The damage that develops at that early response is presented in Figure 5.32 & Figure 5.33 and described here:

- The facade is damaged only at its base due to the vertical bending, while the tympanum is stressed but not damaged. This relatively lower damage (compared with the brick masonry) is due to the larger thickness of the stone masonry.
- However, the horizontal bending of the facade results also in damaging the connections with the return walls, especially at the top part.
- Both of the return walls have slightly damaged at the west side of their base, due to the in-plane bending.
- The north wall appears to be more vulnerable, with high concentration of strains and damage initiation.
- More specifically, there is a crack starting at the low east corner of the window which will grow diagonally, towards the north-east corner.
- Moreover, the west pier shows some damage initiation at its top corner with the window but also a high stress concentration at its base at the height of the window.
- Finally, the spandrel isn't damaged, but has significant strain concentration at its top east area.

Reaching at the load peak, a closer look is necessary in order to understand the mechanism that finally develops:

- As the damage previously described evolves, several areas develop high concentration of stresses and therefore become possible strain localization areas.
- More specifically, the north corner of the door tries to develop a vertical crack towards the tympanum,
- the connection of the facade with the blind wall develops also significant stresses,
- the top east part of the spandrel appears to be also a critical area.
- However, finally the west pier of the north wall develops significant tensile stresses both at its base and top, leading to a brittle failure.

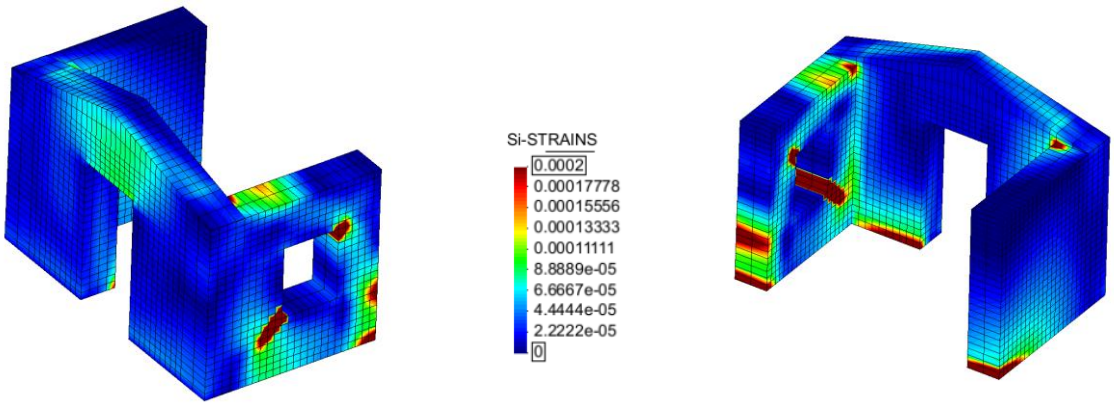

(a) (b)

Figure 5.32 Stone House Pulling (+X): principal strains at peak load (a) NE view and (b) SW view

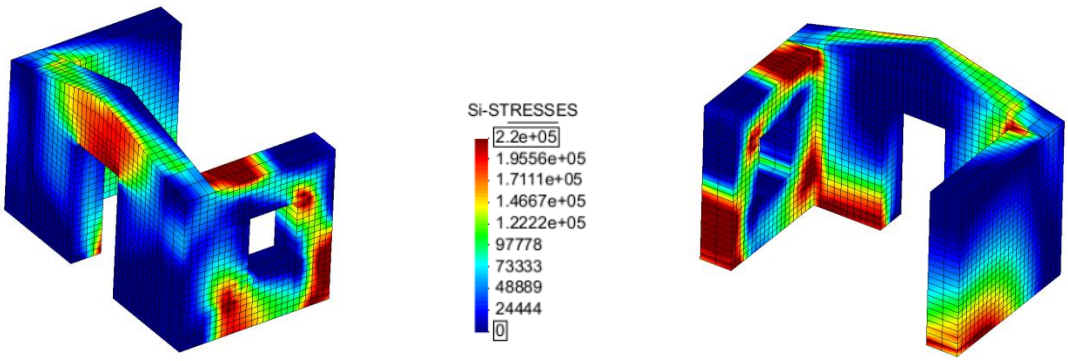

(a) (b)

Figure 5.33 Stone House Pulling (+X): principal stresses at peak load (a) NE view and (b) SW view

As a result of the brittle failure of the west pier, the structure loses notably load capacity and significant stress redistribution is occurring. More specifically, the spandrel of the north wall is unloaded and the whole structure is now having an important torsional response. What's more, the diagonal crack of the east pier of the north wall also advances significantly, reaching and connecting the base crack of the north part of the gable wall. This way, the west pier forms a local mechanism, while a big portion of the north-east corner (including the spandrel, the east pier of the return wall and the north part of the facade) is only weakly connected with the south part of the structure through the gable of the façade. As a result, at the same time amplified by the torsional response, a crack appears at the south top corner of the door and extends until the south top corner of the house, therefore cutting off the connection of the north-east corner of the structure. The results of the analysis are presented in Figure 5.34, Figure 5.35 and Figure 5.36.

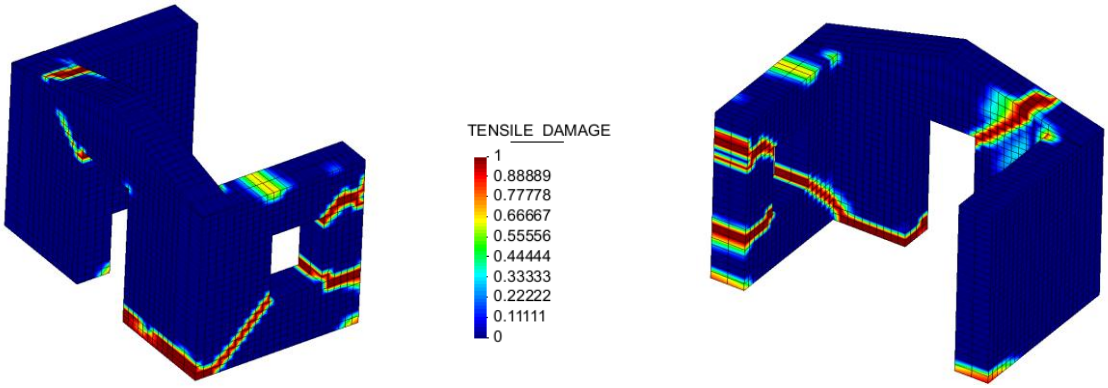

(a) (b)

Figure 5.34 Stone House Pulling (+X): damage at failure (a) NE view and (b) SW view

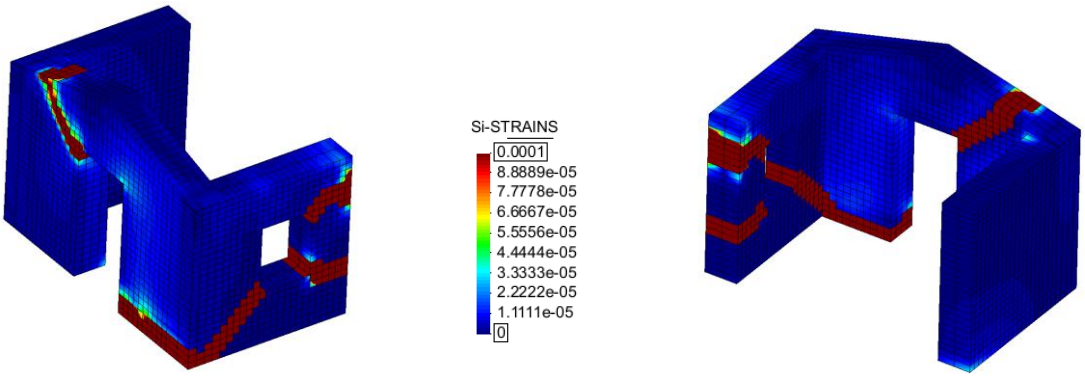

(a) (b)

Figure 5.35 Stone House Pulling (+X): principal strains at failure (a) NE view and (b) SW view

(a) (b)

Figure 5.36 Stone House Pulling (+X) NE view: displacements at failure (a) contour (b) iso-surface

As a result, the collapse mechanism formed includes two macro-elements: the west pier of the north wall and the north-east corner of the structure which in turn includes the spandrel and the east pier of the north side wall and the north pier and gable of the façade.

Pushing (-X)

As already mentioned, the response of the structure is less vulnerable when pushed. The structure responds almost elastically until a base shear of around 250,000 N and reaches a load peak of around 325,000 N.

At this area of the response, damage develops simultaneously in two main parts of the structure (Figure 5.37):

- At the base of the facade, due to vertical bending, and
- at the same time, significant in-plane damage is observed at the north side wall, due to the weakness introduced by the window.
- More specifically, two diagonal cracks develop simultaneously, at the top east and bottom west of the window, towards the corners of the wall

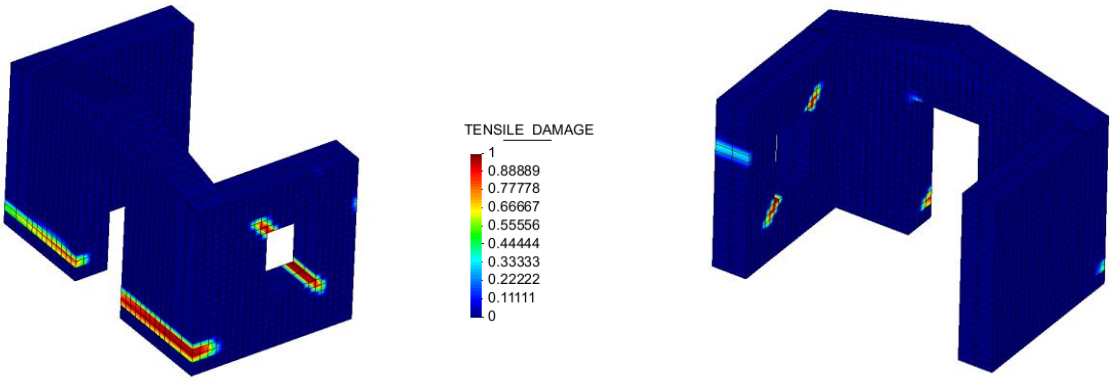

(a) (b)

Figure 5.37 Stone House Pushing (-X): damage at peak load (a) NE view and (b) SW view

As a result, the two diagonal cracks at the north wall develop, causing a loss of load capacity and a brittle failure of the top north-west corner. At that point a local collapse macro-element is formed and therefore the local equilibrium is lost and the analysis stops. The final results of the analysis are presented in Figure 5.38 and Figure 5.39.

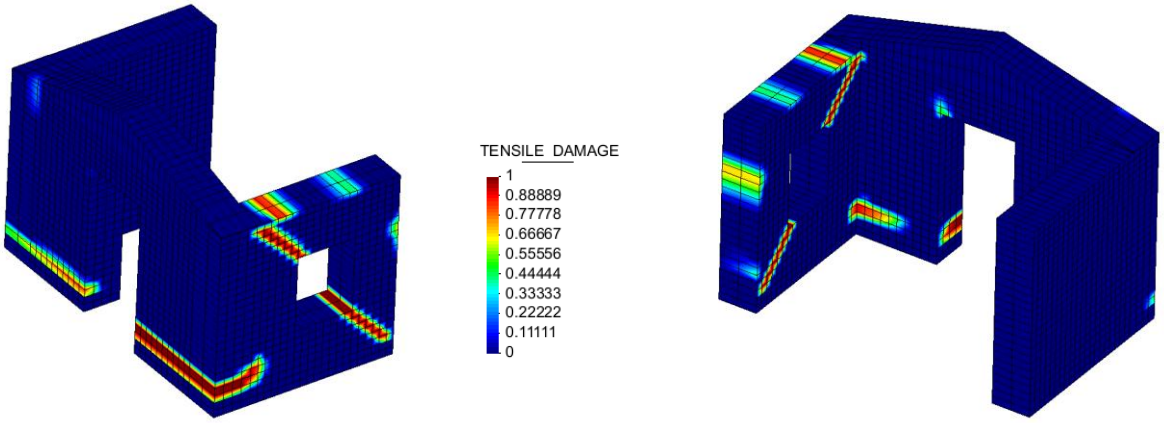

(a) (b)

Figure 5.38 Stone House Pushing (-X): damage at failure (a) NE view and (b) SW view

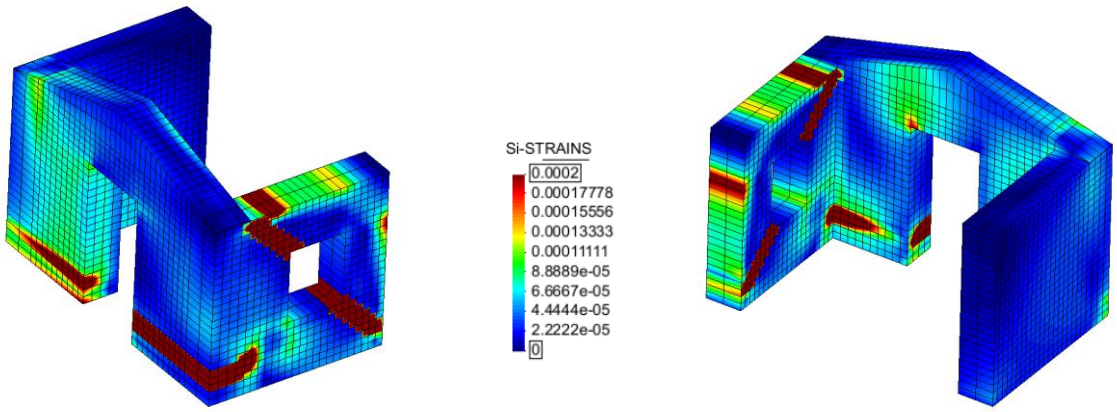

(a) (b)

Figure 5.39 Stone House Pushing (-X): principal strains at failure (a) NE view and (b) SW view

5.2.2 Comparison with Experimental results

In this subsection, the results of the reference model are compared with the results of the experiment in terms of collapse mechanism, PGA and displacements.

Collapse Mechanism

In order to compare the experimental with the numerical collapse mechanisms, a brief summary of the experimental response and failure is presented (Figure 5.40): Besides the initial horizontal crack at the

south wall, the structure started developing cracks at TEST03 and TEST04, while TEST05 marked its ultimate limit state. Already at TEST04, the damage was extended at the north wall, with cracks starting from the corners of the window, and developing diagonally towards the corners of the wall, and significant damage was observed at the façade, dividing it into three parts: north, gable and south. Finally, at TEST05 the collapse process started with 1) the fall of stones at the top west corner of the north wall due to impulses of the lintel and the rocking response of the corresponding pier by a diagonal crack at its base, 2) the rocking response of the east pier initially due to a diagonal crack at the base of the window towards the north-east base corner, and later split into two parts at the height of the window, due to the influence of the lintel and 3) the out-of-plane rocking response of the façade, split in three main parts, the north , the gable and the southern. Finally, we should underline as main influencing points i) the torsional response of the structure due to the weak north side wall, and ii) the important influence of the big lintels that either provided stabilization either “hammered” or stabilized other parts, but also in general the high unit to structure size ratio.

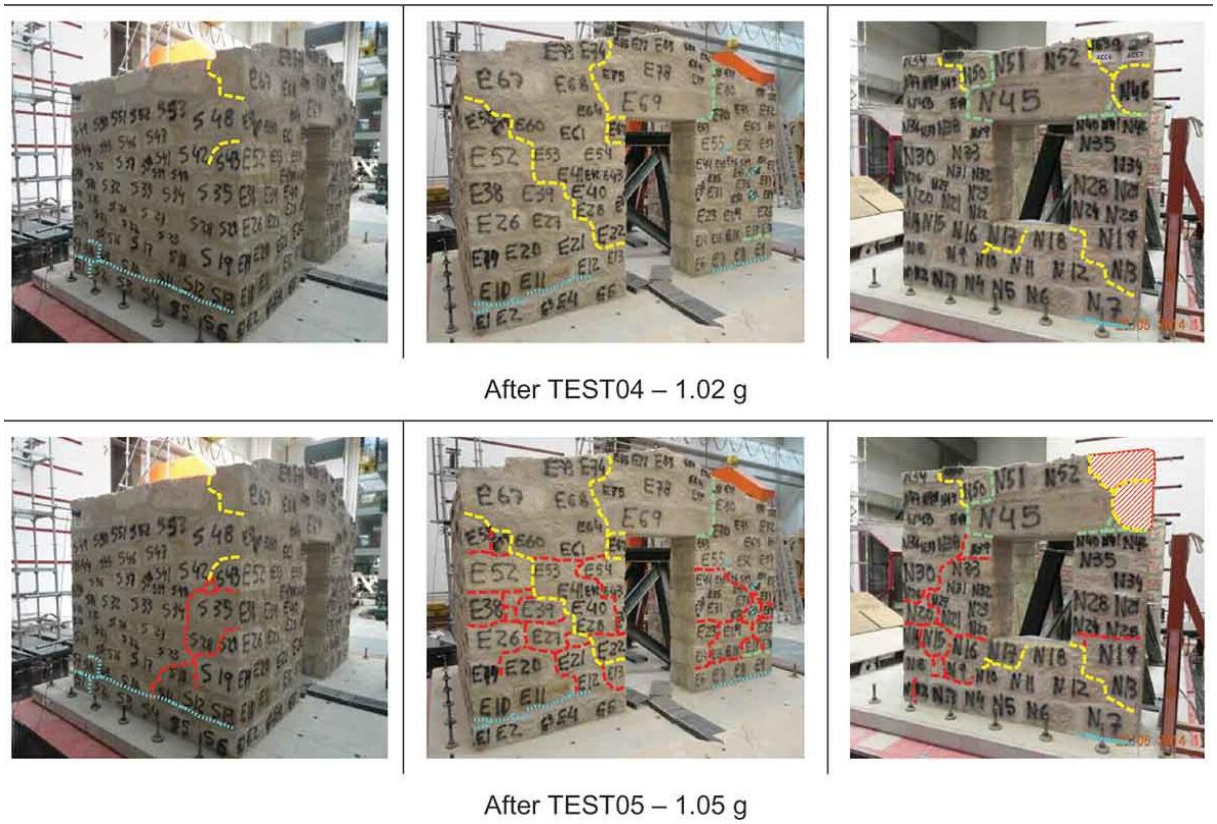

Figure 5.40 Damage evolution and collapse mechanism formation in the Stone structure

(Candeias et al, 2017)

The numerical results obtained with the FEM analysis could reproduce correctly some important aspects of the experimental response, but were also characterized by shortcomings. The comparison is presented in Figure 5.41, Figure 5.42 and Figure 5.43.

More specifically, the initial horizontal damage observed at the base of the structure has been replicated by the numerical model (Figure 5.28), although a straight forward correlation is not certain. More importantly, the in-plane vulnerability and crack development of the north side wall is adequately reproduced by the numerical model, if both directions of the pushover analysis are considered.

However, the main incapability of the model is its continuum homogenized nature, which can't replicate the significant influence of the lintels and in general the high units' size, in combination with the static loading instead of the real dynamic effects taking place in the experiment. More specifically, the impulse and stabilization phenomena created at the north wall changed the initial mechanism formed at the north-east pier, by not allowing the initially formed crack at the lower part of the window to the corner to be the decisive for the collapse mechanism (Figure 5.44), and therefore created a parallel crack motive at a higher level. Moreover, the lintel of the door played also an important role, since it promoted two vertical cracks at its sides and the unconstrained response of three parts of the façade. Finally, the high unit size caused an extensive and distributed damage pattern at the façade, while the numerical model could only provide localized damage patterns.

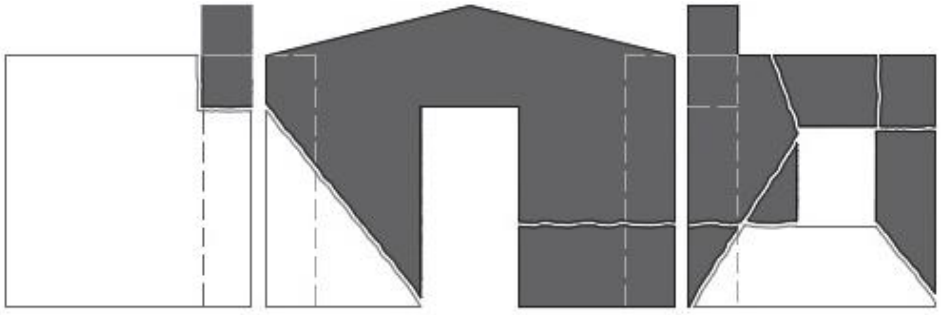

Figure 5.41 Stone house: Experimental collapse mechanism (Mendes et al, 2017)

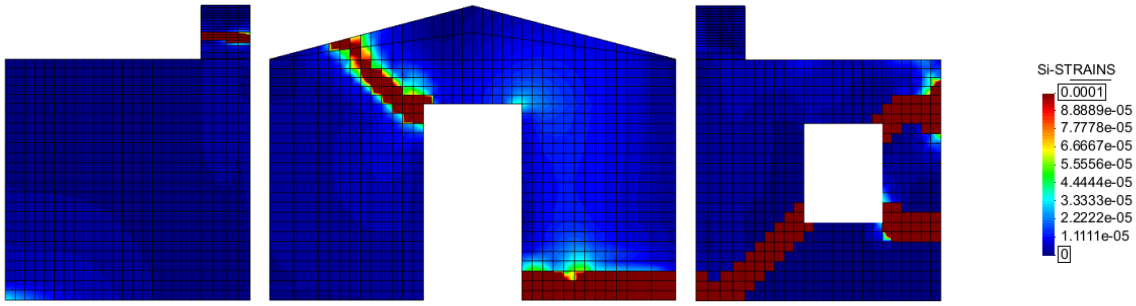

Figure 5.42 Stone house Pulling(+X): Principal strains at failure

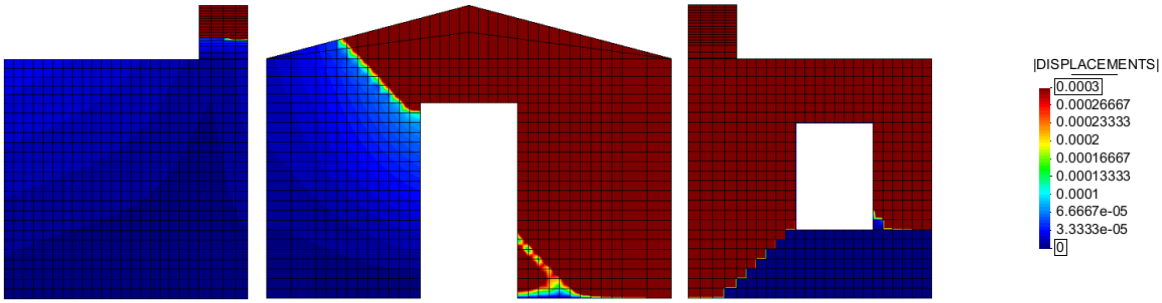

Figure 5.43 Brick house Pulling(+X): Displacements at failure

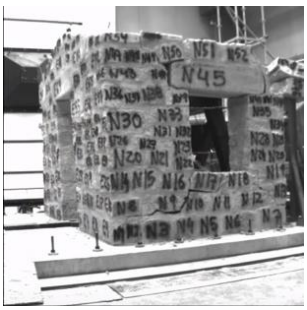

Figure 5.44 Stone house: Snapshot of the shaking table TEST05, showing the initial crack propagation at the low-east corner of the window

Peak load - PGA

A comparison of the numerical and the experimental results in terms of PGA is governed by several difficulties, already presented in the corresponding subsection for the case of brick house (see 5.1.2 Peak load – PGA). As a result any comparison should be considered with care, and is possible only until the collapse mechanism is formed.

According to (Candeias et al, 2017), the collapse mechanism of the stone house started to form at TEST03 and was completed at TEST05 (Figure 3.6). The corresponding base shear of the PGA's of these two TESTs have been plotted together with the pushover curves (). More specifically, the orange line corresponding to TEST03 should highlight the damage initiation of the structure, while the red should indicate the load peak after which the mechanism is formed.

Taking into account all the aforementioned uncertainties and difficulties of this attempt, it can be observed a good correlation between the experimental results and the numerical, specifically for the vulnerable pulling (+X) direction.

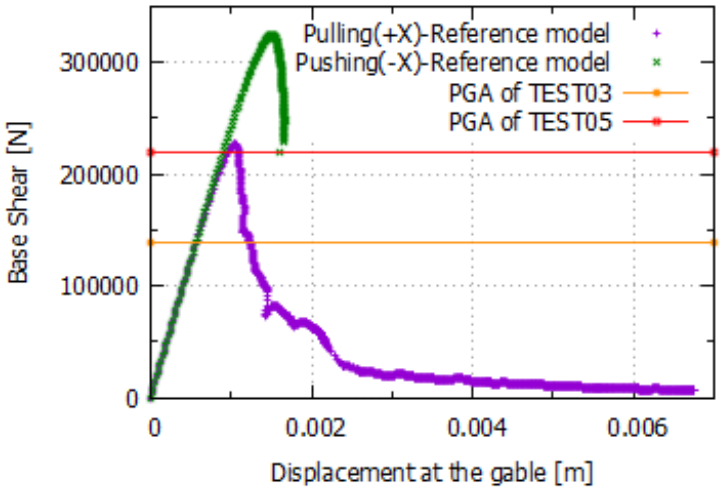

Figure 5.45 Stone House: pushover curves and corresponding PGA's of TEST03 and TEST05

Displacements

An attempt to correlate the numerical results with the experimental ones in terms of displacements would face the same difficulties as the correlation of PGA's. At the same time, the not exact collapse mechanism assessed here plays a significant and sensitive role in the displacement estimation.

Despite all the above, a comparison is attempted here (Figure 5.46), corresponding to completion of the mechanism formation. Similarly with the brick house, the corresponding PGA is selected as the load peak and the displacements at the last point of the capacity curve where the complete mechanism is formed.

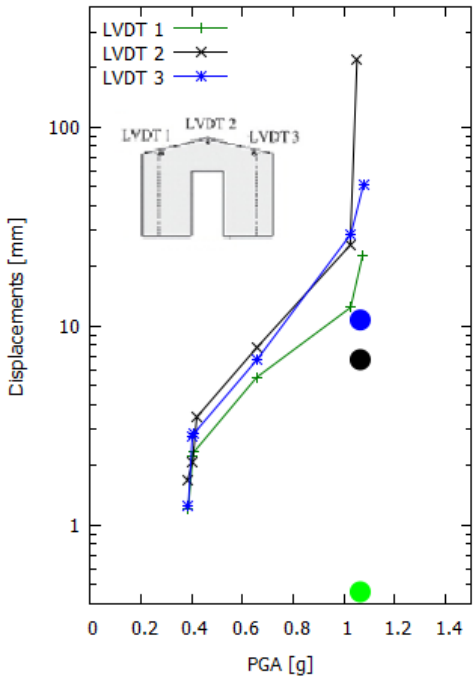

Figure 5.46 Brick house: Displacements of LVDTs during the experiment (lines) & corresponding numerical estimation (dots)

The numerical results appear to significantly underestimate the experimental displacements. As an attempt to provide an explanation of this contrast, some arguments follow. On the one hand, the damage accumulation of the tests history was very high in the stone house, while significant dislocations were observed after each test (Candeias et al, 2017). Moreover, by looking at the damage state of TEST04, we can identify that the collapse mechanism is almost formed, and therefore a much smaller PGA than that of TEST05 would have led to its completion. In addition, significant dynamic amplification of the order of 2 to 3 was observed for the stone house, just after the mechanism formation, in TEST05. Finally, the high divergence of LVDT1 estimation could be explained by the fact

that the numerical collapse mechanism didn't replicate the inclusion of the corner top as in the experiment, while the in-plane response of the blind wall at the experiment was characterized mostly by a rocking than an elastic behaviour due to its initial horizontal crack at its base (prevented in the model, see Chapter 5.2.1).

5.2.3 Comparison with standard elements

The solution obtained using the mixed finite elements is here compared with the solution that is obtained using the standard finite elements, in order to assess the efficiency of the mixed formulation and also identify and point out the shortcomings of the standard formulation that are overcome with the mixed one.

Firstly, a comparison is done in terms of capacity curves in Figure 5.47. Several differences can be identified concerning mainly the load peak of the pulling (+X) direction, the latter divergence in strength during the softening and finally, the different failure obtained for the pushing (-X) direction.

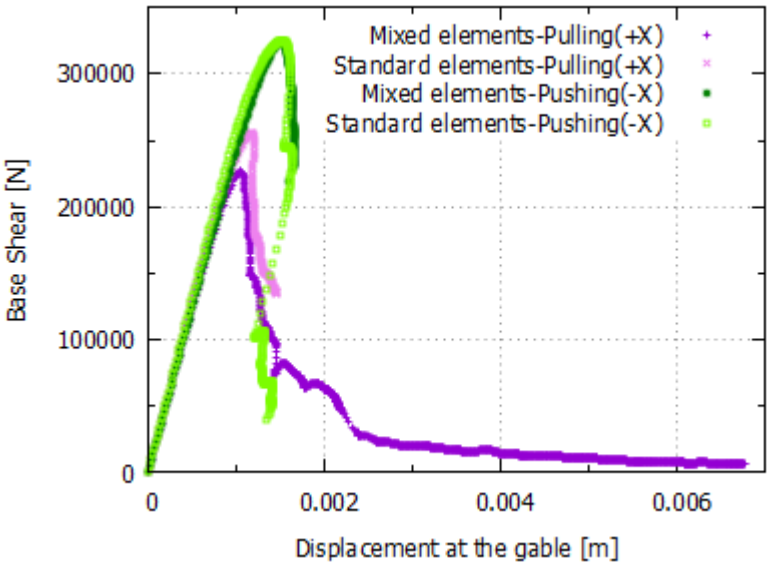

Figure 5.47 Stone house: Capacity curves in both directions for mixed & standard formulation

More specifically, the standard elements present a higher load peak for the pulling (+X) direction and continue similarly at the softening region. This can be more clearly explained by looking also the crack propagation in Figure 5.48. As can be observed, initially, the cracks developing at the west pier are "locked" horizontally, as the mesh orientation for the standard elements, while the corresponding cracks at the mixed elements are more "flexible" during their evolution. Moreover, during the softening region, the standard elements' model is incapable to join the two cracks arriving at the north-east corner, and therefore the crack extending from the side wall is evolving independently at the third layer of elements, due to the mesh orientation. Finally, in the case of pushing (-X), a similar motive is

observed in Figure 5.49, with the horizontal crack developing at the north-east corner not being able to “escape” by the mesh orientation, and as a result a different mechanism is formed, due to the failure at the base, instead of the top north-west corner.

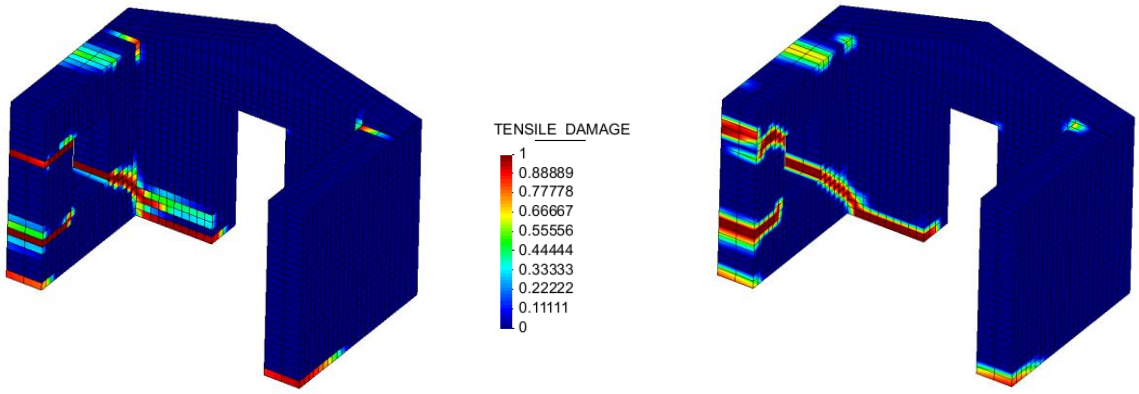

(a) (b)

Figure 5.48 Stone House Pulling(+X) SW view: tensile damage at softening region (a) with Standard elements and (b) with Mixed elements

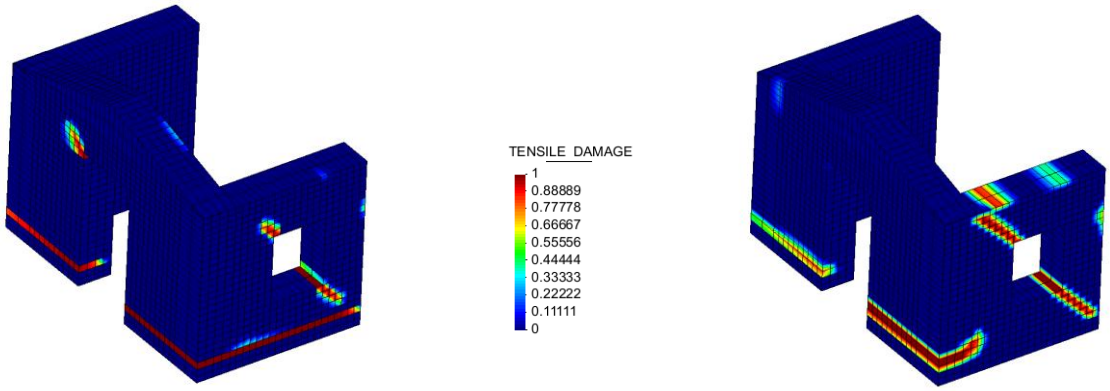

(a) (b)

Figure 5.49 Stone House Pushing(-X) NE view: tensile damage at softening region (a) with Standard elements and (b) with Mixed elements

5.2.4 Comparison with previous simulation attempts

Similarly with the brick house, the results of the numerical model obtained in this study are compared with the results obtained in one of the post-dictions studies (Chácara et al., 2017), in which a similar

modelling technique and analysis strategy were used. Any modelling differences are mentioned for the brick house and therefore are skipped here.

Once more, the comparison between the two different simulations is made both in terms of capacity curves and cracks or mechanisms developed (Figure 5.50 and Figure 5.51).

As a general overview, lower load peaks are achieved with the model developed herein, the damage pattern are comparable, however the capacity curves present a significant difference in the energy dissipation and the complete collapse mechanism is not so clearly formed in the case of the Diana simulation.

More specifically, different initial stiffness is observed for the two simulations, while the possible causes are presented in more detail for the brick house, namely: the different order of elements used and the different integration points' configuration scheme adopted (see Chapter **Σφάλμα! Το αρχείο προέλευσης της αναφοράς δεν βρέθηκε.**). Moreover, a lower load peak is achieved for the model developed in this thesis, especially for the pulling (+X) direction (Figure 5.51). An explanation could be given by looking at the damage pattern: as can be observed the two models develop damage at similar areas, except than the east part of the spandrel, where the simulation developed here doesn't develop significant damage and fails in a brittle way earlier. The same comment concerns the pushing (-X) direction about the damage at the top of the west pier (Figure 5.52). In addition, the models developed with Diana appear to dissipate much more energy during their damage evolution, probably due to the same reason discussed just above.

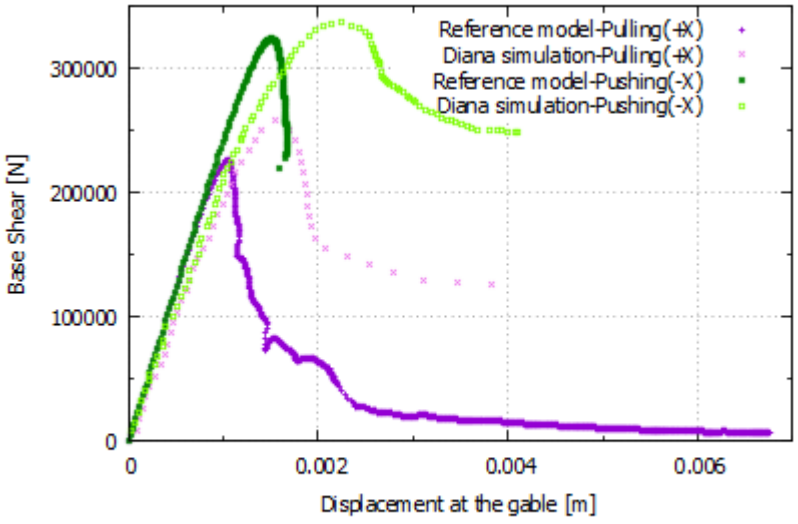

Figure 5.50 Stone House: Comparison of capacity curves of the reference and DIANA simulation

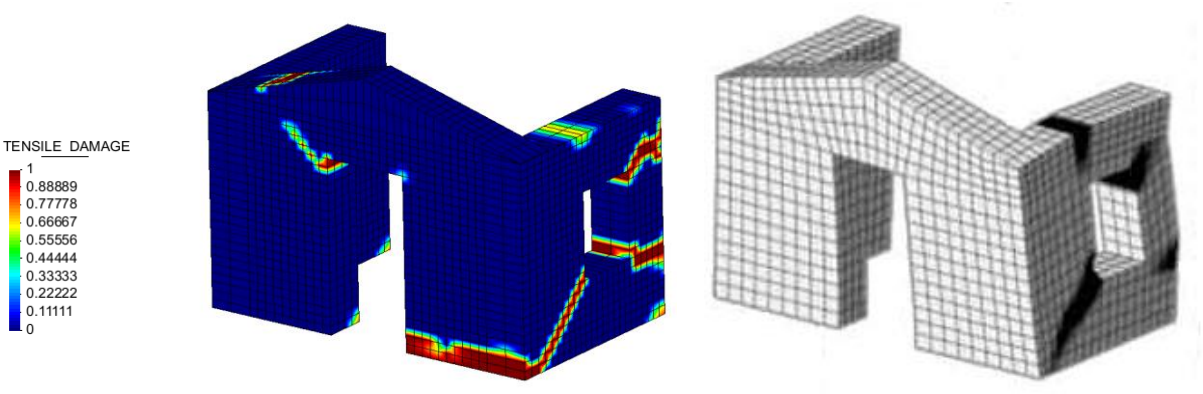

(a) (b)

Figure 5.51 Brick House Pulling(+X): Principal strains (a) reference model and (b) simulation with DIANA

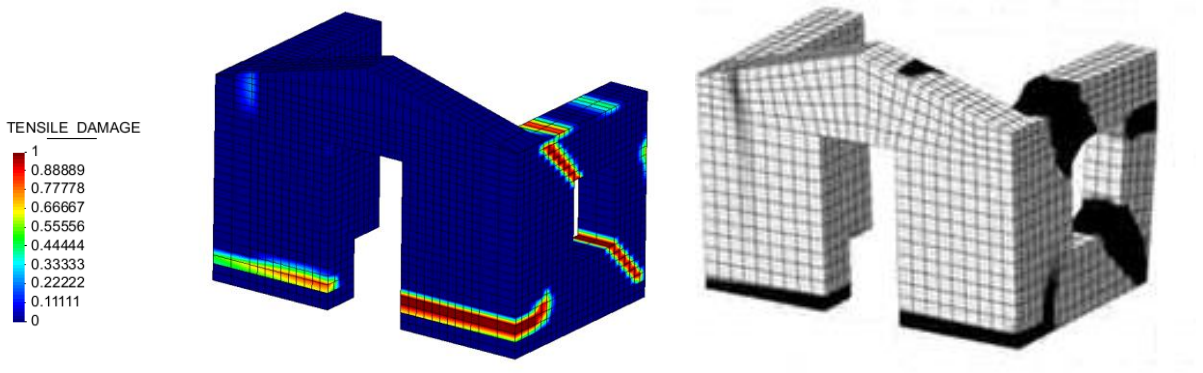

(a) (b)

Figure 5.52 Brick House Pushing(-X): Principal strains (a) reference model and (b) simulation with DIANA

5.3 Sensitivity Analysis

5.3.1 Lintel's effect

The damage evolution of both mock-ups at the corners of the openings (Figure 3.4 & Figure 3.6), indicate a possible influence of the lintels. For this reason, a simple attempt to simulate this influence is presented in this subsection. Only the results of the stone house are shown, since the results of the brick house follow an identical motif.

In order to model the lintel for the stone house (and respectively for the brick house), the corresponding finite elements are assigned with linear elastic properties, to avoid failure, and with a

higher Young modulus of elasticity to replicate the distinct material's properties (Figure 5.53). Specifically for the stone house, two different values used in previous micro-modelling approaches for the stone material (Chácara et al., 2017; Gams et al. 2017) are tested, namely 31.5 GPa and 50 GPa. Nevertheless, both values provide identical results and therefore only one case is presented here. Finally, it should be underlined that none intermediate material, or interface is used between the lintel and the masonry.

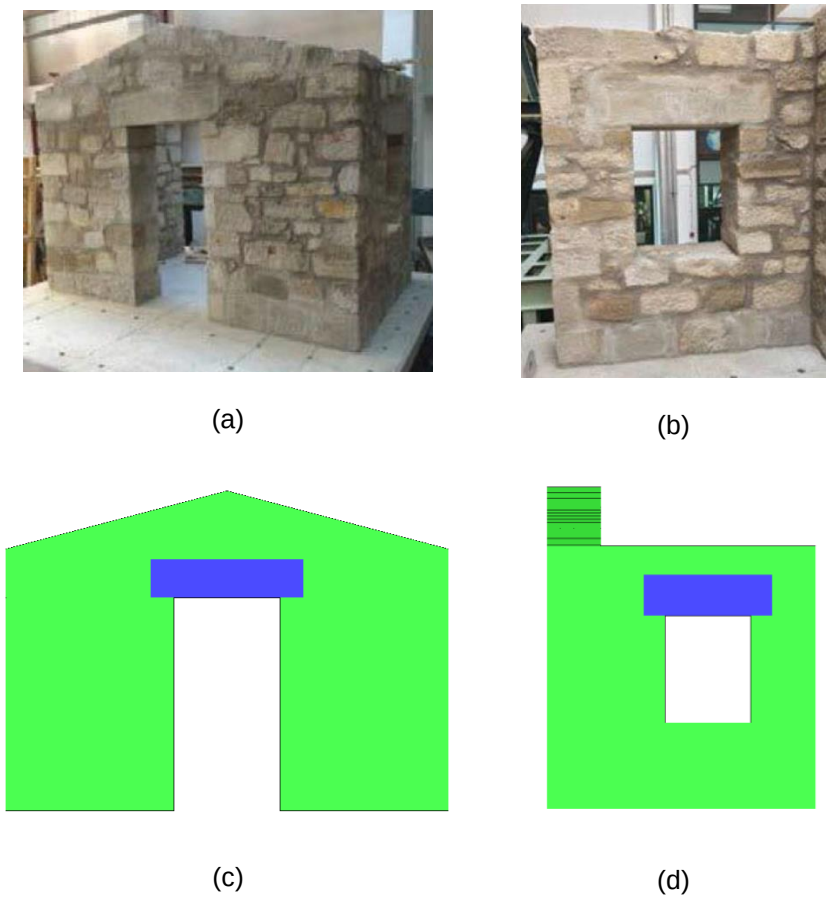

(a) (b)

(c) (d)

Figure 5.53 The lintels of the stone house (a) & (b) as built, and (c) & (d) as modelled

In general, the results of the lintel's simulation and the reference model are almost the same. More specifically, the capacity curves are identical and therefore a presentation and comparison is skipped, while the only remarkable difference appears in the damage/strain pattern, presented in Figure 5.54 and Figure 5.55.

In the case that the lintel is distinctly simulated and pulling (+X) is examined, at an early stage of the response (after the damage initiation, but before the load peak), stresses and strains concentrate at the two corners of the lintel at the façade (Figure 5.54 (b) comparable with Figure 5.32). However, on

the one hand this damage doesn't increase significantly (low values of damage index in Figure 5.55 (a)), and on the other hand, when the response reach the peak load and the north wall loses its capacity, the damage around the lintel stops to develop anymore (since the restrain of the north wall is lost, and the façade is not bending horizontally anymore). As a result, the final collapse mechanism obtained is identical with the reference model (Figure 5.55 (b)).

Exactly identical results are also obtained when pushing (-X) is examined, and therefore the detailed presentation is skipped.

Finally, by comparing these results with the experimental response (Figure 5.54 (a)) we can observe that:

- a better representation of the damage around the lintel is achieved for early damage stages, when the lintel is simulated,
- however, this damage doesn't affect the global response of the structure, which appears to happen, to some extent, in the experimental case.

Concluding, the effect of the lintel is not crucial within the framework of a static analysis that is performed here.

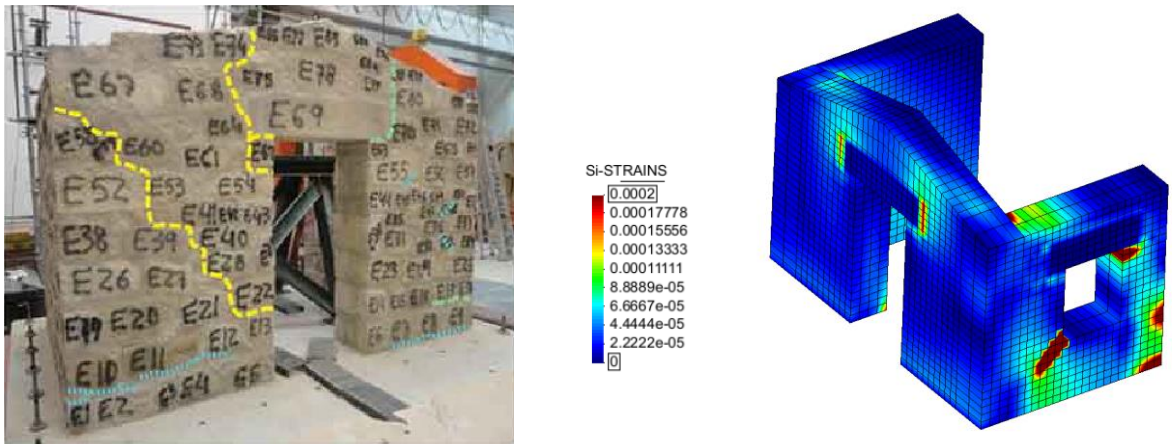

(a) (b)

Figure 5.54 Stone house: (a) damage after TEST04, (b) principal strains when pulling (+X), including the lintels

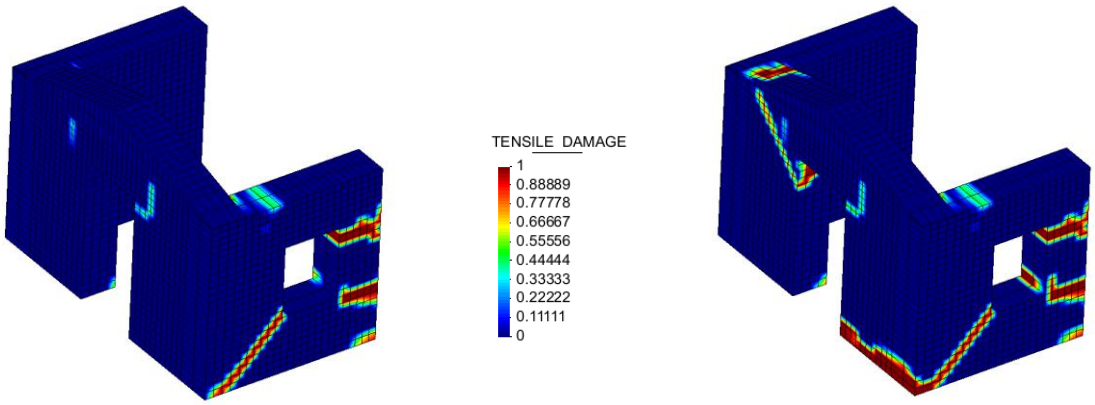

(a) (b)

Figure 5.55 Stone house, including the lintels: damage when pulling (+X) (a) at early stage and (b) at failure

5.3.2 Orthotropic damage model

As already mentioned, an isotropic damage model is used for the reference analysis, since a monotonic loading is being applied to the structure. Although in order to assess this choice, a comparison is also done with an orthotropic damage model (Cervera et al, 2003). For this reason, in order to gain a more clear understanding of the two different damage models, a simple example of a single element is done and presented in the Annex. The main points of this example are the following: i) under monotonic tension or compression test, the two damage models show identical behaviour, ii) under monotonic shear test, the orthotropic damage model retains more strength in the inelastic regime, which never diminishes completely, since no compressive damage is considered iii) when cyclic loading is considered, the orthotropic damage model is stiffer both in Mode 1 or Mode 2 loading, if damage has been previously developed. The numerical explanation of the above outcomes derives from the fact that the isotropic damage model damages the whole stress/strain tensor, while the orthotropic model damages only the tensile part of it in order to replicate the unilateral nature of such materials.

Moving to the analysed structure, the capacity curves that are obtained with both damage models are presented in the Figure 5.56 and Figure 5.57. Generally, the two damage models present very similar response, although not identical. More specifically, firstly the isotropic damage model demonstrates higher load peak behaviour and secondly the orthotropic damage model appears to be retaining more strength in the softening region. Taking into account the point (ii) mentioned above, the second outcome can be easily understood, while the first one seems controversial. Therefore a closer look at the results is necessary, in order to find an adequate explanation or interpretation. More specifically, a

step by step monitoring of the results around the load peak seems necessary, since it appears to be the area of differentiation.

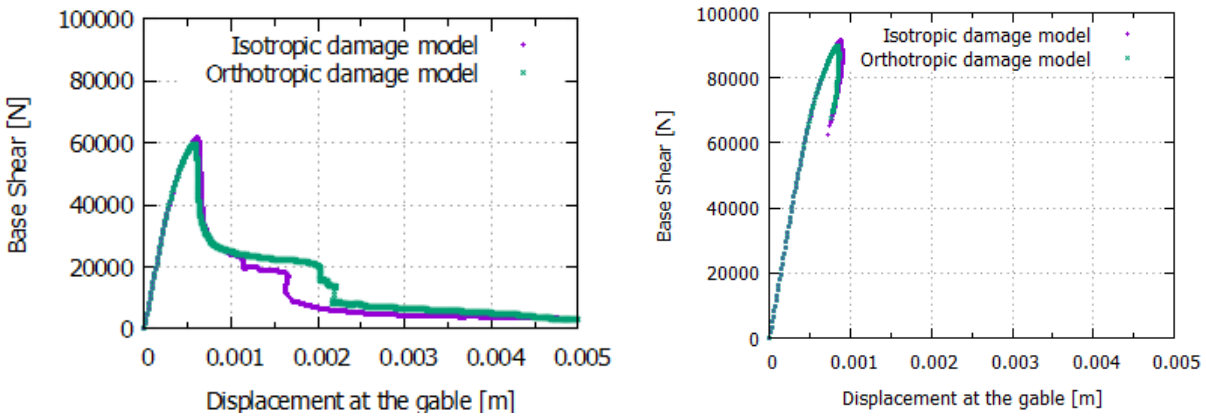

(a) (b)

Figure 5.56 Brick house: Isotropic & Orthotropic damage model (a) for pulling (+X) and (b) for pushing

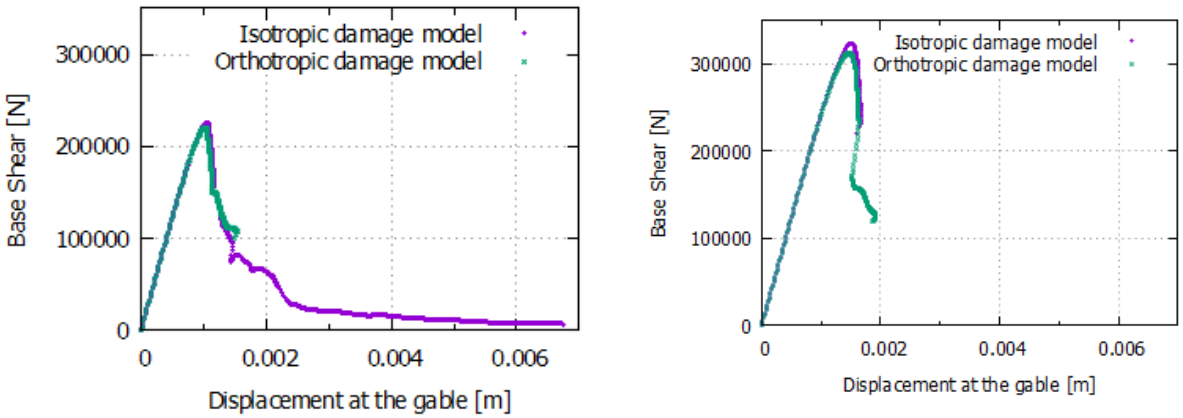

(a) (b)

Figure 5.57 Stone house: Isotropic & Orthotropic damage model (a) for pulling (+X) and (b) for pushing

For simplicity reasons, only one case is presented in detail, the brick house in pulling (+X), while identical reasoning implies to the rest cases. An explanation of the results is given by looking after two crucial points of the forming mechanism, namely the diagonal crack at the low-east side of the window at the north side wall, and the east part of the corresponding spandrel. Figure 5.58 presents the strain values of these two crucial points when using the two different damage models, around the load peak.

These results combined with the aforementioned summaries of the Annex, can reveal the interpretation. Starting by the diagonal crack at the low corner of the window, it is observed that the orthotropic damage model develops less strain, exactly as expected by the point (ii), since it has more retaining strength. At the same time, the crack at the spandrel of the window appears due to bending and is therefore subjected mainly to monotonic tension. As a result both damage models should present the same retaining strength, according to point (i). However, in the Figure 5.58 the strains are higher for the orthotropic damage model. This can be explained by the different stiffness of the inelastic regime of the two models, which is present only at the shear crack, since no compressive damage is considered (ii): as a result, stresses redistribute and concentrate more in areas where the stiffness is even. Consequently, damage accumulates quicker in the spandrel for the orthotropic damage model, which is also the responsible element for brittle loss of capacity. In other words, the stiffer shear part of the orthotropic model leads to easier (or earlier) accumulation of damage at the areas that are under tension; which have the same stiffness for both models. Or physically speaking, orthotropic damage models, which don't consider any compressive damage, promote failure mechanisms that depend on tensile failure, if shear damage is also present. Particularly for the structure analysed here, the former case applies, since the failure mechanism is triggered due to the failure of the spandrel.

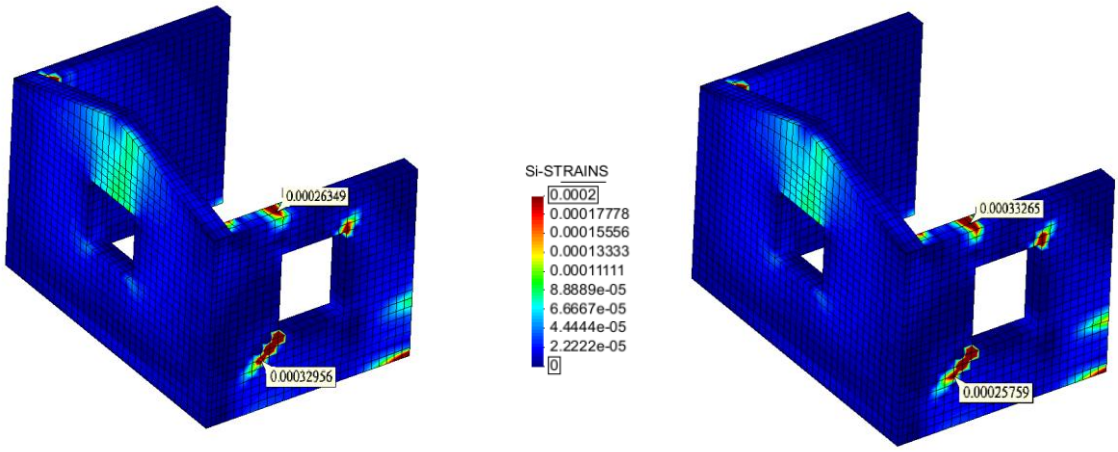

(a) (b)

Figure 5.58 Brick House (+X): principal strains (a) for Isotropic damage model and (b) for Orthotropic damage model

5.3.3 Stabilization parameter

The only additional input parameters needed for the mixed finite element formulation is the stabilization parameter τ_ε, presented in Subsection 2.2.2. It's a necessary parameter in order to ensure a stabilized solution; however, its value is not yet well established, since an arbitrary number is

necessary for its definition (Cervera et al., 2004; Cervera et al. 2010a; Benedetti, 2017). An attempt to define a correct value is far beyond the scope of this thesis, and therefore a simple sensitivity analysis is only performed, in order to have a more practical understanding of the influence of the parameter to the results.

Three different values of the parameter are examined, namely the reference value of 0.1, a limit value of 0.99 that tends to give similar results with the standard formulation, and an in between value of 0.5. All the cases are subjected to this parametric analysis and their results are presented in Figure 5.59 and Figure 5.60. In all cases, the damage evolution is identical, and therefore only the capacity curves are presented here.

The graphs clearly shows that as the value of τ_ε increases, the structure behaves stiffer, has a significantly higher load peak and dissipates more energy, tending to obtain a similar solution with the standard FE formulation.

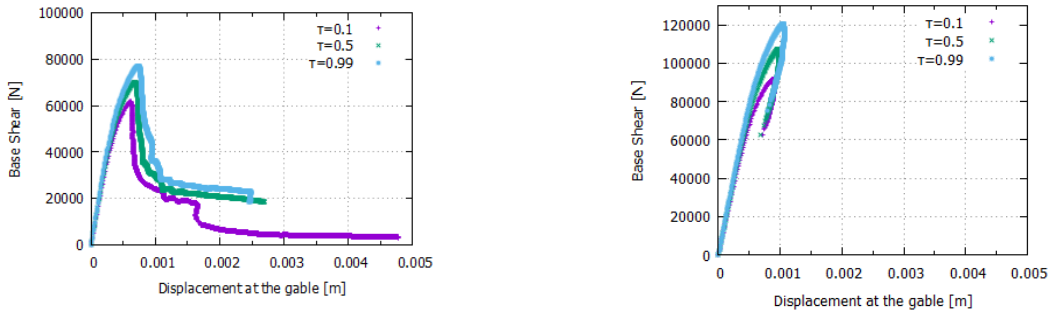

(a) (b)

Figure 5.59 Brick House: Sensitivity analysis of the stabilization parameter τ_ε for (a) pulling (+X) and (b) pushing (-X)

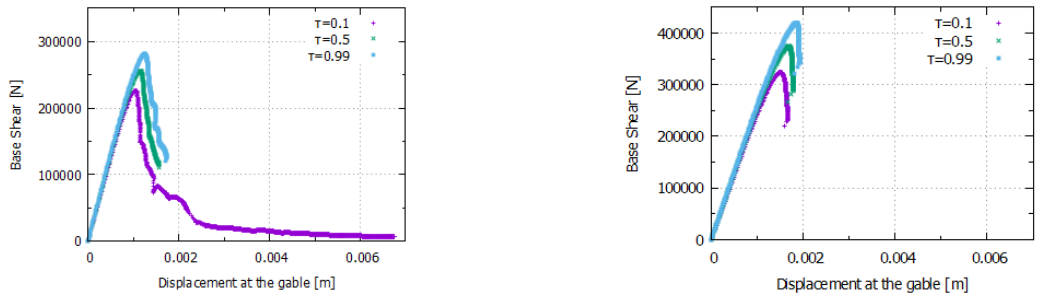

(a) (b)

Figure 5.60 Stone House: Sensitivity analysis of the stabilization parameter τ_ε for (a) pulling (+X) and (b) pushing (-X)

5.3.4 Computational cost

The advantages that the mixed strain/displacement elements present compared with the standard displacement based elements have been clearly shown in Subsections 5.1.3 and 5.2.3. However, this enhanced strain accuracy comes with an increased computational cost, since 9 instead of 3 unknowns are present at each node. On the other hand, the increased accuracy in such high non-linear problems sometimes leads to less iterations needed in order to achieve convergence. Nevertheless, the possible use of any computational tool should always be characterized by a reasonable computational cost, always relevant with the problem examined. For this reason, a simple comparison of the results obtained here is presented in this subsection, followed by a discussion of the future possibilities of such advanced techniques.

The numerical analyses are run on a desktop computer with 4 GB of RAM and a dual core CPU clocking at 2.66 GHz. Moreover, the brick model is composed by 5100 elements and a total number of 7428 nodes, while the stone house by 4712 elements and 6931 nodes.

Since each analysis of each case arrives at a different point of the solution and the comparison should be consisted, the results compared here are chosen in order to have a reference point at the capacity curves. In more detail, for the case of the brick house in pulling (+X) a reference value of displacement of 4 mm is chosen and in pushing (-X) and the final obtained points of the solution are compared. For the stone house in pulling (+X), the last point achieved with the standard elements is chosen with its corresponding in the mixed elements' solution, while for the stone in pushing (-X), the peak load is chosen as more representative, since a different mechanism is afterwards evolving.

The comparison is done in terms of CPU time (in seconds) needed and RAM memory requirements (in MB), and is presented in Table 4.

Table 4 CPU and RAM requirements for mixed and standard finite elements

	Case	Formulation	pseudo-time steps needed	CPU (seconds)	RAM (MB)
Brick House	pulling (+X)	Mixed	3241	4165	31.34
		Standard	3614	1474	22.21
	pushing (-X)	Mixed	283	500	31.64
		Standard	327	151	22.32
Stone House	pulling (+X)	Mixed	244	453	29.37
		Standard	231	106	20.67
	pushing (-X)	Mixed	99	215	29.65
		Standard	115	38	20.79

The average values of the above table show an increase of CPU time needed of 300% and 42% of RAM memory.

At this moment, it is clear that the mixed formulation can provide a more consistent solution but with a relatively increased computational cost needed. Therefore, a strategy that could reduce this cost but keep the precision high would be of great importance. In fact, the first steps of this development have already been done in recent works (Benedetti, 2017; Benedetti et al., 2017) and are based on the important capability of the mixed formulation of being compatible with the standard formulation (Figure 5.61). More specifically, due to this compatibility, the mixed elements can be used a priori in areas that damage is expected to appear, while standard elements can be used elsewhere, managing to reduce therefore significantly the computational cost needed. Moreover, a possible future strategy could be to automatically call and substitute the standard elements with the mixed, in areas of strain localization, and therefore avoid any a priori guess.

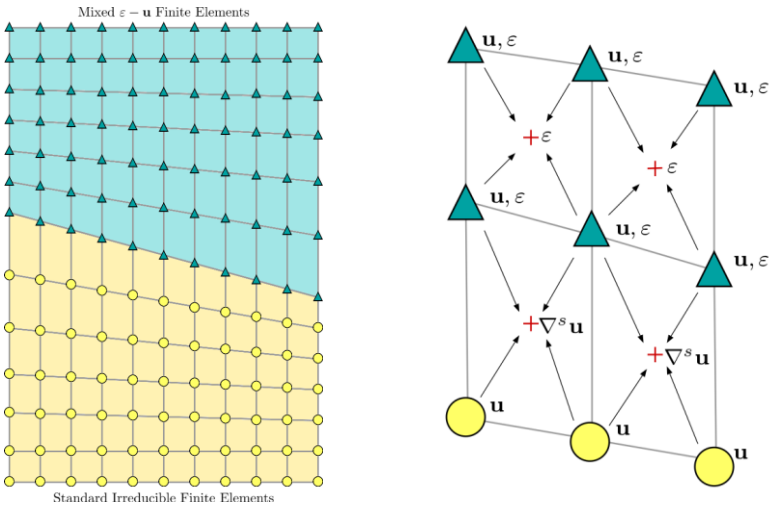

(a) (b)

Figure 5.61 FE mesh with combined standard and mixed formulations (Benedetti, 2017)

6. CONCLUSION

6.1 Summary of the adopted methodology

The out-of-plane response is a complex and at the same time crucial aspect of the seismic vulnerability of masonry structures. It depends on several factors, some of which are the material properties, the quality of the walls, the geometry of the structure, the connections between structural elements and the stiffness of the diaphragms. Despite its importance and due to the related difficulties, there is still lack of a robust and straightforward assessment technique. More specifically, although the tools available may significantly contribute to the estimate of seismic safety of existing masonry structures, they appear themselves either extremely sophisticated and costly, either not yet completely sufficient for a refined prediction of the failure mechanism and a reliable estimate of the seismic displacement demand. Bearing in mind the above, the objective of this thesis is to explore the possibilities of a novel finite element technique for the assessment of the out-of-plane response of masonry structures.

A full scale experimental campaign of two masonry structures subjected to shaking-table test is chosen here as case study (Candeias et al, 2017). The main characteristics that played a decisive role on the response of the mock-ups were the effective wall-corners connections, the weak north wall that led to torsional behavior, and finally the presence of the opening at the façade. As a result, a combined both in-plane and out-plane mechanism appeared in both cases.

A finite element macro-modelling approach is adopted in the thesis, considered as an adequate method for modelling the non-linear response of masonry structures, in compromise with a reasonable computational cost and input parameters needed. Furthermore, the non-linear static analysis (pushover) is used here as a simple but sufficient tool that can provide an assessment of the collapse mechanisms that might form, if applied in all directions.

However, macro-modelling approaches usually results to the non-realistic representation of localized cracks and to the dependency of the numerical solution to the used finite element mesh. This mesh bias dependency problem has caught the attention of many researchers in the last decades, and recently the mixed strain/displacement finite element formulation has been proposed as a remedy. The main characteristic of the mixed formulation is that it is intended to estimate also the strains, in addition to the displacements. Therefore, an enhanced accuracy for the strains is achieved in strain localization and crack propagation problems, leading to more correct assessment of the load peak, the crack path and the failure mechanism. As a result, due to the advantages that the mixed formulation has shown both in theory and practice, it is adopted for the highly non-linear problem examined here, being at the same time the first real-scale application.

Nevertheless, several shortcomings characterize the general methodology adopted and their influence should be underlined before any results are presented. More specifically, 1) a finite element model is

not capable of reproducing rocking phenomena, while 2) a macro-modelling approach excludes the ability to represent phenomena related to the units' lay-out, i.e the anisotropic behaviour of masonry, lintels' effect, interlocking of units, high unit/structure size ratio of the stone house etc. Moreover, the pushover analysis 3) due to its intrinsic static monotonic nature, is not able to reproduce any inertial dynamic effects and cyclic damage accumulation, while 4) a complete ability of the analysis to predict the exact collapse displacement, cannot be claimed; since such a task cannot be achieved by a numerical tool that might lose its convergence due to loss of stability/equilibrium in the horizontal direction, while it is the vertical one which is in the end the determinant factor for the collapse or not of the structure. In addition, 5) the experimental procedure included a sequence of 8 steadily increasing excitations until the collapse, with the damage accumulating at every step, while the numerical simulation involves only one excitation until the loss of stability. Finally, 6) as identified by (Costa, 2012), the specific characteristics of the ground motion may significantly influence the out-of-plane behavior, while a pushover analysis would always provide the same results.

Considering all the above, the main objectives of the thesis are defined as:

- To assess the proposed model by comparing it with the experimental results, mainly in terms of collapse mechanism, and secondly in terms of peak load and displacements.
- To assess the performance of the mixed finite elements by comparing with the results obtained with the standard elements, in order to highlight the advantages claimed by the former.
- To assess the proposed model by comparing it with a previous similar attempt, where the DIANA software was employed.
- To perform sensitivity analyses and examine the influence of secondary parameters, such as the stabilization parameter, the damage model used or the lintel's effect.

6.2 Conclusions

Starting with the comparison of the proposed models with the experimental results in terms of collapse mechanism, a good overall estimation is observed, since similar portions of the structure are included, while several local differences are mainly attributed to the aforementioned shortcomings. More specifically:

- Both numerical models are able to replicate correctly the vulnerability of the structures in the pulling (+X) direction
- The in-plane response and early failure of the weak side walls, including the created torsional effects, are correctly represented in the numerical simulations,
- The numerical models can't reproduce correctly the out-of-plane damage created around the openings of the facades,

- In the case of the brick house, the horizontal crack at the north-east corner can't be reproduced by the model and instead a diagonal crack appears. This is attributed to the orthotropic behavior of the brick masonry which is neglected at the numerical model,
- The numerical tool employed is unable to replicate the secondary mechanism that was activated in the brick house, since it is incapable to simulate rocking phenomena and therefore a possible secondary mechanism formation within an existing one.
- In the case of the stone house, the high unit to structure size ratio had a significant influence on the response, leading to either stabilization phenomena, either to spread damage distribution. On the other hand, the numerical model is unable to replicate all the above, due to its continuum nature. However, the similarity of the crack propagation before the former effects is notable (see Figure 5.44).
- Finally, the crack which appeared at the base of the blind wall of the stone house, although not clearly explained at the experiment, is also indicated by the numerical model.

A comparison of the experimental and the numerical results in terms of PGA, being possible only until the collapse mechanism formation, is also attempted. Two damage states are compared: the damage initiation and the completion of the collapse mechanism formation. Despite the several difficulties that characterize such an attempt, a very good correlation is obtained for both structures.

Furthermore, for the case of displacement comparison, satisfactory results are obtained only for the brick house and not for the stone. More specifically:

- A sufficient agreement of the acquired displacements is observed for the brick house, while the small differences can be attributed to the secondary mechanism formed,
- On the contrary, in the case of the stone house, the numerical model appears to underestimate the experimental displacements, while a possible explanation can indicate the significant damage accumulation and dislocation created by the test sequence during the experiment. At the same time, the high divergence of the south part of the façade is attributed to the small local difference of the mechanism and the rocking response of the south wall due to the base crack, neglected in the reference model.

The enhanced accuracy provided by the mixed formulation is highlighted by comparing the results with the standard formulation. Specifically, the standard formulation presents higher stiffness, higher strength and significant retaining strength at the softening region, since some cracks are "locked" by the mesh orientation. On the other hand, the results of the mixed formulation don't appear to suffer by any mesh dependency, justifying their superiority.

Finally, the results of the developed models are set side by side with a previous simulation attempt (Chácara et al., 2017), in order to investigate possible shortcomings or advantages of both models. As

a general view, the two different simulations present almost similar response until the peak load, but then the solutions diverge, with the DIANA simulation retaining strength and dissipating much more energy, in contrast with the brittle loss of capacity by the herein developed model. More specifically:

- In the case of the brick house, although the solutions of the two models are in good agreement until the load peak, then a difference mechanism starts to develop, focused at the façade and the corners in the case of DIANA and at the north wall in the herein developed model.
- For the case of the stone house, the mechanism formation is similar, but a much higher retaining strength is again observed.
- In the end, if the identification of the collapse mechanism is set as the main task of this modelling strategy, then the herein developed model can be claimed to be more adequate for its purpose.

Furthermore, the lintels' effect is examined by simulating them with distinct material parameters. A better representation of the damage is achieved for early damage stage, however, the final global response is not influenced.

Regarding the damage model, an isotropic damage model is used in the reference model, since a monotonic loading is applied. However, in order to assess this option, a comparison with an orthotropic damage model, which can simulate the crack re-closure, is done. The results of the analyses are almost identical. However, an unexpected slightly higher load peak of the isotropic damage model is noticed and is further investigated. Therefore, as an outcome, it is pointed out that orthotropic damage models, which don't consider any compressive damage, promote failure mechanisms that depend on tensile failure, if shear is also present, as is also the case of the examined structures.

Since the only additional parameter needed by the mixed formulation, namely the stabilization parameter τ_ε, is not well established yet, a sensitivity analysis is implemented in order to study its influence on the final results. Three values are studied which cover its possible range. The results of the analyses show that as the value of τ_ε increases, the results tends to the standard FE solution.

The last part of the thesis consists an investigation of the additional computational cost needed by the mixed elements, compared with the standard. The comparison is done for all analyzed cases, in terms of RAM memory and CPU demand. An average increase of around 300% of CPU and 42% of RAM is observed, highlighting that the mixed formulation can provide a more consistent solution but with a relatively increased computational cost needed.

6.3 Future works

The workflow of this study has highlighted several shortcomings of the adopted methodology, and therefore a possible future work on the topic could focus to overcome them. Some of the possible research lines could be:

- the use of modeling strategy that could replicate the orthotropic material behavior of the masonry, or at least an orthotropic damage model with distinct damage criteria under tension and compression. Such a development could be done either within the macro-modelling framework, either with a different scale model, such as micro-modelling. Several models have already been proposed for such considerations (Lourenço 2000; Trovalusci & Masiani, 2003; Pela et al, 2011; Petracca et al, 2017), coming of course with a higher computational cost, and the need of knowledge of the anisotropic properties of the materials.
- To implement and perform a dynamic analysis, in order to overcome all the drawbacks arising by the use of a static and monotonic analysis. It is somehow the "natural continuation" (Benedetti et al, 2017) of the development of the mixed formulation to be implemented for dynamic problems, and the advantages are expected to be significant.
- To create a strategy that could reduce the additional computational cost of the mixed elements. A first discussion is already done in Subsection 5.3.4, and can be based on the compatibility of the mixed elements with the standard. Therefore, a possible strategy could be to automatically call and substitute the standard elements with mixed, in areas of strain localization, in order to enhance locally the accuracy, and at the same time minimize the additional computational cost.
- To combine the present methodology with other existing methodologies, towards an holistic technique for the seismic assessment of masonry structures. As is pointed out, the main advantage and contribution of this work is to identify correctly the collapse mechanism of a masonry structure. At the same time, several of other existing methodologies present as their main shortcoming the definition of the collapse mechanism, as a premise for any application (see Section 1.2). Therefore, a combination of the presented methodology with such methods could create a complete and straightforward procedure. An example of this possible development is given based on the flowchart proposed by Costa, 2012 in Figure 6.1.

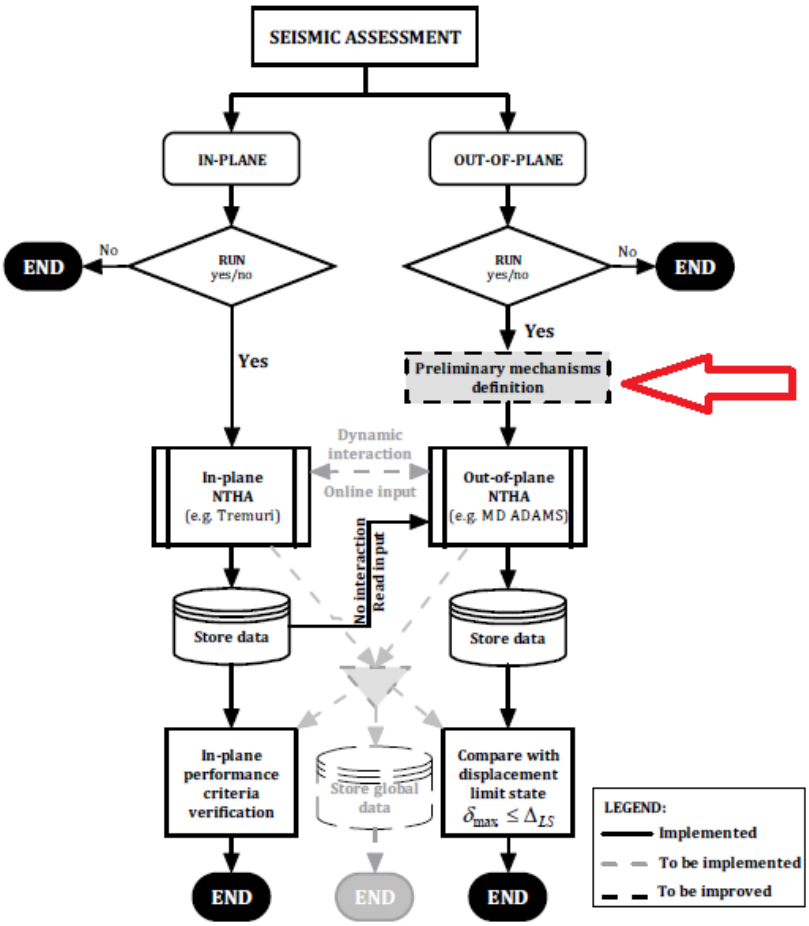

Figure 6.1 Flowchart of the proposed methodology for the seismic assessment of masonry structures by (Costa, 2012), (the red arrow indicates the possible contribution of the present work)

REFERENCES

Abrams, D. P., Angel, R., & Uzarski, J. (1996). Out-of-plane strength of unreinforced masonry infill panels. *Earthquake Spectra*, *12*(4), 825-844.

Abrams, D. P., AlShawa, O., Lourenço, P. B., & Sorrentino, L. (2017). Out-of-Plane Seismic Response of Unreinforced Masonry Walls: Conceptual Discussion, Research Needs, and Modeling Issues. International Journal of Architectural Heritage, 11(1), 22-30.

Alexandris, A., E. Protopapa, and I. Psycharis. (2004). Collapse mechanisms of masonry buildings derived by the distinct element method. In *Proceedings of the 13th World Conference on Earthquake Engineering* Vancouver, B.C., Canada, August 1–6, 2004. Paper no. 548. Canadian Association for Earthquake Engineering and International Association for Earthquake Engineering.

AlShawa, O., Sorrentino, L., & Liberatore, D. (2017). Simulation of shake table tests on out-of-plane masonry buildings. Part (II): combined finite-discrete elements. International Journal of Architectural Heritage, 11(1), 79-93.

Bažant, Zdeněk P., and B. Oh. 1983. "Crack Band Theory for Fracture of Concrete." Materials and Structures 16: 155–77. doi:10.1007/BF02486267.

Benedetti L., (2017). Mixed finite element formulations for strain localization and failure in plasticity. PHD Thesis, Universitat Politecnica de Catalunya.

Benedetti, L., Cervera, M., & Chiumenti, M. (2017). 3D numerical modelling of twisting cracks under bending and torsion of skew notched beams. Engineering Fracture Mechanics, 176, 235-256.

Binda L., Saidi A., & Tedeschi C., (2006). Compatibility of materials used for repair of masonry buildings: research and applications. *Fracture and Failure of Natural Building Stones.* S. K. Kourkoulis, Springer Netherlands, Part I, pp: 167-182.

Block, P., Ciblac, T., & Ochsendorf, J. (2006). Real-time limit analysis of vaulted masonry buildings. *Computers & Structures*, *84*(29), 1841-1852.

Brezzi, F. (1974). On the existence, uniqueness and approximation of saddle-point problems arising from Lagrangian multipliers. Revue française d'automatique, informatique, recherche opérationnelle. Analyse numérique, 8(R2), 129-151

Bruneau, M. (1994). Seismic evaluation of unreinforced masonry buildings—A state-of-the-art report. *Canadian Journal of Civil Engineering*, *21*(3), 512-539.

Candeias, P. X., Campos Costa, A., Mendes, N., Costa, A. A., & Lourenço, P. B. (2017). Experimental Assessment of the Out-of-Plane Performance of Masonry Buildings Through Shaking Table Tests. International Journal of Architectural Heritage, 11(1), 31-58.

Cannizzaro, F., & Lourenço, P. B. (2017). Simulation of Shake Table Tests on Out-of-Plane Masonry Buildings. Part (VI): Discrete Element Approach. International Journal of Architectural Heritage, 11(1), 125-142.

Casapulla, C. (1999). Resistenze attritive in una parete muraria soggetta ad azioni normali al suo piano medio. In *L'Ingegneria Sismica in Italia: Atti IX Convegno Nazionale ANIDIS*. Torino, Italy, September 20–23, 1999.

Casapulla, C., & D'Ayala, D. (2006, November). In plane collapse behaviour of masonry walls with frictional resistance and openings. In *Structural analysis of historical constructions. Possibilities of numerical and experimental techniques. Proceedings of the 5th International Conference, Macmillan India Ltd, New Delhi* (pp. 1153-1160).

Casolo, S. (1999). Rigid element model for non-linear analysis of masonry facades subjected to out-of-plane loading. *Communications in Numerical Methods in Engineering 15*(7):457–468.

Casolo, S. (2000). Modelling the out-of-plane seismic behaviour of masonry walls by rigid elements. *Earthquake Engineering & Structural Dynamics 29*(12):1797–1813.

Casolo, S., & Milani, G. (2010). A simplified homogenization-discrete element model for the non-linear static analysis of masonry walls out-of-plane loaded. *Engineering Structures*, *32*(8), 2352-2366.

Casolo, S., & Milani, G. (2013). Simplified out-of-plane modelling of three-leaf masonry walls accounting for the material texture. *Construction and Building Materials*, *40*, 330-351.

Cecchi, A., & Sab, K. (2002). Out of plane model for heterogeneous periodic materials: the case of masonry. *European Journal of Mechanics-A/Solids*, *21*(5), 715-746.

Cecchi, A., Milani, G., & Tralli, A. (2007). A Reissner–Mindlin limit analysis model for out-of-plane loaded running bond masonry walls. *International journal of solids and structures*, *44*(5), 1438-1460.

Cervera M., Agelet de Saracibar C., & Chiumenti M., (2002), COMET: Coupled Mechanical and Thermal analysis, Data Input Manual, Version 5.0, Technical report IT-308, Available from http://www.cimne.com/comet/cvdata/cntr1/dtos/img/mdia/COMET_Data_Input_manual.pdf.

Cervera, M., Chiumenti, M., Valverde, Q., Agelet de Saracibar, C. (2003) "Mixed linear/linear simplicial elements for incompressible elasticity and plasticity" Computer Methods and Applied Mechanics in Engineering, 192 (49-50), pp. 5249-5263

Cervera, M., Chiumenti, M., & de Saracibar, C. A. (2004). Shear band localization via local J 2 continuum damage mechanics. Computer Methods in Applied Mechanics and Engineering, 193(9), 849-880.

Cervera M., Chiumenti M., & Codina R. (2010a). Mixed Stabilized Finite Element Methods in Nonlinear Solid Mechanics. Part I: Formulation. Computer Methods in Applied Mechanics and Engineering, 199(37-40), 2559-2570.

Cervera, M., Chiumenti, M., & Codina, R. (2010b). Mixed stabilized finite element methods in nonlinear solid mechanics: Part ii: Strain localization. Computer Methods in Applied Mechanics and Engineering, 199(37), 2571-2589.

Cervera, M., Chiumenti, M., & Codina, R. (2011). Mesh objective modeling of cracks using continuous linear strain and displacement interpolations. *International Journal for Numerical Methods in Engineering*, *87*(10), 962-987.

Cervera, M., Chiumenti, M., Benedetti, L., & Codina, R. (2015). Mixed stabilized finite element methods in nonlinear solid mechanics. Part III: Compressible and incompressible plasticity. Computer Methods in Applied Mechanics and Engineering, 285, 752-775.

Cervera, M., Barbat, G. B. and Chiumenti, M. "Finite element modelling of quasi-brittle cracks in 2D and 3D with enhanced strain accuracy" (2017) Computational Mechanics, in press, http://dx.doi.org/10.1007/s00466-017-1438-8

Chácara, C., Mendes, N., & Lourenço, P. B. (2017). Simulation of shake table tests on out-of-plane masonry buildings. Part (IV): macro and micro FEM based approaches. International Journal of Architectural Heritage, 11(1), 103-116.

Codina, R. (2000). Stabilization of incompressibility and convection through orthogonal sub-scales in finite element methods. *Computer methods in applied mechanics and engineering*, *190*(13), 1579-1599.

Costa, A. A., A. Arêde, A. Campos Costa, A. Penna, and A. Costa. (2013a). Out-of-plane behaviour of a full scale stone masonry facade. Part 1: Specimen and ground motion selection. Earthquake Engineering & Structural Dynamics 42(14), 2081–2095.

Costa, A. A. M. G. (2012). *Seismic assessment of the out-of-plane performance of traditional stone masonry walls* (Doctoral dissertation, Universidade do Porto (Portugal)).

D'Ayala, D., & Speranza, E. (2003). Definition of collapse mechanisms and seismic vulnerability of historic masonry buildings. Earthquake Spectra, 19(3), 479-509.

D'Ayala, D., & Shi, Y. (2011). Modeling masonry historic buildings by multi-body dynamics. *International Journal of Architectural Heritage*, *5*(4-5), 483-512.

Decanini, L., De Sortis, A., Goretti, A., Langenbach, R., Mollaioli, F., & Rasulo, A. (2004). Performance of masonry buildings during the 2002 Molise, Italy, earthquake. *Earthquake Spectra*, *20*(S1), S191-S220.

de Borst, R. (2002). Fracture in quasi-brittle materials: a review of continuum damage-based approaches. *Engineering fracture mechanics*, *69*(2), 95-112.

DeJong, M. J. (2009). *Seismic assessment strategies for masonry structures* (Doctoral dissertation, Massachusetts Institute of Technology).

Del Piero, G. (1989). Constitutive equation and compatibility of the external loads for linear elastic masonry-like materials. *Meccanica*, *24*(3), 150-162.

Derakhshan, H., Griffith, M. C., & Ingham, J. M. (2011). Out-of-plane behavior of one-way spanning unreinforced masonry walls. *Journal of Engineering Mechanics*, *139*(4), 409-417

Derakhshan, H., Griffith, M. C., & Ingham, J. M. (2011). Out-of-plane behavior of one-way spanning unreinforced masonry walls. *Journal of Engineering Mechanics*, *139*(4), 409-417.

Derakhshan, H., Nakamura, Y., Ingham, J. M., & Griffith, M. C. (2017). Simulation of shake table tests on out-of-plane masonry buildings. Part (I): displacement-based approach using simple failure mechanisms. International Journal of Architectural Heritage, 11(1), 72-78.

Doherty, K. T. (2000). *An investigation of the weak links in the seismic load path of unreinforced masonary buildings* (Doctoral dissertation).

Doherty, K., Griffith, M. C., Lam, N., & Wilson, J. (2002). Displacement-based seismic analysis for out-of-plane bending of unreinforced masonry walls. *Earthquake engineering & structural dynamics*, *31*(4), 833-850.

Drei, A., C. S. Oliveira, P. B. Lourenço, and P. Roca. (2001). The seismic behaviour of the “Aqueduto da Amoreira” in Elvas using distinct element modelling. In *Proceedings of the 3rd International Seminar on Historical Constructions*, eds., P. B. Lourenço and P. Roca, Guimarães, Portugal November 7–9, 2001, 903–912.

Felice, G. D., & Giannini, R. (2001). Out-of-plane seismic resistance of masonry walls. *Journal of earthquake engineering*, *5*(02), 253-271.

Felice, G. D. (2005). Out-of-plane fragility of historic masonry walls. In *Structural analysis of historical constructions*, eds., C. Modena, P. B. Lourenço, and P. Roca. London, UK: Taylor & Francis, vol. 2: 1143–1148.

Felice, G., De Santis, S., Lourenço, P. B., & Mendes, N. (2017). Methods and Challenges for the Seismic Assessment of Historic Masonry Structures. International Journal of Architectural Heritage, 11(1), 143-160.

Ferreira, T. M., Costa, A. A., & Costa, A. (2015). Analysis of the out-of-plane seismic behavior of unreinforced masonry: A literature review. *International Journal of Architectural Heritage*, *9*(8), 949-972.

Ferreira, T. M. D. S. (2015). Out-of-plane seismic performance of stone masonry walls: experimental and analytical assessment. PHD Thesis, Universidade de Aveiro.

Gabellieri, R., L. Landi, and P. P. Diotallevi. (2013). A 2–DOF model for the dynamic analysis of unreinforced masonry walls in out-of-plane bending. In *Proceedings of the 4th ECCOMAS Thematic Conference on Computational Methods in Structural Dynamics and Earthquake Engineering: COMPDYN 2013*, eds., M. Papadrakakis, V. Papadopoulos, and V.Plevris. Kos Island, Greece, June 12–14, 2013.

Gams, M., Anžlin, A., & Kramar, M. (2017). Simulation of shake table tests on out-of-plane masonry buildings. Part (III): two-step FEM approach. International Journal of Architectural Heritage, 11(1), 94-102.

Giaquinta, M., & Giusti, E. (1985). Researches on the equilibrium of masonry structures. *Archive for Rational Mechanics and Analysis*, *88*(4), 359-392.

GiD: the personal pre and post-processor. (2002) CIMNE, Technical University of Catalonia; http://gid.cimne.upc.es

Giuffrè, A. (1990). Letture sulla meccanica delle murature storiche.

Giuffrè, A., C. Carocci, C. Baggio, and GNDT–SSN. (1993). Sicurezza e conservazione dei centri storici: Il caso Ortigia: Codice di pratica per gli interventi antisismici nel centro storico. Italy: Editori Laterza.

Griffith, M. C., Magenes, G., Melis, G., & Picchi, L. (2003). Evaluation of out-of-plane stability of unreinforced masonry walls subjected to seismic excitation. *Journal of Earthquake Engineering*, *7*(spec01), 141-169.

Hart, G. C., Kariotis, J., & Noland, J. L. (1988). The Whittier Narrows, California Earthquake of October 1, 1987—Masonry Building Performance Survey. *Earthquake spectra*, *4*(1), 181-196.

Hendry, A. W., Sinha, B. P., & Davies, S. R. (1997). Design of masonry structures E & FN Spon.

Heyman, J. (1966). The stone skeleton. *International Journal of solids and structures*, *2*(2), 249-279.

Housner, G. W. (1963). The behavior of inverted pendulum structures during earthquakes. *Bulletin of the seismological society of America*, *53*(2), 403-417.

Jirásek, M., & Bauer, M. (2012). Numerical aspects of the crack band approach. Computers & Structures, 110, 60-78.

Kawai, T. (1978). New discrete models and their application to seismic response analysis of structures. *Nuclear Engineering and Design*, *48*(1), 207-229.

Lagomarsino, S. (1998, October). Seismic damage survey of the churches in Umbria. In *Proc. of the Workshop on Seismic Performance of Monuments (Monument-98), Lisbon* (pp. 167-176).

Lagomarsino, S., & Podesta, S. (2004). Damage and vulnerability assessment of churches after the 2002 Molise, Italy, earthquake. *Earthquake Spectra*, *20*(S1), S271-S283.

Lagomarsino, S. (2015). Seismic assessment of rocking masonry structures. *Bulletin of earthquake engineering*, *13*(1), 97.

Lemos, J. V. (2007). Discrete element modeling of masonry structures. *International Journal of Architectural Heritage*, *1*(2), 190-213.

Lemos, J. V., Campos-Costa, A. (2017). Simulation of Shake Table Tests on Out-of-Plane Masonry Buildings. Part (V): Discrete Element Approach. International Journal of Architectural Heritage, 11(1), 117-124.

Lourenço, P. B., & Rots, J. G. (1997). Multisurface interface model for analysis of masonry structures. *Journal of engineering mechanics*, *123*(7), 660-668.

Lourenço, P. B. (2000). Anisotropic softening model for masonry plates and shells. *Journal of structural engineering*, *126*(9), 1008-1016.

Lourenço, P. B. (2002). Computations on historic masonry structures. *Progress in Structural Engineering and Materials*, *4*(3), 301-319.

Lourenço, P. B. (2009). Recent advances in masonry modelling: micromodelling and homogenisation. Multiscale Model. Solid Mech. Comput. Approaches, 3, 251-294.

Lourenço, P. B., Mendes, N., Costa, A. A., & Campos-Costa, A. (2017). Methods and Challenges on the Out-of-Plane Assessment of Existing Masonry Buildings. International Journal of Architectural Heritage, 11(1), 1.

Macorini, L., & Izzuddin, B. A. (2011). A non-linear interface element for 3D mesoscale analysis of brick-masonry structures. *International Journal for numerical methods in Engineering*, *85*(12), 1584-1608.

Makris, N., & Konstantinidis, D. (2003). The rocking spectrum and the limitations of practical design methodologies. *Earthquake engineering & structural dynamics*, *32*(2), 265-289.

Mendes, N., Costa, A. A., Lourenço, P. B., Bento, R., Beyer, K., de Felice, G., ... & Lemos, J. V. (2017). Methods and approaches for blind test predictions of out-of-plane behavior of masonry walls: A numerical comparative study. International Journal of Architectural Heritage, 11(1), 59-71.

Menon, A., & Magenes, G. (2008). *Out-of-plane seismic response of unreinforced masonry: definition of seismic input*. Rose School, IUSS Press

Milani, G., Lourenço, P., & Tralli, A. (2006). Homogenization approach for the limit analysis of out-of-plane loaded masonry walls. *Journal of structural engineering*, *132*(10), 1650-1663.

Milani, G., & Venturini, G. (2011). Automatic fragility curve evaluation of masonry churches accounting for partial collapses by means of 3D FE homogenized limit analysis. *Computers & Structures*, *89*(17), 1628-1648.

Milani, G., Pizzolato, M., & Tralli, A. (2013). Simple numerical model with second order effects for out-of-plane loaded masonry walls. *Engineering Structures*, *48*, 98-120.

Milano, L., Mannella, A., Morisi, C., & Martinelli, A. (2008). Schede illustrative dei principali meccanismi di collasso locali negli edifici esistenti in muratura e dei relativi modelli cinematici di analisi. Allegato alle Linee Guida per la Riparazione e il Rafforzamento di elementi strutturali, Tamponature e Partizioni (2008)

Milizia (1554). Principij di architettura. Venezia, Italy.

Moore, T. A., Kobzeff, J. H., Diri, J., & Arnold, C. (1988). The Whittier Narrows, California earthquake of October 1, 1987—preliminary evaluation of the performance of strengthened unreinforced masonry buildings. *Earthquake spectra*, *4*(1), 197-212.

Mosler, J., & Meschke, G. (2004). Embedded crack vs. smeared crack models: a comparison of elementwise discontinuous crack path approaches with emphasis on mesh bias. *Computer Methods in Applied Mechanics and Engineering*, *193*(30), 3351-3375

Novelli, V., & D'Ayala, D. (2012). Seismic vulnerability assessment of the Casbah of Algiers. In *Proceeding of 8th International conference of structural analysis of historical constructions* (pp. 2939-2947).

Oliver, J. (1989). A consistent characteristic length for smeared cracking models. International Journal for Numerical Methods in Engineering, 28(2), 461-474.

Oliveira, C. S., J. V. Lemos, and G. E. Sincraian, (2002). Modelling large displacements of structures damaged by earthquake motions. *European Earthquake Engineering 16*(3):56–71.

Page, A. W. (1978). Finite element model for masonry. *Journal of the Structural Division*, *104*(8), 1267-1285.

Papa, S., Di Pasquale, G., Podestà, S., & Brignola, A. (2011). Manuale per la compilazione della scheda per il rilievo del danno ai beni culturali. Chiese, Modello A-DC.

Pelà, L. (2009). Continuum damage model for nonlinear analysis of masonry structures. PhD Thesis. Universitat Politecnica de Catalunya & Università degli studi di Ferrara

Pelà, L., Cervera, M., & Roca, P. (2011). Continuum damage model for orthotropic materials: Application to masonry. Computer Methods in Applied Mechanics and Engineering, 200(9), 917-930.

Penazzi, D., Valluzzi, M. R., Cardani, G., Binda, L., Baronio, G., & Modena, C. (2000, June). Behaviour of historic masonry buildings in seismic areas: lessons learned from the Umbria-Marche earthquake. In *Proceedings of the 12th international conference of IBBMac* (Vol. 1, pp. 217-235).

Petracca, M., Pelà, L., Rossi, R., Oller, S., Camata, G., & Spacone, E. (2017). Multiscale computational first order homogenization of thick shells for the analysis of out-of-plane loaded masonry walls. Computer Methods in Applied Mechanics and Engineering, 315, 273-301.

Picchi, L. (2002). Risposta sismica per azioni fuori dal plano di parete murarie. Pavia, Italy: Università Degli Studi di Pavia.

Priestley, M. J. N., Evison, R. J., & Carr, A. J. (1978). Seismic response of structures free to rock on their foundations. *Bulletin of the New Zealand National Society for Earthquake Engineering*, *11*(3), 141-150.

Priestley, M. J. N. (1985). Seismic behaviour of unreinforced masonry walls. *Bulletin of the New Zealand National Society for Earthquake Engineering*, *18*(2), 191-205.

Psycharis, I. N. (1990). Dynamic behaviour of rocking two-block assemblies. *Earthquake Engineering & Structural Dynamics*, *19*(4), 555-575.

Rabczuk, T. (2013). Computational methods for fracture in brittle and quasi-brittle solids: state-of-the-art review and future perspectives. *ISRN Applied Mathematics*, *2013.*

Restrepo-Vélez, L. F. (2004). Seismic Risk of Unreinforced Masonry Buildings, Individual Study. ROSE. School, Pavia, Italy.

Reitherman, R. (1985). The Borah Peak, Idaho earthquake of October 28, 1983—performance of unreinforced masonry buildings in Mackay, Idaho. *Earthquake spectra*, *2*(1), 205-224.

Roberti, G. M., and O. Spina. (2001). Discrete element analysis on the Sardinian' Nuaraghe. In *Proceedings of the 3rd International Seminar on Historical Constructions*, eds., P. B. Lourenço and P. Roca, Guimarães, Portugal, November 2001, 719–727.

Rondelet J.B., (1802). Théorie et pratique de l'art de bâtir. Paris, France.

Shawa, O. A., Felice, G., Mauro, A., & Sorrentino, L. (2012). Out-of-plane seismic behaviour of rocking masonry walls. *Earthquake Engineering & Structural Dynamics*, *41*(5), 949-968.

Sincraian, G. E., Oliveira, C. S., and Lemos, J. V. (1998). Assessment of the seismic behaviour of a stone masonry aqueduct using the discrete element method. In *Proceedings of the 11th European Conference on Earthquake Engineering*, eds., P. Bisch, P. Labbé, and A. Pecker. Paris, France, September 1998. Rotterdam, Netherlands: Balkema.

Sorrentino, L., Masiani, R., & Decanini, L. D. (2006). Overturning of rocking rigid bodies under transient ground motions. *Structural Engineering and Mechanics*, *22*(3), 293-310.

Sorrentino, L., Kunnath, S., Monti, G., & Scalora, G. (2008). Seismically induced one-sided rocking response of unreinforced masonry façades. *Engineering Structures*, *30*(8), 2140-2153.

Sorrentino, L., D'Ayala, D., de Felice, G., Griffith, M. C., Lagomarsino, S., & Magenes, G. (2017). Review of out-of-plane seismic assessment techniques applied to existing masonry buildings. International Journal of Architectural Heritage, 11(1), 2-21.

Spanos, P. D., Roussis, P. C., & Politis, N. P. (2001). Dynamic analysis of stacked rigid blocks. *Soil Dynamics and Earthquake Engineering*, *21*(7), 559-578.

Stevin, S. (1586). De beghinselen der weeghconst. *The Principal Works of Simon Stevin*, *1*.

Theodossopoulos, D., & Sinha, B. (2013). A review of analytical methods in the current design processes and assessment of performance of masonry structures. *Construction and Building Materials*, *41*, 990-1001.

Tomaževič, M. (1997). *Seismic resistance verification of masonry buildings: Following the new trends.*

Trovalusci, P., & Masiani, R. (2003). Non-linear micropolar and classical continua for anisotropic discontinuous materials. International Journal of Solids and Structures, 40(5), 1281-1297.

Valluzzi, M. R. (2007). On the vulnerability of historical masonry structures: analysis and mitigation. *Materials and structures*, *40*(7), 723-743.

Venture, A. A. J. (1981). *Methodology for Mitigation of Seismic Hazards in Existing Unreinforced Masonry Buildings: Wall-testing, Out-of-plane*. The Corporation.

Yim, C. S., Chopra, A. K., & Penzien, J. (1980). Rocking response of rigid blocks to earthquakes. *Earthquake Engineering & Structural Dynamics*, *8*(6), 565-587.

Zienkiewicz, O. C., Taylor, R. L., & Zhu, J. Z. (2005). The Finite Element Method: Its Basis and Fundamental, Elselvier.

Zuccarello, F. A., Milani, G., Olivito, R. S., & Tralli, A. (2009). A numerical and experimental analysis of unbonded brickwork panels laterally loaded. *Construction and Building Materials*, *23*(5), 2093-2106

ANNEX

Used Isotropic and Orthotropic damage models: single element comparison

Geomaterials, such as masonry, present a unilateral nature of damage, meaning that the damage might be active or not, depending on the loading direction (Pela, 2009). For example, if damage has occurred in tension, the compressive response wouldn't be affected in case of reverse loading Figure 0.1.

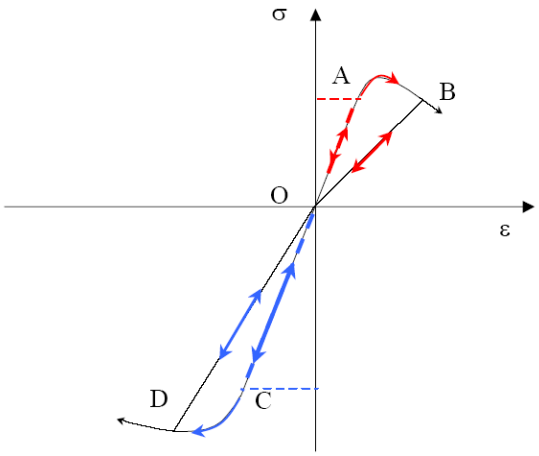

Figure 0.1 Unilateral effect under cyclic loading (Pela, 2009)

As a consequence, unilateral damage models have been developed, which are able to reproduce this crack-closure phenomenon. The isotropic damage model, used in this thesis as reference damage model, is not able to reproduce such phenomena. For this reason another damage model is also been tested, denoted as orthotropic damage model, being able to do so. The main characteristic of the model is that it splits the stress tensor into two parts: the tensile (σ^+) and the compressive (σ^-) part. Moreover, two separate damage indexes are assumed, in order to track the damage under tension (d^+) and compression (d^-), respectively. In this way the model is able to reproduce the unilateral behavior of such materials.

$$\boldsymbol{\sigma} = (1 - d^+)\bar{\boldsymbol{\sigma}}^+ + (1 - d^-)\bar{\boldsymbol{\sigma}}^- \tag{17}$$

Nevertheless, it is important to underline that no compressive damage is considered in this thesis, and therefore the damage index d^- is always zero.

In order to obtain a more intuitive understanding of this difference, a simple example of one element was implemented. A single cubic element, similar with the ones used in this thesis, is subjected to

Mode I and Mode II cyclic tests, using and comparing the two different damage models, namely the isotropic and the orthotropic. Their responses are presented in Figure 0.2.

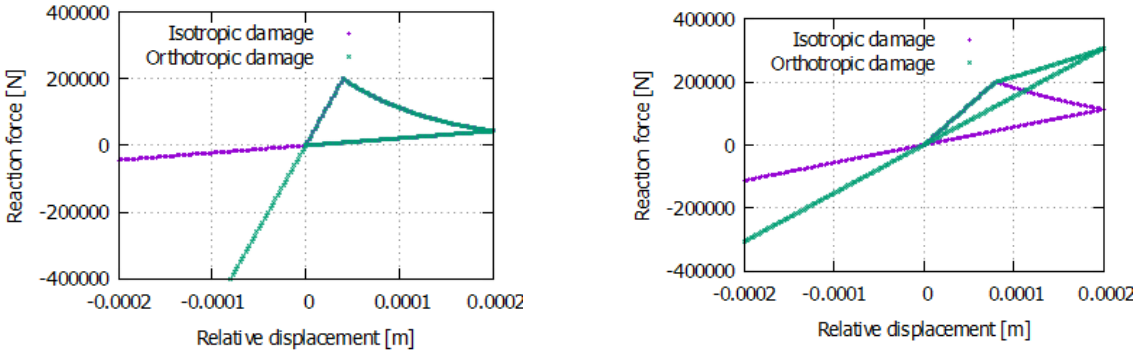

(a) (b)

Figure 0.2 Single cubic element under cyclic loading with Isotropic & Orthotropic damage models (a) for Mode I and (b) for Mode II

As can be seen in Mode I testing, the two models present identical response when subjected to monotonic tension, but when compression is after that acted, the isotropic damage model appears to "keep" the tensile damage, while the orthotropic damage model represents correctly the crack closure phenomenon with the undamaged stiffness.

When the cube is subjected to Mode II loading, things change even in the monotonic loading. More specifically, the shear loading leads to both tensile and compressive stresses to appear. Therefore, since the isotropic damage model damages the whole stress tensor, a similar softening with Mode I is observed. On the other hand, the orthotropic damage model results in damaging only the tensile part of the tensor (since compressive damage is not considered), and therefore a retaining strength is always present, corresponding to the compressive part of the tensor. Moving to the reverse direction of loading, the same stiffness of that time is kept, since there is no physical difference.

Summarizing, the main points of this example are the following:

- under monotonic tension or compression test, the two damage models show identical behaviour,
- under monotonic shear test, the orthotropic damage model retains more strength in the inelastic regime, which never diminishes completely, since no compressive damage is considered
- when cyclic loading is considered, the orthotropic damage model is stiffer both in Mode I or Mode II loading, if damage has been previously developed.